AWPP
H25p
1990

A dissertation entitled

PERCOLATIVE TRANSPORT AND CLUSTER DIFFUSION
NEAR AND BELOW THE PERCOLATION THRESHOLD
OF A POROUS POLYMERIC SYSTEM

submitted to the Graduate School of the
University of Wisconsin-Madison
in partial fulfillment of the requirements for the
degree of Doctor of Philosophy

by

JAYNE ELIZABETH HASTEDT

Degree to be awarded: December 1990 May 19___ August 19___

Approved by Dissertation Readers:

George Zografi — August 22, 1990
Major Professor — Date of Examination

Kenneth G. Comm

Ronald R. Bruetto

John D. Wiley
Dean, Graduate School

PERCOLATIVE TRANSPORT AND CLUSTER DIFFUSION NEAR AND BELOW THE PERCOLATION THRESHOLD OF A POROUS POLYMERIC SYSTEM

by

JAYNE ELIZABETH HASTEDT

A thesis submitted in partial fulfillment of the

requirements for the degree of

Doctor of Philosophy

(Pharmaceutics)

at the

UNIVERSITY OF WISCONSIN - MADISON

1990

Phar
AW
#25

PERCOLATIVE TRANSPORT AND CLUSTER DIFFUSION NEAR AND BELOW THE PERCOLATION THRESHOLD OF A POROUS POLYMERIC SYSTEM

Jayne Elizabeth Hastedt
Under the supervision of
Assistant Professor James L. Wright and Professor George Zografi
at the University of Wisconsin - Madison

ABSTRACT

Deviation from classical percolative transport was observed near and below the percolation threshold of a system containing benzoic acid and poly(vinyl stearate). Analysis of the polymer material properties, the morphology of the porous microstructures of several tablets, and the transport properties of the system below the threshold lead to the conclusion of nonclassical anomalous diffusion. A percolative transport model incorporating nonclassical cluster diffusion and classical percolative transport mechanisms was developed. The model successfully predicted the release characteristics of the biphasic percolating matrix both below and near and above the system's percolation threshold.

The percolation threshold of the system was determined to be 0.09 ± 0.02 which corresponds to a coordination of 28 ± 7 at 95% confidence. The low threshold, and subsequently high coordination, was determined to be an inherent property of the system caused by the complexity of the underlying microstructure.

George Zografi
Professor George Zografi, Major Professor

August 22, 1990
Date

UWMN Graduate School

AUG 23 1990

DEDICATION

To Jamshed, my inspiration.

ACKNOWLEDGEMENTS

This research was generously funded in part by the American Chemical Society Chapter of the Petroleum Research Foundation, Glaxo Inc., and the Burroughs Wellcome Fund.

The assistance of Tom Pienkowski in the microtoming studies and Gary Girdaukas in stereo-imaging of the three-dimensional reconstructions was greatly appreciated. Without these two people, the difficult task of generating three-dimensional images of the pore structures would not have been possible.

My appreciation also goes to my very talented husband, Jamshed Ghandhi, who made pieces of equipment too numerous to list in order to keep my experiments running and me happy. Without his support, both mentally and technically, none of this would have been possible.

I am also grateful to my father, Harold W. Hastedt, for his help in the design and manufacture of the diffusion cell assembly utilized in this research. He was also beneficial in lending his talented eye for drawing and detail to the figures presented in this dissertation.

I would like to thank Professor George Zografi for taking the time and effort to take on the responsibility of monitoring my research efforts and exploring pertinent percolation concepts. The encouragement offered was, and will always be, greatly appreciated.

My gratitude and appreciation also goes to Dr. James Wright who guided me through much of this via long distance phone calls and unbiased criticisms. Without these discussions, none of this would have been possible, at least not in this form. Thank you Jim.

TABLE OF CONTENTS

Title — Page

Abstract ii
Dedication iii
Acknowledgements iv
Table of Contents v
List of Figures ix
List of Tables xi
I. Introduction 1
A. The Research Objective 1
B. The Approach 2
C. Background 4
1. Percolation Theory 4
a) Percolation Morphological Parameters 6
b) Percolation Transport Parameters 13
c) Scaling Laws of Percolation Theory Above the Percolation Threshold 17
d) Percolation Clusters and Scaling 22
e) The Bethe Lattice 25
2. Transport in Porous Media 30
a) Diffusion in Heterogeneous Materials 30
b) Percolation and Transport 31
3. Combining Percolation Theory and Diffusion in Heterogeneous Materials 32
D. Percolative Transport Results Above the Percolation Threshold 35
E. The Proposed Solution 42
1. Transport Near and Below the Percolation Threshold 42
2. Nonclassical and Nonuniversal Percolative Transport Systems 42
a) Changing Microstructure 43
b) Biphasic Conductivity and Nonclassical Behavior 43
c) Complex Microstructure and Nonuniversal Behavior 44

Title Page

d) System Size 45
(i) Finite-Size Scaling 45
(ii) Renormalization Group 47
F. Expected Results and Contributions 51
II. Experimental 53
A. Chemicals and Reagents 53
B. Methodology 54
1. Previous Analysis 54
2. Current Analysis 56
3. Release Kinetics 56
a) Tablet Manufacture 56
b) Dissolution 61
c) Analysis 62
4. Physicochemical Properties 64
a) Determination of the Pycnometric Densities of Benzoic Acid and Poly(vinyl stearate) 64
b) Osmometry 66
c) Intrinsic Viscosity and Viscosity Average Molecular Weight of Poly(vinyl stearate) 67
d) Melting Point and Enthalpy of Fusion of Poly(vinyl stearate) 70
e) Transport Through Poly(vinyl stearate) Films and Discs 71
5. Analysis of the Microstructure Morphology 76
a) Microtoming 76
b) Microscopy 76
c) Three-Dimensional Reconstructions 83
III. Data Treatment and Results 85
A. Percolative Transport Near and Below the Percolation Threshold 85
1. Data From Transport Near and Below the Percolation Threshold 85
2. Volume Fraction Accessible Near and Below the Percolation Threshold 89
3. Volume Fraction Effective Near and Below the Percolation Threshold 94

Title Page

B. Analysis of Nonclassical Percolating Systems 99
1. Changing Microstructure 99
a) Contribution of Osmotic Pressure to Transport 99
2. Characterization of Biphasic Conducting Systems 102
a) Viscosity Average Molecular Weight of Poly(vinyl stearate) 102
b) Melting Point and Heat of Fusion of Poly(vinyl stearate) 105
c) Biphasic Conductivity 106
(i) Permeability Model 106
(ii) Permeability Results 108
3. Characterization of the Porous Microstructure 112
a) Three-Dimensional Reconstructions 112
b) Estimation of Porosity Based on Reconstructions 119
C. Overall System Results 121
1. Osmotic Pressure Results 121
2. Transport Through Poly(vinyl stearate) Results 121
3. Microstructure Morphology Results 124
4. Conclusions 126
IV. Discussion 127
A. Development of the Nonclassical Percolative Transport Model 127
1. The System 128
a) Transport Near and Above the Percolation Threshold 128
b) Transport Below the Percolation Threshold 131
2. Determination of the Percolation Threshold 133
3. Nonlinear Regression Analysis 137
a) Estimation of the Nonclassical Percolative Transport Model Parameters Below the Percolation Threshold 137
b) Estimation of the Nonclassical Percolative Transport Model Parameters Near and Above the Percolation Threshold 139
B. Evaluation of the Nonclassical Percolative Transport Model 142
1. Comparison to Experimental Bulk Diffusivities 142

Title Page

2. Comparison to Scaling Theory....144
a) The Percolation Threshold....144
b) Percolative Scaling....146
3. Contributions to Bulk Transport....149
4. The Kinetics Model....152
V. Summary and Conclusions....155
A. Analysis and Characterization of the System....155
1. The Percolative Transport and Cluster Diffusion Model....156
2. The Mechanism of Transport Through the Polymer....158
B. Deviation From Classical and Universal Percolating Systems....160
1. Biphasic Conductivity and Nonclassical Behavior....160
2. Microscopic Ordering and Nonuniversal Behavior....161
C. Difficulties and Limitations of This Research....162
1. The Kinetics Model....162
2. Limitations of the Model....163
a) Cluster Size Far Below the Percolation Threshold....163
b) Morphological versus Percolative Contributions to Transport....163
D. Questions....164
1. Volume Fraction Effective From Conductivity Measurements....164
2. Meaning of Pre-Exponential Factors....164
3. Evaluation of Coordination....166
4. Testing the Model....166
E. Applications....167
VI. References....168
VII. Appendix....177
Appendix A
Derivation of the Release Kinetics Model....177
Appendix B
Photomicrograph Data for Three-Dimensional Reconstructions....181
Appendix C
Kinetic Release Data....187

LIST OF FIGURES

Figure	Title	Page
Figure 1.1	The Tablet Constituents	3
Figure 1.2	A Two-Dimensional Square Lattice	8
Figure 1.3	Examples of Coordination in Two Dimensions	9
Figure 1.4	Percolation Threshold as a Function of Coordination Number for Three-Dimensional Lattices	11
Figure 1.5	Percolation Parameters Of the Cubic Lattice as a Function of Volume Fraction Conducting	16
Figure 1.6	A Bethe Lattice of Coordination Three	26
Figure 1.7	Square Root Of Time Release Profiles From Initial Kinetics Experiments	36
Figure 1.8	Initial Volume Fraction Accessible Results Above the Percolation Threshold	37
Figure 1.9	Initial Volume Fraction Effective Results Above the Percolation Threshold	38
Figure 1.10	Initial Experimental Volume Fraction Effective Results Compared to the Calculated Percolation Profile Above the Percolation Threshold	41
Figure 1.11	Renormalization Group Scale Transformation of a Body-Centered Cubic Lattice	48
Figure 1.12	Simulated Profile of a Percolative Renormalization Group Analysis	50
Figure 2.1	The Rotating Disk Assembly	58
Figure 2.2	The Diffusion Cell Assembly	72
Figure 2.3	Stainless Steel Chuck and Tablet Assembly	79
Figure 2.4	Square Grid Reticle for Photomicroscopy	80
Figure 2.5	X-Y Micropositioning Stage for Photomicroscopy	81
Figure 2.6	Two-Dimensional Photomicrograph of the Porous Microstructure	84
Figure 3.1	Square Root of Time Release Profile for EXP 3	87
Figure 3.2	Square Root of Time Release Profile for EXP 4	88
Figure 3.3	Experimental Volume Fraction Accessible Results for the Benzoic Acid/Poly(vinyl stearate) System Compared to Theory	93

Figure	Title	Page
Figure 3.4	Experimental Volume Fraction Effective Results for the Benzoic Acid/Poly(vinyl stearate) System Compared to Theory	98
Figure 3.5	Determination of the Intrinsic Viscosity of Poly(vinyl stearate) Based on Reduced Viscosity Results	104
Figure 3.6	Permeability of Poly(vinyl stearate) Discs and Films to Benzoic Acid	109
Figure 3.7	Photomicrograph of Compressed Disc of Poly(vinyl stearate) Surface	110
Figure 3.8	Three-Dimensional Reconstructions of the Pore Structure. Dimensions of 100 μm × 100 μm × 167 μm or 83 μm.	114
Figure 3.9	Three-Dimensional Reconstructions of the Pore Structure. Dimensions of 100 μm × 50 μm × 167 μm or 83 μm.	115
Figure 3.10	Three-Dimensional Reconstruction for Stereo Viewing, Total Porosity = 0.051	116
Figure 3.11	Three-Dimensional Reconstruction for Stereo Viewing, Total Porosity = 0.141	117
Figure 3.12	Three-Dimensional Reconstruction for Stereo Viewing, Total Porosity = 0.263	118
Figure 3.13	Scanning Electron Photomicrograph of Micronized Particles of Pure Benzoic Acid Powder	125
Figure 4.1	Estimation of the Percolation Threshold of the Benzoic Acid/ Poly(vinyl stearate) Tablet Matrix	135
Figure 4.2	Residuals Plotted as a Function of Porosity for Transport Below the Percolation Threshold	138
Figure 4.3	Residuals Plotted as a Function of Porosity for Transport Near and Above the Percolation Threshold	140
Figure 4.4	Comparison of Experimental Results to Percolative Transport and Cluster Diffusion Model	143
Figure 4.5	Assessment of the Percolation Threshold Estimation Method	145
Figure 4.6	Scaling Relationship for the Calculated Profile	147
Figure 4.7	Cluster and Percolative Contributions to Bulk Diffusion	150
Figure 7.1	Schematic Diagram of the Pseudosteady-State Diffusion Problem for the Benzoic Acid/Poly(vinyl stearate) Matrix System.	180

LIST OF TABLES

Table	Title	Page
Table 1.1	Critical Percolation Exponents	19
Table 2.1	Previously Measured Physicochemical Properties of the Tablet Constituents	55
Table 2.2a	Parameters for Release Experiment 3	59
Table 2.2b	Parameters for Release Experiment 4	60
Table 2.3	Pycnometric Density Determination of the Tablet Constituents	65
Table 2.4	Sample Descriptions and Chamber Volumes for Transport Through Poly(vinyl stearate) Experiments	75
Table 2.5	Technical Pan Film Processing Conditions	82
Table 3.1	Volume Fraction Accessible Results From EXP 4 Plateau Values	91
Table 3.2	Summary of Total Accessible and Isolated Volume Fraction Data Obtained for The Benzoic Acid/Poly(vinyl stearate) Matrix	92
Table 3.3	Linear Regression Analysis of EXP 3 and EXP 4 Square Root of Time Release Profiles	96
Table 3.4	Summary of All Percolation Parameters Obtained From Experimental Results	97
Table 3.5	Isosmotic Solution Preparation	101
Table 3.6	Comparison of Benzoic Acid Release Rates into Osmotically Matched and Unmatched Buffer Solutions	101
Table 3.7	Reduced Viscosities for Poly(vinyl stearate)/Benzene Solutions at 25°C	103
Table 3.8	Permeability Results From Poly(vinyl stearate) Cast Films and Compressed Discs	111
Table 3.9	Comparison of Experimental Porosities to PC3D Calculated Values for the Microtomed Tablets	120
Table 4.1	Linear Regression Analysis For the Percolation Threshold Estimation of the Benzoic Acid/Poly(vinyl stearate) System	136
Table 4.2	Statistical Evaluation of the Nonclassical Percolative Transport Model Parameter Estimates	141

I. INTRODUCTION

Transport of material through porous media is a phenomenon studied in a variety of disciplines. For the pharmaceutical scientist, the transport characteristics of a drug entity diffusing through a noneroding porous delivery device dictate the extent and duration of delivery of the active ingredient. The ability to control the transport characteristics of a dosage form is therefore a crucial goal in determining product viability. An understanding of the transport mechanisms associated with the drug delivery provides the fundamental knowledge required to achieve this control.

In a noneroding, hydrophobic porous matrix, the physicochemical properties of the drug entity alone do not dictate transport; the morphology of the matrix plays a major role in defining the transport kinetics. Characterization of the morphology, a combination of topology and geometry of the pore space, is crucial to understanding transport through such systems. Network models, percolation theory being one, provide insight into the connection between morphology and transport.

A. The Research Objective

The objective of this research was to develop a quantitative transport model which described the release of a drug entity from a porous hydrophobic polymeric delivery device. The current research is an extension of an earlier preliminary study[1] and focuses on the correlation between morphology and transport. An understanding of the transport mechanisms and the morphology of the pore space was sought through the application of percolation theory, specifically in a realm which is designated as nonclassical in terms of percolation principles.

B. The Approach

The system studied contained benzoic acid as a classically "conducting" material and poly(vinyl stearate) as a classically "nonconducting" material (Figure 1.1). The terms "conducting" and "nonconducting" refer to the ability or inability of a material to contribute to transport or form conducting sites. For instance, in the benzoic acid/poly(vinyl stearate) system investigated in this research, a directly compressed tablet composed of the two excipients was placed in a dissolution vessel containing dissolution medium. The benzoic acid dissolved and diffused away from the tablet matrix to leave behind a tortuous porous structure through which other dissolved molecules of benzoic acid had to diffuse in order to reach the outer surface of the matrix. The benzoic acid and the pore space it produces comprise the conducting phase of the matrix.

Throughout the release kinetics experiments conducted, the poly(vinyl stearate) porous matrix remained intact and did not dissolve in the dissolution medium. It was initially assumed that the benzoic acid was not soluble in the poly(vinyl stearate); this assumption justifies the use of the term "nonconducting" to describe the polymer.

By evaluation of the matrix transport characteristics as a function of drug load, the percolative nature of the system can be deduced. The evaluation of pertinent percolation parameters provides information about the pore topology (the interconnectedness of the pore space) and geometry (the shape of the pore space). Through this approach, the connection between morphology and transport will be investigated.

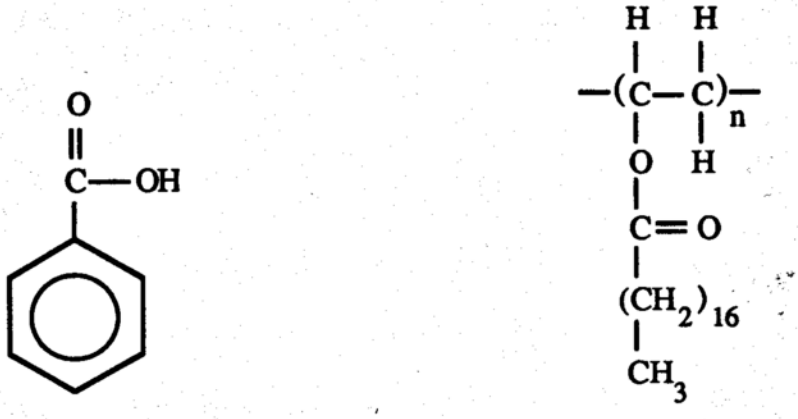


Figure 1.1 The Tablet Constituents: Benzoic Acid and Poly(vinyl stearate). (a) Structure of benzoic acid and (b) structure of poly(vinyl stearate).

C. Background

This Section will acquaint the reader with the concepts of percolation theory utilized in this research and present the initial model and data obtained from the earlier study.[1] The questions derived from the initial research will be discussed in the section entitled "The Proposed Solution," which will effectively outline the experimental efforts to be described henceforth. The Section will conclude with a discussion of the expected results and possible contributions of this research.

1. PERCOLATION THEORY

Percolation theory is a mathematical tool which provides a statistical description of the morphology and the associated transport properties of heterogeneous or porous materials by the use of simple scaling laws. The percolative transport characteristics of a porous system provide information about its internal morphology. One of the important advantages percolation theory offers is that it does not use adjustable parameters, such as tortuosity, to describe transport or morphology.

Percolation basically describes a phase transition; the phase transition is defined as the phenomenon associated with a qualitative change in a system occurring at a sharply defined parameter value. The parameter value of percolation theory is the percolation threshold, $\emptyset_c$, and the qualitative change involves the formation of a sample spanning cluster; both of these will be described below. Due to the phase transition characterization of percolation, the theory itself is derived for a system of infinite size. Only in such a system can a true phase transition occur. Therefore, in percolation theory there are some finite-size effects which must be considered. However, as the system size becomes large relative to what is known as the correlation length (a value proportional to the typical cluster diameter of the system), these finite-size effects become negligible and the system can be adequately

described with the classical theory. The aspect of finite-size scaling is described in a subsection of Section E of this Chapter.

Percolation processes can be described by two models: site percolation and bond percolation. In site percolation the tablet matrix (or lattice) is broken down into a random distribution of occupied and unoccupied sites. The occupied sites contribute to transport (pores) while the unoccupied sites do not contribute to transport (solid matrix material). Similarly, bond percolation deals with sites connected by bonds which can be occupied (open) or unoccupied (closed). The interconnectedness of these sites or bonds (cluster formation) as well as the volume fraction which are occupied dictate the transport characteristic of the matrix. Basically, bond and site percolation use the same scaling laws, but they use different critical exponents and lattices of identical coordination have different threshold values. The research described in this dissertation is described by site percolation.

Historically, the initial onset of percolation theory can be traced back to Flory's work of the 1940's dealing with the phase transitions produced in the gelation process of branched macromolecules.[2] The mathematical model derived by Flory in his research is today known as the Bethe lattice or Cayley tree. Flory, however, didn't use the term "percolation" to describe the mathematics of his model and actually the physicists of more recent times derived the names "Bethe lattice" and "Cayley tree". Therefore, the actual advent of percolation theory is attributed to two researchers, Broadbent and Hammersley,[3] who, in 1957, actually coined the term "percolation" and developed the mathematics associated with the theory. These two scientists were studying the critical phenomena associated with crystallization.

Since its onset, percolation theory has been used in such varied applications as galaxy formation,[4] the spreading of forest fires,[5] electrical conductivity,[6] reaction in porous catalysts,[7] and transport through porous polymeric matrices,[8] just to name a few. The

increased interest in percolation stems from the advent of computers and the increased interest in disordered systems. The increased performance of main-frame computers has enabled percolation scientists to evaluate the critical exponents of percolation theory, which will be discussed in detail later. Due to the extensive number of configurations that individual lattice sites are able to assume, the probability calculations for system sizes approaching "infinity" is very time consuming even on the fastest main-frame.

a) Percolation Morphological Parameters

Percolation parameters can be broken down into morphological and transport parameters. The transport characteristics of the matrix are described by the volume fraction effective, which is discussed in the next section. The morphological properties of the matrix include the percolation threshold, the coordination number of the lattice or matrix, the volume fraction conducting, the volume fraction accessible, the backbone volume fraction, the dead end clusters, and the isolated clusters. Morphological properties are defined as those which can be represented by the physical pore space of the system. Since the volume fraction effective is a transport coefficient, it cannot be described by the physical pore structure and is instead a property dictated by the morphology.

As discussed previously, the mathematics of percolation theory is based on probability and statistics. The percolative morphological properties involve clusters of randomly distributed conducting and nonconducting sites situated in a lattice as simulated in Figure 1.2. Percolation theory deals with the number and properties of these clusters. The probability that a site in a lattice is occupied, or conducting, is denoted as $\emptyset$ while the probability that a site is unoccupied, or nonconducting, is $(1 - \emptyset)$. The volume fraction conducting, $\emptyset$, is the porosity of the matrix.

Each lattice in percolation theory is described by how the sites are distributed within the lattice space. The number of nearest neighbors, or coordination number, a particular site has is defined as the maximum possible number of sites which are in direct contact with that site. Figure 1.2 is a square lattice and has a coordination, z, of 4. The simple cubic lattice, its three-dimensional counterpart, has a coordination of 6. Figure 1.3 shows a two-dimensional triangular lattice, z = 3, and a two-dimensional hexagonal, z = 6, lattice. These lattices can be constructed by tessellating the lattice space of the system. A tessellation is an aggregate of nonoverlapping polygons, polyhedra, or other analog of higher dimension, that completely fill an n-dimensional continuum.[9] Tessellations are mainly utilized in computer simulation studies.

More complicated lattice types are generated from random tessellations. A random tessellation is formed by constructing random polyhedra around randomly distributed points on a lattice. The coordination number in such a system is defined as the average number of faces a polyhedra could statistically have. In a three-dimensional model, the Voronoi tessellation, the coordination was determined to be an average value of 15.54 by Meijering.[10] The Voronoi tessellation was shown to be an irregular, highly connected structure with a consequently low threshold.[9]

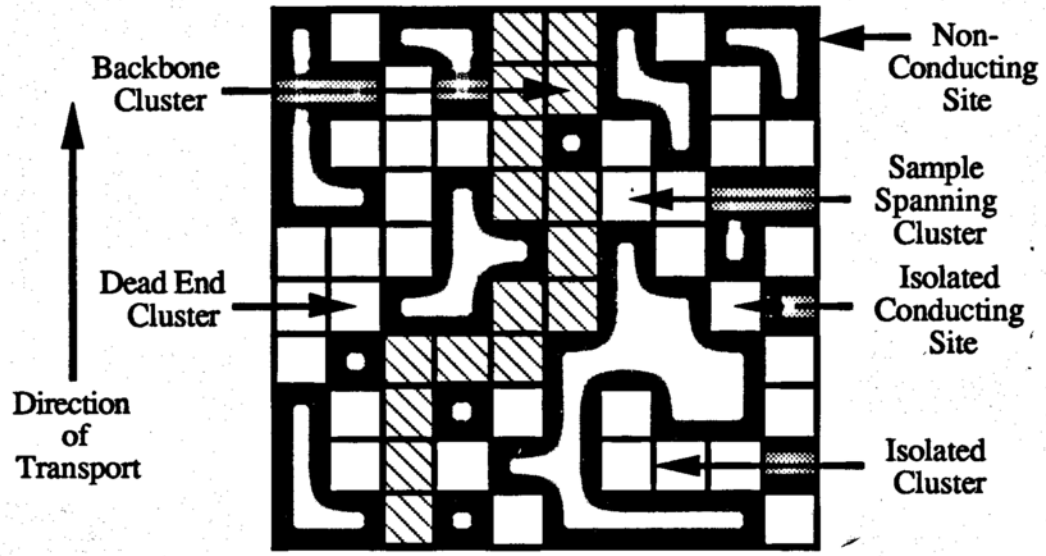
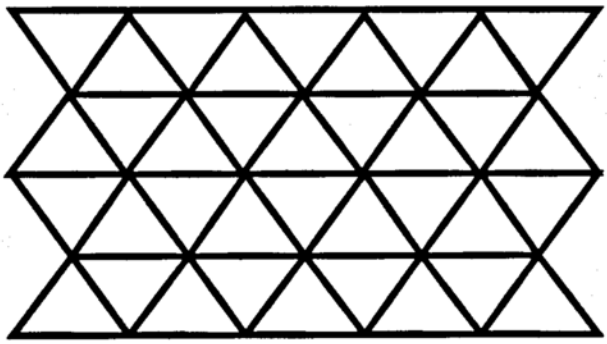
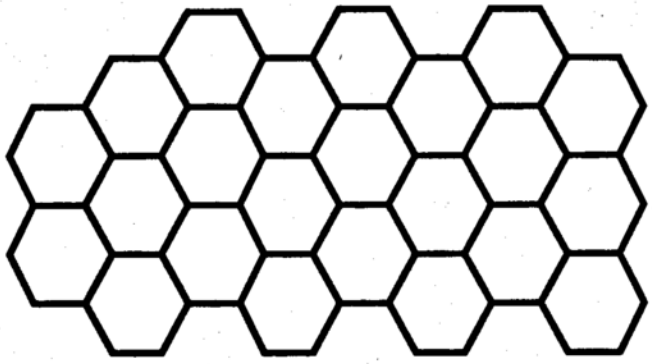


Figure 1.2 A Two-Dimensional Square Lattice. $\emptyset = 0.50$, $z = 4$. Conducting sites are white, nonconducting sites are black.



(a)



(b)

Figure 1.3 Examples of Coordination in Two Dimensions.
(a) Triangular lattice, z = 3; (b) hexagonal lattice, z = 6.

Clusters which span the entire width of a lattice in the direction of transport are known as sample spanning clusters (Figure 1.2). The concentration or volume fraction of conducting sites within a lattice, $\emptyset$, dictates whether or not a sample spanning cluster is capable of being formed. It is readily evident that a critical concentration exists, referred to as the critical percolation threshold ($\emptyset_c$), below which the sample spanning cluster doesn't exist and above which the sample spanning cluster does exist. As long as a sample spanning cluster exists in a matrix, transport can occur from one side of the matrix to the other. Therefore, at concentrations above the percolation threshold, transport is possible, whereas below the threshold, transport does not occur.

A relationship exists between the coordination number of a lattice and its percolation threshold. Figure 1.4 is produced from literature values[11,12] of various three-dimensional lattice percolation threshold and coordination values. The fitted relationship derived from these literature values is

$$\emptyset_c = \frac{1}{1 + 0.356 \cdot z}. \qquad (1.1)$$

The fitted parameter, 0.356, based on 11 literature values, had a standard error of 0.005.

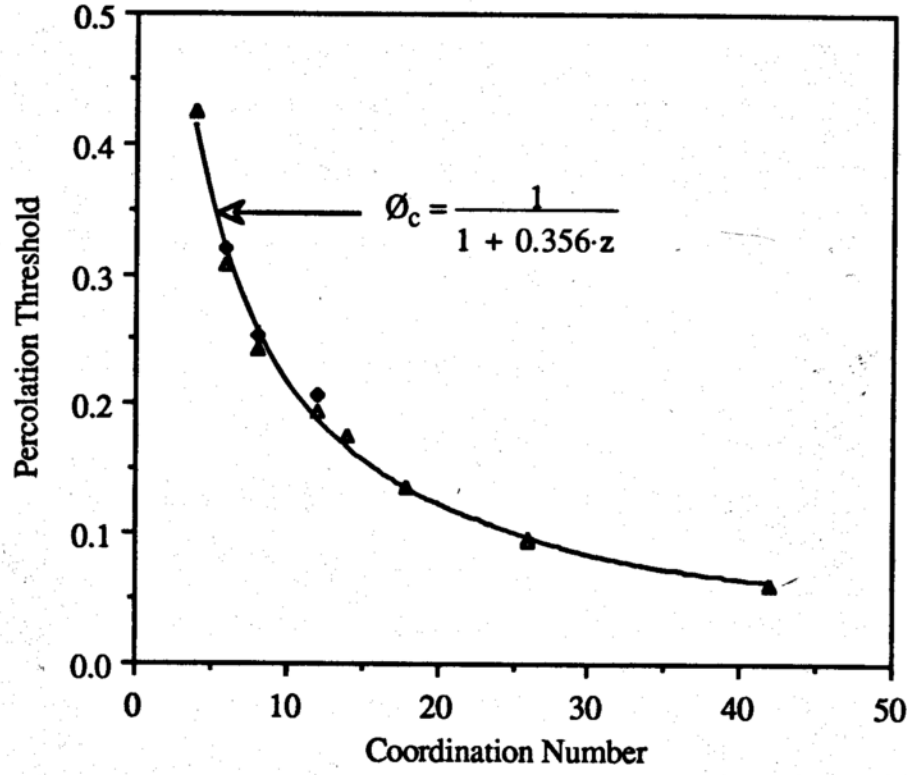


Figure 1.4 Percolation Threshold as a Function of Coordination Number for Three-Dimensional Lattices. Points are literature values: Open triangles,[11] closed diamonds.[12] Solid line is the fitted profile as labelled.

The volume fraction of conducting sites in the sample spanning cluster is referred to as the volume fraction accessible, $\emptyset^A$. The volume fraction accessible summarizes the topological characteristics of the pore structure. Since the sample spanning cluster does not exist below the percolation threshold, the volume fraction accessible is zero below the threshold. Below the percolation threshold all clusters of conducting material are isolated. The volume fraction of isolated conducting sites in the matrix is called the volume fraction isolated, $\emptyset^I$. Above and near the percolation threshold a fraction of the pore space contributes to the sample spanning cluster and the remainder of the pore space exists as isolated clusters.

As the concentration of conducting sites increases above the percolation threshold, the value of the accessible volume fraction increases due to the joining of dead end clusters and the coalescence of isolated clusters. The sum of the volume fraction accessible and the volume fraction of isolated material is the total volume fraction, or porosity, of the matrix,

$$\emptyset = \emptyset^A + \emptyset^I . \tag{1.2}$$

The volume fraction accessible can also be broken down into two components, the backbone volume fraction, $\emptyset^B$, and the dead end clusters, $\emptyset^D$,

$$\emptyset^A = \emptyset^B + \emptyset^D . \tag{1.3}$$

The backbone volume fraction is defined as the tortuous interconnected region of the sample spanning cluster through which transport is possible. The dead end clusters are extensions off the backbone which are so far removed from the transport path that they do not contribute to transport. Therefore, the dead end clusters, under steady-state conditions, act

similarly to the isolated clusters in that neither one contributes to transport in a classical percolating system. During nonsteady-state transport the dead end clusters would contribute to transport by entrapping solute.

b) Percolation Transport Parameters

The volume fraction effective, $\emptyset^E$, is the important transport parameter of a matrix. The volume fraction effective is defined as the effective transport coefficient of the matrix. Equation (1.4) shows the relationship between $\emptyset^E$ and D_B, the bulk diffusivity, and D_{Aq}, the aqueous diffusion coefficient,

$$\emptyset^E = \frac{D_B}{D_{Aq}}. \qquad (1.4)$$

The aqueous diffusion coefficient is defined as the diffusion coefficient of the solute in pure solvent. In the case of the benzoic acid/poly(vinyl stearate) system, D_{Aq} is the diffusion coefficient of benzoic acid in the dissolution medium. The bulk diffusivity reflects the transport through the pore structure. Therefore, the bulk diffusivity is always less than or equal to the value of D_{Aq} due to the tortuous nature of the pore space.

From Equation (1.4) it is easy to see the limits of the volume fraction effective. Since transport below the percolation threshold is not possible due to the absence of the sample spanning cluster, $\emptyset^E = 0$ below $\emptyset_c$. Therefore, the value of the bulk diffusivity must be zero below the threshold in order to satisfy this condition. Also, when $\emptyset = 1$, or the entire matrix is conducting, the volume fraction effective must equal one. Therefore, this stipulation dictates that the bulk diffusivity equals the aqueous diffusion coefficient when $\emptyset = 1$.

The volume fraction effective is strongly correlated to the accessible and the backbone volume fraction. The relationship between the morphological percolation parameters and the volume fraction effective is shown in Figure 1.5 for a three-dimensional cubic lattice taken from literature values.[13,14]

It has been proposed,[15] that the ratio of the effective volume fraction to the backbone volume fraction roughly approximates the tortuosity of the matrix. The tortuosity cannot be precisely described by this ratio because the complicated structure of the backbone also influences transport. In general,

$$\emptyset^E \leq \emptyset^B \leq \emptyset^A . \qquad (1.5)$$

The volume fraction accessible is always greater than the effective volume fraction due to the tortuous nature of the sample spanning cluster. Essentially, not all that is accessible to transport is totally effective to transport. The effective volume fraction, backbone volume fraction, and accessible volume fraction are all equal at two points of the percolation parameter profile, at the percolation threshold and when the volume fraction conducting equals one.

Basically,

$$\emptyset^E = \emptyset^B = \emptyset^A = 0, \qquad \emptyset < \emptyset_c \qquad (1.6)$$

$$\emptyset^E = \emptyset^B = \emptyset^A = 1, \qquad \emptyset = 1 . \qquad (1.7)$$

The backbone volume fraction becomes equal to the accessible volume fraction when the dead end clusters no longer exist. The concentration of dead end clusters rises rapidly above the percolation threshold as the tortuous nature of the matrix increases. As the

concentration of conducting material increases, the dead end cluster concentration decreases in almost an exponential manner. Essentially, as more and more conducting material fills the matrix, the sample spanning cluster becomes so extensive that the isolated clusters coalesce into the sample spanning cluster, the dead end clusters become part of the backbone cluster, which in turn becomes an increasing fraction of the accessible volume fraction. When the backbone volume fraction equals the accessible volume fraction, all material within the matrix is essentially accessible to transport and $\emptyset^A = \emptyset$. Therefore,

$$\emptyset^A = \emptyset^B = \emptyset, \qquad \emptyset^D = \emptyset^I = 0 . \tag{1.8}$$

The volume fraction isolated rises linearly as a function of porosity until it reaches a maximum at the percolation threshold. Above the threshold, the volume fraction isolated drops off as the accessible volume fraction increases due to the incorporation of isolated clusters into the sample spanning cluster. The porosity of the matrix becomes equal to the accessible volume fraction when all the isolated clusters have been taken up by the sample spanning cluster, as indicated in Equation (1.8). Below the threshold all conducting material exists in the form of isolated clusters and therefore,

$$\emptyset = \emptyset^I, \quad \emptyset < \emptyset_c . \tag{1.9}$$

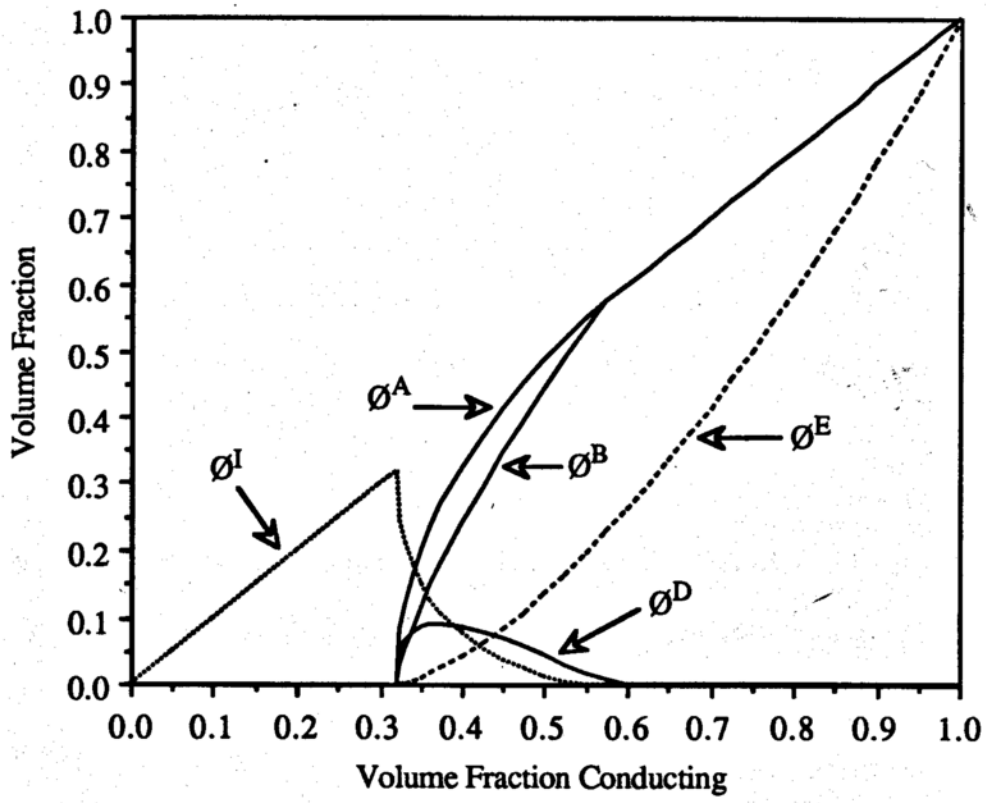


Figure 1.5 Percolation Parameters Of the Cubic Lattice as a Function of Volume Fraction Conducting. The volume fractions accessible, backbone, and dead end clusters are shown as solid lines; the isolated clusters and effective volume fraction are dashed lines.[13,14]

c) Scaling Laws of Percolation Theory Above the Percolation Threshold

Percolation parameters follow scaling laws which essentially relate the critical exponents of different parameters. The scaling laws of bulk percolation parameters take the form

$$\emptyset^i(\emptyset) \propto (\emptyset - \emptyset_c)^j, \qquad \emptyset \rightarrow \emptyset_c, \tag{1.10}$$

which states that the percolation parameter, $\emptyset^i$, as a function of $\emptyset$ near the percolation threshold, scales as the difference between the volume fraction conducting and the critical percolation threshold of the system raised to some exponent *j*. The exponent, *j*, is called the critical exponent of the parameter. The value $(\emptyset - \emptyset_c)$ is called the gap exponent.

The scaling relationships are derived from cluster properties and cluster exponents and therefore, the concepts of percolation clusters and scaling will be discussed in the next section. In general, this section will deal with the scaling relationships of the bulk percolative properties crucial to the understanding of this research; specifically the effective, accessible, and backbone volume fraction scaling laws.

As can be seen in Figure 1.5, the profiles for the accessible, effective and backbone volume fractions are smooth functions above the percolation threshold. From percolation theory, the scaling relationships for these three parameters take the following forms

$$\emptyset^E \propto (\emptyset - \emptyset_c)^\mu, \qquad \emptyset > \emptyset_c \tag{1.11}$$

$$\emptyset^A \propto (\emptyset - \emptyset_c)^\beta, \qquad \emptyset > \emptyset_c \tag{1.12}$$

$$\emptyset^B \propto (\emptyset - \emptyset_c)^{\gamma_b}, \qquad \emptyset > \emptyset_c \tag{1.13}$$

where μ, β, and γ_b are the critical exponents for conductivity ($\emptyset^E$), the strength of the infinite network ($\emptyset^A$), and the backbone volume fraction ($\emptyset^B$) respectively. These relationships are only valid near the percolation threshold, in what is known as the scaling region. Table 1.1 lists the most current values of various percolation exponents in two and three dimensions and for the special case of the Bethe lattice.[15,16,17]

Critical exponents of percolation theory are generally thought of as being independent of coordination and dependent only on dimensionality. In this respect, the critical exponents are thought to be "universal." In three dimensions, the values of μ, β, and γ_b have been reported to be 2.0,[16] 0.4,[16] and 0.9.[17] Therefore, the accessible and the backbone volume fractions approach zero with an infinite slope and the effective volume fraction approaches zero with a zero slope as the concentration of conducting material tends to the threshold from above.

The critical exponents themselves are derived from the "singular" or critical part of the percolation property. This refers to the leading nonanalytic term of the equation describing the property, and does not necessarily mean that the property goes to infinity. For instance, the critical exponent for the volume fraction accessible is derived from

$$\left[\emptyset^A\right]_{sing} = \left[\emptyset - \sum_s s \cdot n_s(\emptyset)\right]_{sing} \propto (\emptyset - \emptyset_c)^\beta, \qquad (1.14)$$

where s is the number of sites in a particular cluster and n_s is the average number (per lattice site) of s-clusters averaged over many different distributions of occupied sites within the lattice.

TABLE 1.1 CRITICAL PERCOLATION EXPONENTS‡

Critical Exponent	Percolation Parameter	Two-Dimensional Systems	Three-Dimensional Systems	Bethe Lattice
μ	$\emptyset^E$	1.3	2.0	3
γ_b	$\emptyset^B$	0.5 – 0.6	0.9	2
β	$\emptyset^A$	5/36	0.4	1
ν	ξ	4/3	0.9	1/2
σ	Cluster numbers; $\emptyset = \emptyset_c$	36/91	0.45	1/2
τ	Cluster numbers; $\emptyset = \emptyset_c$	187/91	2.2	5/2
$\zeta\ (\emptyset < \emptyset_c)$	Asymptotic exponential decay	1	3/2	5/2
$\zeta\ (\emptyset > \emptyset_c)$	of cluster numbers	1/2	2/3	1

‡Rational numbers are exact results, others are estimates.

Critical exponent values taken from references 15, 16, and 17.

Therefore, $s \cdot n_s$ is the probability that any lattice site belongs to a finite s-cluster. The summation is therefore the probability that a lattice site belongs to an isolated cluster or the volume fraction isolated. Therefore, $\emptyset - \emptyset^I$ is the accessible volume fraction. Other aspects of n_s will be addressed in the section on percolation clusters and scaling to follow.

Taking an example from Stauffer[18] to describe the singularity aspect more clearly: if a quantity φ varies as

$$\varphi = \varphi_o + \varphi_1(\emptyset - \emptyset_c) + \varphi_2(\emptyset - \emptyset_c)^{1.355} + \varphi_3(\emptyset - \emptyset_c)^{1.855} + \varphi_4(\emptyset - \emptyset_c)^2, \quad (1.15)$$

then the singular part, φ_{sing}, is given as

$$\varphi_{sing} = \varphi_2(\emptyset - \emptyset_c)^{1.355}, \quad (1.16)$$

and the "analytic background", $\varphi_{analytic}$, is given as

$$\varphi_{analytic} = \varphi_o + \varphi_1(\emptyset - \emptyset_c) + \varphi_4(\emptyset - \emptyset_c)^2, \quad (1.17)$$

and the "background to scaling", $\varphi_{background}$, is given as

$$\varphi_{background} = \varphi_3(\emptyset - \emptyset_c)^{1.855}. \quad (1.18)$$

Percolation theory, in the classical sense, deals with the singularities of these relationships.

A few of the exponents have been calculated exactly, but in general, the aim of scaling in percolation theory is to determine the inter-relationship of the critical exponents. In this manner, the values reported for specific exponents may change as better estimates are

determined. In general, the critical exponent values in two dimensions are better known than their three-dimensional counterparts.

Some percolation scientists have used their experimental data or computer simulations to obtain values of critical exponents by plotting the logarithm of the percolation parameter as a function of the logarithm of the gap exponent. The value of the critical exponent is obtained from the slope. For some percolation parameters, this is the only method currently available to estimate critical exponents. Generally a more precise estimate is not available due to a lack of the algorithm describing the parameter and/or the correlation of the exponent to other scaling exponents. The advent of faster main-frame computers will eventually allow percolation scientists to achieve better estimates of these "theoretical" exponents.

The difficulty in accurately determining critical exponent values has led many percolation scientists to use the Bethe lattice to estimate the percolative behavior of their real lattices. The advantage of using the Bethe lattice lies in the fact that values of $\emptyset_c$, $\emptyset^A$, $\emptyset^D$, $\emptyset^E$, and therefore $\emptyset^I$ and $\emptyset^B$, can be solved exactly for arbitrary values of $\emptyset$, z, the pore size distribution, and the local transport coefficient of the matrix. The Bethe lattice will be discussed in the last section of this percolation review.

d) Percolation Clusters and Scaling

As is quite evident by now, percolation clusters basically dictate the observed bulk behavior of a percolating system; therefore, cluster properties are crucial to the understanding of transport. The cluster properties themselves depend on cluster size.

Clusters of conducting material exist both below and above the percolation threshold. The behavior of clusters is different on each side of the threshold due to the exclusive nature of the sample spanning cluster. Stauffer[16,18] as well as other authors[19,20,21,22,23] have written extensively on clusters and diffusion on percolating clusters.

The general scaling relationship for cluster numbers (n_s) near the percolation threshold can be defined in terms of $n_s(\emptyset)$,

$$n_s(\emptyset) = s^{-\tau} f[(\emptyset - \emptyset_c)s^{\sigma}] \quad (\emptyset \to \emptyset_c, s \to \infty), \tag{1.19}$$

where τ and σ are critical exponents and s is the cluster size expressed as the number of occupied sites. This relationship implies that the actual scaling function for clusters near the threshold must be determined by numerical techniques and cannot be predicted a priori by percolation theory.

Cluster numbers away from the percolation threshold at a fixed porosity below and above the threshold behave as shown in Equation (1.20), where the value of ζ is different depending on whether the clusters are below or above the threshold as defined in Equation (1.21),

$$\log n_s \propto -s^{\zeta}, \quad s \to \infty, \emptyset \text{ fixed} \tag{1.20}$$

$$\zeta(\emptyset < \emptyset_c) = 1, \quad \zeta(\emptyset > \emptyset_c) = 1 - \frac{1}{d}, \tag{1.21}$$

where d is the dimensionality of the pore space. Note that both scaling relationships for cluster numbers are only valid for large s-clusters.

In the region where $\emptyset$ is close to $\emptyset_c$ but s is so large that the quantity $|\emptyset - \emptyset_c| \cdot s^{\sigma}$ of Equation (1.19) is much larger than one, both Equations (1.19) and (1.20) apply. Therefore, the function in Equation (1.19) can be evaluated by a percolation scientist working in this $\emptyset$ range.

In terms of scaling and clusters, the evaluation of critical exponents is made simpler since all cluster numbers scale with two known exponents, σ and τ. These two exponents, which were introduced in Equation (1.19), are descriptors of cluster numbers at $\emptyset = \emptyset_c$. τ is called the Fisher exponent,[24] and σ is a surface exponent. Everything in clusters depends on only these two critical exponents, and the scaling relationship of Equation (1.19) is a generalized version of the Fisher droplet model.[24] The Fisher droplet model was derived to model the cluster expansion of real gases and the gas-to-liquid transition.

Before leaving this discussion on clusters, it is interesting to look at the cluster numbers in terms of their k-th moment, M_k,

$$M_k = \sum_s s^k \cdot n_s \ . \tag{1.22}$$

The mean cluster size of a lattice is the second moment, the volume fraction accessible is the first moment, and the total number of clusters is the zeroth moment. This relationship can be written in terms of the gap exponent, τ, and σ,

$$M_k \propto |\emptyset - \emptyset_c|^{(\tau - 1 - k)/\sigma}, \tag{1.23}$$

which is a generalized scaling relationship and an example of how cluster distributions can be described with just two critical exponents. The scaling relationship for the volume fraction accessible therefore becomes

$$\emptyset^A \propto (\emptyset - \emptyset_c)^\beta \propto (\emptyset - \emptyset_c)^{(\tau - 2)/\sigma}, \tag{1.24}$$

and the relationship of β to τ and σ is simply

$$\beta = \frac{(\tau - 2)}{\sigma}. \tag{1.25}$$

Knowing the values of τ and σ in three dimensions to be 2.2 and 0.45 respectively, the value of β is calculated to be 0.4. Obviously, this is a powerful tool for determining critical exponents and this example identifies the power of scaling in percolation theory.

e) The Bethe Lattice

The Bethe lattice is the only lattice structure in percolation theory of dimensionality greater than one which provides exact solutions for percolation parameters. The Bethe lattice is defined by one coordination number and is totally void of closed loops (Figure 1.6). The combination of the absence of closed loops and the mono-coordinated lattice structure provide a mathematically simple system to evaluate analytically compared to the higher order tessellations. Despite its simplicity, however, similarities exist between the Bethe lattice and real lattices. A major asset of the Bethe lattice is that it does not require a large main frame computer to determine the critical percolation parameters; all the exact solutions for the lattice have been solved by Fisher and Essam[25] and Stinchcombe.[26] Many researchers have successfully used the Bethe lattice to model real percolating systems.[7,14,15,27,28,29,30]

The first step in transforming a real percolating lattice over to the realm of the Bethe lattice involves calculating the coordination in Bethe-space from

$$\emptyset_c = \frac{1}{(z-1)}, \tag{1.26}$$

where $\emptyset_c$ is the experimentally determined percolation threshold of the real percolating system and z is the calculated coordination of the Bethe lattice with that exact threshold value.

The accessible volume fraction relationships for the Bethe lattice are given by

$$\emptyset^A(\emptyset) = 0, \quad \emptyset < \emptyset_c \tag{1.27}$$

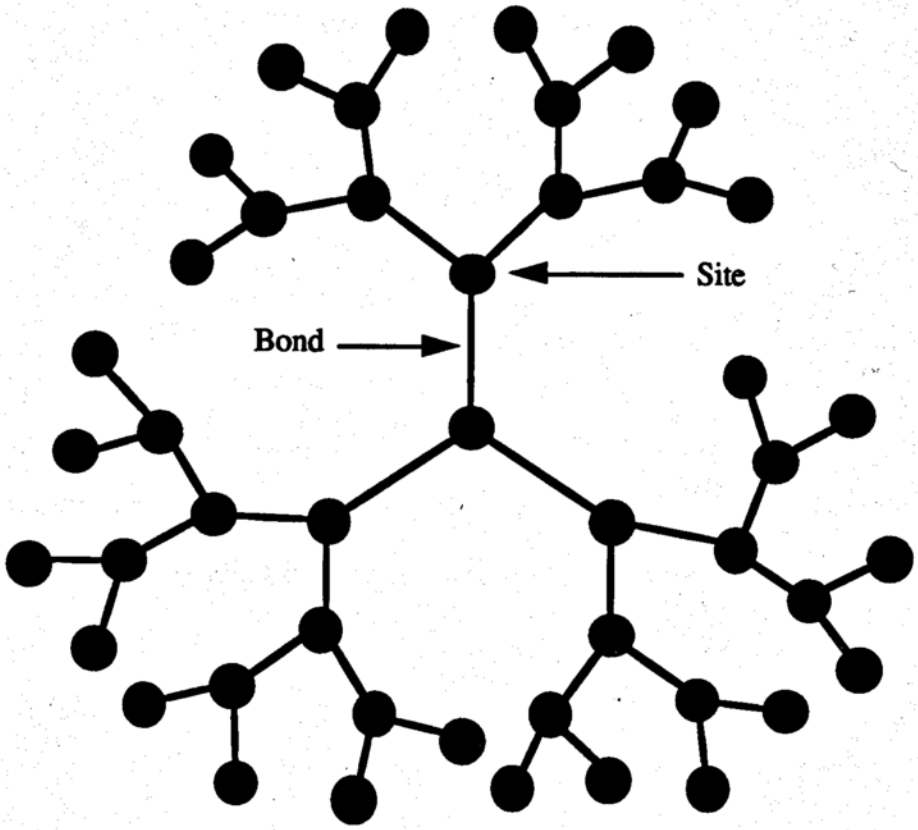


Figure 1.6 A Bethe Lattice of Coordination Three.

$$\emptyset^A(\emptyset) = \emptyset\cdot\left(1-\left[\emptyset^R/\emptyset\right]^{(2z-2)/(z-2)}\right), \qquad \emptyset \geq \emptyset_c \tag{1.28}$$

where $\emptyset^R$ is the root of

$$\emptyset^R\left(1-\emptyset^R\right)^{(z-2)} - \emptyset\cdot(1-\emptyset)^{(z-2)} = 0\,. \tag{1.29}$$

The dead end volume fraction is calculated[30] from

$$\emptyset^D(\emptyset) = 2\cdot\left[\emptyset^A - \emptyset + \sqrt{\emptyset\cdot\left(\emptyset-\emptyset^A\right)}\right]. \tag{1.30}$$

The calculation of the effective volume fraction is much more complex, and therefore, the interested reader is directed to the work of Stinchombe[26] and Reyes and Jensen.[7] In general, the relationship describing transport on a Bethe lattice is given as

$$\emptyset^E = -\left(\frac{z-1}{z-2}\right)\cdot\frac{C'(0)}{D_{Aq}}, \tag{1.31}$$

where D_{Aq} is the aqueous diffusion coefficient, as described earlier, and C' is a power series expansion accurate to order $(z-1)^{-4}$. Equation (1.32) gives the relationship for $C'(0)$,

$$C'(0) = -\langle L\rangle[\emptyset - \emptyset_c], \tag{1.32}$$

where $\langle L\rangle$ is a harmonic average of the local transport coefficient. This equation is an approximation in the sense that the harmonic average value is used to approximate the actual

value of L. The harmonic average, in turn, is described by

$$\langle L \rangle = \left\{ \int_0^\infty \frac{F(L)}{L} dL \right\}^{-1}, \tag{1.33}$$

where F(L) is defined by

$$F(L(r)) = f(r) \cdot \frac{dr}{dL(r)}, \tag{1.34}$$

where $f(r)$ is the normalized pore size distribution of the porous solid.

A simplified relationship for $\emptyset^E$ in the near-percolation range defined as $(\emptyset - \emptyset_c) < 1/z$ is given by

$$\emptyset^E = 1.522 \cdot \frac{(z-1)}{(z-2)^2} \cdot \frac{\langle L \rangle}{D_{Aq}} \cdot \left(\frac{\emptyset - \emptyset_c}{\emptyset_c} \right)^2. \tag{1.35}$$

Therefore, by using the above equations, values for the percolation parameters can be calculated and simulations of real higher order tessellations can be easily made by using the Bethe lattice model. The accessible and the dead end volume fractions as a function of $\emptyset$ can be calculated simply by knowing z, which is obtained from Equation (1.26). The calculation of the volume fraction effective is more complicated since, besides the coordination in Bethe-space, the pore size distribution, $f(r)$, and estimates of the local transport coefficients must be known.

Due to the fact that closed loops are absent in a Bethe lattice, there is one major difference between the Bethe lattice and higher order tessellations. As the total volume fraction of material within the lattice approaches the critical volume fraction, the sample spanning pathway of real tessellations becomes infinitely tortuous while that of the Bethe lattice becomes a constant. Therefore, the slope of the volume fraction accessible profile at the critical percolation threshold is finite in the Bethe lattice while it is infinite in a real system.

2. TRANSPORT IN POROUS MEDIA

a) Diffusion in Heterogeneous Materials

Diffusion in heterogeneous solids has been a topic of interest for many years prior to the existence of percolation theory. In the pharmaceutical literature of 1963, T. Higuchi derived a model describing the release of a soluble drug substance from a porous heterogeneous matrix.[31] Specifically, it is this work which will be the basis of the kinetic transport model described later in this section. More recent research endeavors involved the elimination of the pseudosteady-state approximation originally invoked by T. Higuchi[31,32] and the subsequent derivation of the nonsteady-state solution based on empirical parameters[33] or approximate analytical solutions.[34] In many instances, the modeling of diffusional release through porous systems has been based on empirical relationships or adjustable parameters such as tortuosity factors.[11,31,35,36,37] Some investigators have attempted to define pore structure by utilizing adjusted porosity values[38] and diffusion-controlled or dissolution-controlled regimes[39] to model the release of water-soluble drugs from porous hydrophobic polymeric delivery systems. Statistical Monte Carlo approaches have also been utilized[40] to simulate two-dimensional pore structures and the diffusion through constricted pores. Microstructural models have been derived to describe diffusive transport in porous polymers.[41]

The major obstacle encountered by all the investigators describing diffusion in heterogeneous materials has been the description of the topology and the geometry of the extracted matrix. Heterogeneous porous materials are characteristically composed of tortuous pore structures and channels which are unique to individual materials and processing techniques. Transport within porous materials has therefore almost exclusively been empirically modeled in the previous literature. This aspect is discussed in the first chapter of a recent text on the controlled release of drugs.[42] In this chapter, Siegel describes the

modeling of drug release from porous polymers in an overview format, citing percolation theory as a viable option in describing transport.

b) Percolation and Transport

Transport in porous media has also been addressed recently by many percolation scientists. Diffusion on percolating clusters near the percolation threshold has been described by Straley.[43] In this research, the author obtained singularities of the diffusion constant and related the critical exponent to percolation conduction problem exponents. Mitescu[19] and Stanley and Coniglio[21] have each written chapters in a text on percolation structures and processes. Mitescu concentrated on diffusion on percolation clusters while Stanley and Coniglio discussed the fractal structure of the sample spanning cluster. Havlin, Ben-Avraham, and Sompolinsky[22] discuss the scaling behavior of diffusion on percolating clusters and describe their Monte Carlo method utilized in obtaining values of the critical exponent for conductivity in two and three dimensions. These three authors describe diffusion both above and below the percolation threshold and define a single scaling relationship which contains a crossover time signalling the change from one regime to the other. Stauffer, Wilke, Gefen, Ilkovic, and Aharony[23] describe diffusion on random clusters below the critical percolation threshold and label this a parasite problem.

Unfortunately, many of the earliest percolation studies described above were obtained by computer simulation techniques. In many instances the data obtained from computer simulations do not satisfactorily describe real systems. Instead of performing percolation computer simulations, many researchers have more recently utilized percolation theory as a model to describe their real experimental systems, as described below.

Percolation experiments in two dimensions have been performed by Mehr, Grossman, Kristianpoller, and Gefen.[44] Two researchers, Smith and Stermer,[45] have used

percolation theory to characterize random microsphere packing data obtained by mercury porosimetry. Three-dimensional conductivity experiments on a conductor-insulator composite have been modeled with percolation theory.[46] In terms of fluid mechanics, three-dimensional pore entrance and exit behavior of osmosis has been attempted with percolation models.[47] An interesting series of three articles by Yanuka describes percolation processes and porous media by first describing a morphological model,[48] obtaining percolation probabilities and cluster formation by computer simulations,[49] and finally predicting capillary hysteresis[50] based on the first two findings. Photoconductivity has been explored in terms of the aspects of percolation theory by Domes, Leyrer, Haarer, and Blumen.[51] In engineering, numerous researchers have successfully utilized percolation theory to model such situations as char oxidation and fragmentation,[14,27,28,52] reactivity and transport in disordered composite media,[15] and the estimation of effective transport coefficients in porous solids.[7] Much of this last set of sited work was based on the Bethe lattice approximation and has been done almost exclusively at the University of Minnesota Department of Chemical Engineering and Materials Science.

3. Combining Percolation Theory and Diffusion in Heterogeneous Materials

As discussed in the first paragraph of this Section, the kinetic transport model utilized in this research is derived from T. Higuchi's early work on diffusion in heterogeneous materials.[31] A brief overview of Higuchi's model and the percolation version derived for this research will be presented here.

In the original work by Higuchi,[31] a pseudosteady-state solution was described for the release of a solid water-soluble drug from a solid matrix. The drug and matrix material were assumed to be randomly dispersed in one another. Higuchi's model results in

$$Q = \sqrt{D_e(2A - \emptyset C_s) C_s t}, \tag{1.36}$$

where Q is the amount of drug released per unit of exposed surface area, D_e is the effective diffusion coefficient, A is the drug load in units of mass per unit volume, Ø is the porosity of the matrix, C_s is the drug solubility, and t is time.

Higuchi defined the effective diffusion coefficient as

$$D_e = \frac{D_{Aq} \cdot \emptyset}{\tau}, \tag{1.37}$$

where D_{Aq} is the aqueous diffusion coefficient, Ø is again the porosity, and τ is the tortuosity of the matrix. In general, it was felt that the tortuosity of a capillary was approximately 3.

Today, it is generally accepted that tortuosity is an empirical correction factor that is obtained from curve fitting and that has no physical meaning. The "effective" diffusion coefficient of Higuchi (Equation (1.37)) is really a steady-state bulk diffusion coefficient.[42] Siegel[42] has redefined the effective diffusion coefficient in terms of diffusion in a pore, as

$$D_e = \frac{D_{Aq}}{\tau^2}, \tag{1.38}$$

based on the observation that tortuosity is defined as the mechanism of diffusion retardation and that porosity has no intrinsic bearing on mobility especially in the nonsteady-state regime.

From the above discussion, it is obvious that a more satisfactory description of the effective diffusion coefficient is required before the relationship between pore structure and release rates in porous systems is understood. Percolation theory can be used to

quantitatively describe and predict transport properties in porous polymeric materials as a function of porosity by using the simple scaling laws of percolation theory previously discussed.

Modification of T. Higuchi's original relationship begins with the flux equation

$$J_B = \frac{dM_t}{Sdt} = \frac{dQ}{dt} = -D_B \frac{dC}{dx}, \tag{1.39}$$

where J_B is the steady-state flux through a unit surface area of the bulk material, C is the concentration of the solute in the water-filled pores, M_t is the amount of drug released at time t, S is the surface area of release, D_B is the bulk diffusion coefficient of the solute through the bulk porous material at steady-state, x is distance, and Q is as defined previously. The solution of this equation in terms of percolation parameters is given in Equation (1.40). The derivation of this result is similar to that provided by T. Higuchi and will therefore not be restated here, but appears in Appendix A for the interested reader.

$$Q = \sqrt{D_B C_s \left(2\emptyset_d^A \rho - \left(\emptyset_d^A + \varepsilon\right) C_s\right) t} \tag{1.40}$$

$\emptyset_d^A$ is the accessible volume fraction of the drug, ρ is the solid state density of the drug, and ε is the inherent porosity of the matrix.

As is readily evident, Q is still a function of the square root of time as in Higuchi's original equation. Therefore, a plot of the amount released versus square root of time will be linear with the slope equal to

$$Slope = S\sqrt{D_B C_s \left(2\emptyset_d^A \rho - \left(\emptyset_d^A + \varepsilon\right) C_s\right)}. \tag{1.41}$$

Therefore, from experimentally determined values of C_s, ρ, ϵ, S, and $\emptyset_d^A$, values of the bulk diffusion coefficient, D_B, can be obtained at various porosities. From the values of D_B and the experimentally determined value of D_{Aq}, the volume fraction effective, the percolation threshold, and lattice coordination can be evaluated based on the previously discussed scaling laws of percolation theory.

D. Percolative Transport Results Above the Percolation Threshold

A series of experiments was performed in a region determined to be above the percolation threshold of the benzoic acid/poly(vinyl stearate) system.[8] The details of the kinetics experiments are discussed in Chapter II. Square root of time release profiles were generated at different drug loads and a sample of these profiles is shown in Figure 1.7. The bulk diffusion coefficient data were obtained from the slope using Equation (1.41) and the volume fraction effective data were obtained from Equation (1.4). The volume fraction accessible data were calculated from the plateau values of the square root of time plots for those experiments which were allowed to run to complete extraction.

The resulting volume fraction accessible and volume fraction effective percolation profiles are shown in Figures 1.8 and 1.9 respectively. From the volume fraction accessible profile in Figure 1.8 it is difficult to determine the percolation threshold of the system. The coordination, based on the literature profiles, appears to be greater than or equal to 12. The accessible volume fraction does appear to follow the percolation trends; however, the results are insufficient for characterization of the system.

The volume fraction effective percolation profile in Figure 1.9 also appears to follow the percolation trends. The coordination of the benzoic acid/poly(vinyl stearate) system, based on the effective results, appears to be greater than the Voronoi tessellation ($z = 15.54$), which indicates a very complex structure.

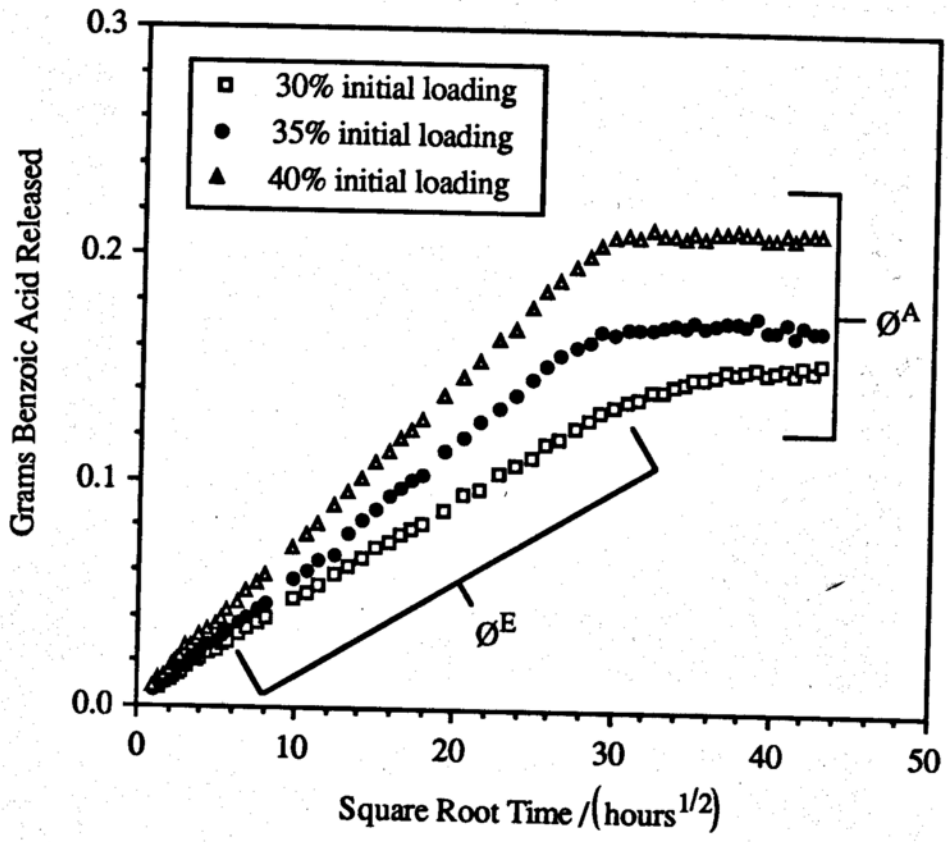


Figure 1.7 Square Root Of Time Release Profiles From Initial Kinetics Experiments. Legend indicates tablet composition in terms of weight percentage benzoic acid. Volume fraction effective data are calculated from slopes and volume fraction accessible data are calculated from plateaus as shown.

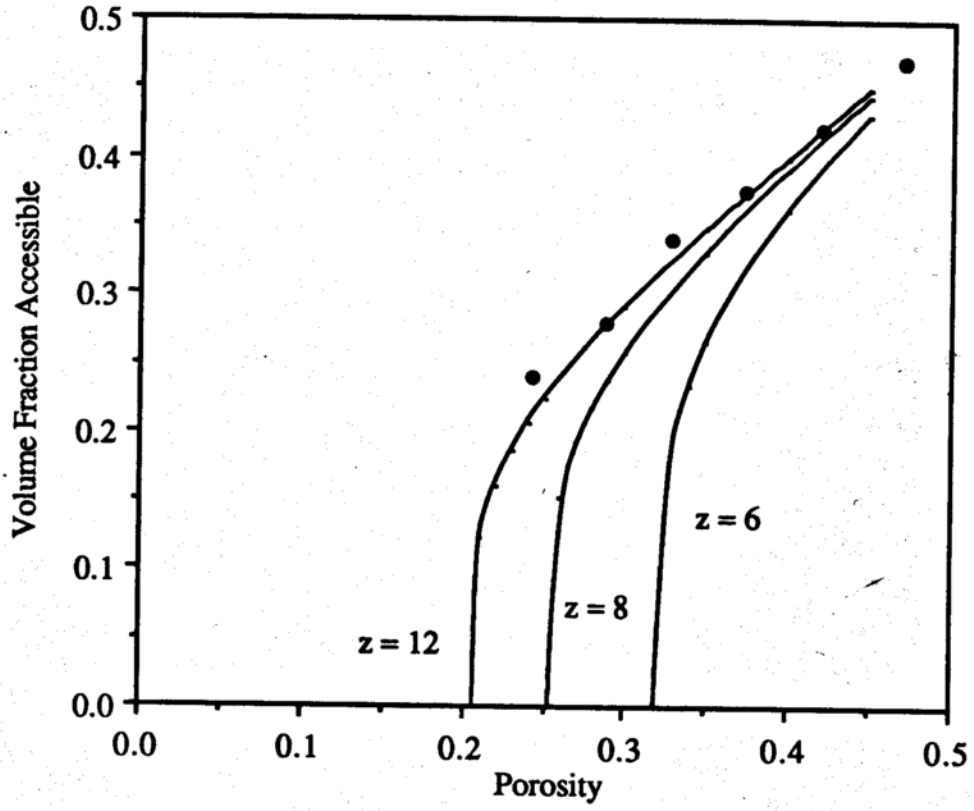


Figure 1.8 Initial Volume Fraction Accessible Results Above the Percolation Threshold. The closed circles are experimental values, the solid lines are literature profiles for the simple cubic (z = 6) lattice, body-centered cubic (z = 8), and the face-centered cubic (z = 12).[12]

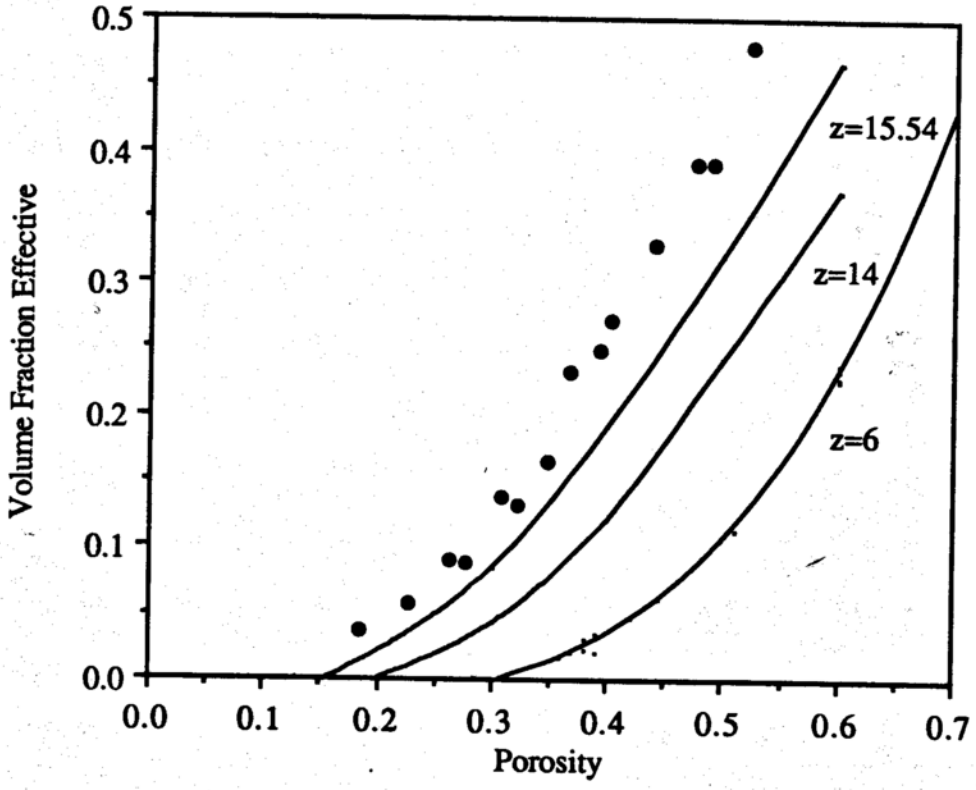


Figure 1.9 Initial Volume Fraction Effective Results Above the Percolation Threshold. The closed circles are experimental results, the lines are literature values; the Voronoi (z = 15.54) and tetrakaidecahedral (z = 14) tessellations,[9] and the simple cubic (z = 6) lattice.[13]

The volume fraction effective profile can be described by the percolation scaling law for conductivity stated in Equation (1.11). By fitting the 14 sets of volume fraction effective as a function of porosity data to the scaling law,

$$\emptyset^E = 2.3 \cdot (\emptyset - 0.07)^{2.0}, \tag{1.42}$$

where the pre-exponential constant was determined to be 2.3 ± 0.1 and the classical percolation threshold was determined to be 0.07 ± 0.01 at 95% confidence. The critical exponent, μ, was not fit and its value was taken as 2.0. Figure 1.10 is a plot of the experimental volume fraction effective results compared to the calculated profile.

The coordination of the benzoic acid/poly(vinyl stearate) system can be calculated from the inter-relationship of the percolation threshold and the coordination as was shown in Figure 1.4 and described by Equation (1.1). By using Equation (1.1) and the percolation threshold value of 0.07, the coordination of the benzoic acid/poly(vinyl stearate) system was determined to be 37.

The results of this section present some very interesting questions about the benzoic acid/poly(vinyl stearate) system. First, why is the threshold so low and therefore the coordination so high? There are very few systems in the literature with thresholds below that of the Voronoi tessellation. Is the internal microstructure of the benzoic acid/poly(vinyl stearate) system so complex that it warrants such a high coordination? Second, why does all the benzoic acid appear to be accessible in the volume fraction accessible profile? As the porosity approaches the percolation threshold from above, the volume fraction accessible is

no longer equal to the porosity of the system. In the benzoic acid/poly(vinyl stearate) system, all results obtained to date indicate that all the benzoic acid is available for transport even when concentrations tend to the threshold from above. The following Section will address these questions and provide some possible solutions.

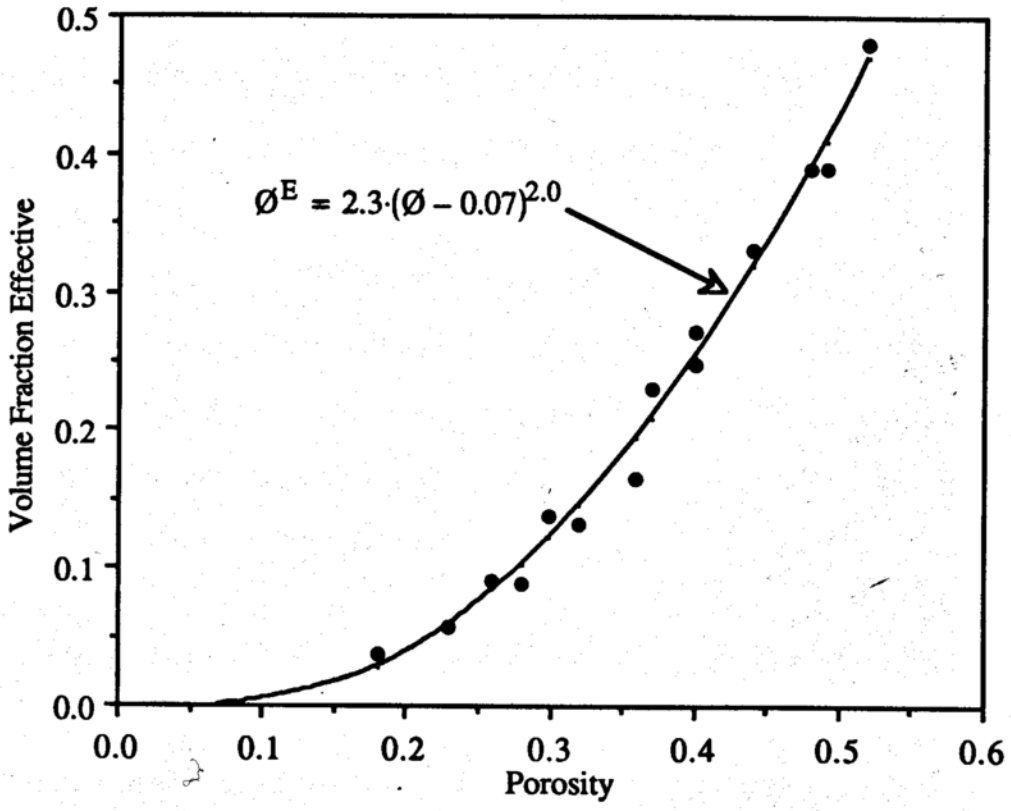


Figure 1.10 Initial Experimental Volume Fraction Effective Results Compared to the Calculated Percolation Profile Above the Percolation Threshold. Closed circles are experimental values, the solid line is the fitted percolation profile as indicated.

E. The Proposed Solution

This Section will address some of the concerns and questions brought up in the last Section; specifically the aspects of the percolation threshold and the coordination of the benzoic acid/poly(vinyl stearate) matrix.

1. Transport Near and Below the Percolation Threshold

In order to fully characterize the transport characteristics of the benzoic acid/poly(vinyl stearate) system, a full volume fraction effective profile is required. Experiments will be conducted near and below the threshold value of 0.07 in an attempt to acquire more volume fraction accessible and effective data and to better determine the coordination and threshold. The experimental results presented in the previous Section will therefore be combined with those obtained from the current research ventures in an attempt to fully characterize the system in terms of percolative transport.

2. Nonclassical and Nonuniversal Percolative Transport Systems

If the percolation threshold of 0.07 is real, why is it so low? In order to answer this question, the benzoic acid/poly(vinyl stearate) system will be analyzed in terms of nonclassical or anomalous percolative transport. The nonclassical nature of the system is defined as the inability to scale percolation parameters with classical percolation scaling laws. Some possible explanations for nonclassical behavior in percolating systems are given on the following pages. The brunt of the experimental analysis forthcoming involves the evaluation of the benzoic acid/poly(vinyl stearate) system in terms of these nonclassical models.

a) Changing Microstructure

Classical percolation theory assumes that the coordination of a lattice is a fixed or averaged constant dependent only on the connectivity or arrangement in space of conducting and nonconducting sites and is independent of the initial porosity or volume fraction conducting of the matrix. A system which has the ability to change its coordination as a function of time or volume fraction conducting also changes its microstructure and is therefore an example of a nonclassical percolating system. The transition of nonconducting sites to conducting sites within such a matrix would result in enhanced transport and conduction below the classical percolation threshold of the system. Since increasing coordination results in an increasing number of conducting pathways accessible to transport, the percolation threshold for such a system would be a variable instead of the classical constant.

b) Biphasic Conductivity and Nonclassical Behavior

Classical percolating systems are composed of two phases, one conducting and one nonconducting. Transport through such systems occurs only along the conducting pathways, that is along the sample spanning clusters. If conducting material is surrounded entirely by nonconducting material then it is called isolated. Isolated conducting material will never be available for transport and will remain in the lattice for an indefinite amount of time. In classical percolation theory the conducting phase or solute is not soluble in and does not have the ability to traverse sections of nonconducting material by any means other than the sample spanning cluster. A system which does not abide by these rules of percolation theory is called nonclassical since it will not adhere to the classical scaling laws.

In the percolation literature, there are reports of systems which exhibit this type of behavior.[53,54] Transport in such systems is called "termite" diffusion. Termite diffusion is described as the situation where a diffusing substance (the termite) has the ability to "gnaw"

its way slowly through a classically nonconducting phase until it reaches conducting material, it then rapidly traverses the classically conducting phase until it reaches the nonconducting phase again, then slowly continues on through the nonconducting phase. In this manner, the termite diffuses through the matrix and has the ability to jump from isolated clusters to sample spanning clusters or between separate branches of the sample spanning cluster or even between individual isolated clusters.

Systems characterized by this diffusion process in the percolation literature are superconductors which exhibit classical percolative transport above the percolation threshold, and nonclassical termite diffusion below the percolation threshold. In a polymeric system, the nature of the polymer (percent crystallinity, molecular weight, melting point, etc.) will dictate whether the solute in the system will act like a termite.

c) Complex Microstructure and Nonuniversal Behavior

There are reports in the literature of systems having lower percolation thresholds than the Voronoi tessellation. Aerogels[55] and aluminum oxide fleece[56] are both reported to have thresholds around 3%. The very low threshold value observed for these two systems has been attributed to complex microstructure and specifically microscopic ordering. A bias in one direction of transport is a case of a nonuniversal percolating system. Nonuniversal behavior is classified as scaling dependent on different or variable values of the "universal" exponent than stated in classical percolation theory. Classical percolation theory deals with randomly dispersed phases. If the microstructure of a percolating system is nonrandom or biased, scaling is expected to be nonuniversal.

The percolation literature addresses the aspect of biased percolative transport. A recent publication by Stauffer, et al.[57] discusses the subject of "bootstrap" percolation. This type of percolation involves taking an originally random system and making it biased by

permanently emptying occupied lattice sites in an iterative manner. The diffusion of particles with attractive interactions has also been addressed in the percolation literature.[58] In this research, the authors derived a model which takes into account the short-range attractive interactions between diffusing particles. Two physicists have studied, by Monte Carlo methods, percolation in anisotropic systems near the percolation threshold.[59] In their research, the physicists found that they could model their system by using the gap exponent of scaling theory, but the "universal" exponent they raised the gap exponent to did not coincide with classical values.

d) System Size

(i) FINITE-SIZE SCALING:

As discussed in the Section on Percolation Theory, the theory is derived for infinite systems. If a finite system is large enough such that its dimension in the direction of transport greatly exceeds the correlation length, the system acts like an infinite percolating system. The correlation length in the percolating system is associated with the average cluster size. As the correlation length approaches the system size a rounding of the percolation profile occurs because a finite fraction of clusters remain conducting over all porosities.

In percolation theory, the correlation length is the important underlying foundation of scaling theory. All critical behavior in a percolating system is dominated by one, and only one, length, ξ. The scaling law for the correlation length is

$$\xi \propto |\emptyset - \emptyset_d|^{-\nu}, \tag{1.43}$$

where ξ is the correlation length and ν is the critical exponent for the divergence of the

correlation length at the critical percolation threshold. The value of ν in three dimensions is approximately 0.9.

The aspect of finite-size scaling is an important issue in the application of percolation theory to real systems. Discussions offered by the percolation scientists Mitescu, Allain, Guyon, and Clerc,[60] Jerauld, Scriven, and Davis,[61] Stauffer,[16] and Efros[62] indicate that when a real system approaches the percolation threshold, the correlation length approaches the system length. It is this region where deviation will be observed.

The deviation of the effective percolation threshold of the finite system from the actual percolation threshold of the infinite system is described by

$$\emptyset_{eff} - \emptyset_c \propto L^{-1/\nu}, \tag{1.44}$$

where $\emptyset_{eff}$ is the effective percolation threshold, L is the system size (length), and ν is the correlation length exponent.

In the work done by Mitescu, Allain, Guyon, and Clerc,[60] a square lattice was investigated in terms of finite-size scaling of the volume fraction effective profile. The two-dimensional bond percolating system showed no appreciable deviation from the predicted percolation threshold above a finite system size of 50×50 sites.

In the benzoic acid/poly(vinyl stearate) system studied here, the system size is on the order of 500 particles in the direction of transport. This number is calculated based on the average particle diameter of both materials and the average tablet thickness. Based on this calculation and the observations of Mitescu, et al.,[60] it will be assumed that the nonclassical/nonuniversal nature of the benzoic acid/poly(vinyl stearate) system is not due to finite-size effects. The experimental system size is large enough in terms of the number of sites such that the finite-size contributions to transport are negligible.

(ii) RENORMALIZATION GROUP:

The method of renormalization group is discussed here in the context of finite-size scaling to demonstrate how some percolation scientists approach the problem of finite-sized systems. It is not a method which will be explored in this research due to the difficulty involved with performing this technique on an actual physical system.

Besides finite-size scaling, renormalization group, a computer simulation method, can be used to obtain information about critical percolation exponents near the critical percolation threshold. The basis of the renormalization group method is the examination of physical quantities near their critical point on different length scales. The method was first introduced in 1971 by K. Wilson[63] and later, in 1981, he was awarded the Nobel prize in Physics for his work on renormalization group. Wilson's first application of renormalization group dealt with thermodynamic phase transitions, but it is easily applied to percolation theory. Renormalization group is generally used in conjunction with Monte Carlo methods and is sometimes called position space renormalization or real space renormalization.

Basically the method involves partitioning the lattice into cells which cover the lattice but still maintain the original symmetry of the lattice. Figure 1.11 is a representation of a scale transformation on a body-centered cubic lattice by using this partitioning method. As can be seen in the Figure, the unit cell containing eight sites, one on each corner, is collapsed into one "super site" which is a site representing the contributions of all eight sites.

The partitioning is performed in a sequential manner such that a series of lattices are constructed from the original lattice but at various length scales. All new renormalized lattices have length scales that vary from the previous lattice by a factor b, where b is the linear dimension of the cell. These partitioned cells are examined to determine $p^*(b)$, the probability that the system of length scale b, percolates. $p^*(b)$ therefore corresponds to the percolation threshold of the renormalized lattice.

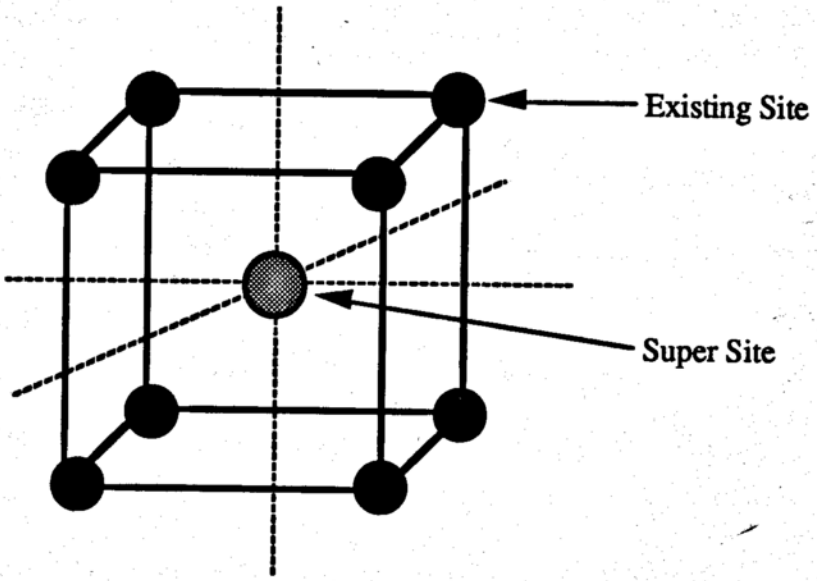


Figure 1.11 Renormalization Group Scale Transformation of a Body-Centered Cubic Lattice.

From the series of data collected, a plot of $b^{-1/\nu}$ versus $p^*(b)$ can be linearly extrapolated to the abscissa. The extrapolated value is the percolation threshold of the infinite lattice. Equation (1.45) is the relationship used in this linear extrapolation.

$$p^*(b) - \emptyset_c(b = \infty) \propto b^{-1/\nu} \tag{1.45}$$

where ν is the critical exponent of the correlation length. The similarity of this equation to Equation (1.44) is not accidental since the methodology of renormalization group and finite-size scaling are more or less equivalent in position space renormalization. A simulated profile is shown in Figure 1.12.

Once the relationship between $b^{-1/\nu}$ and $p^*(b)$ is established, it is trivial to determine the percolation threshold for the system of linear dimension equal to the size of the benzoic acid/poly(vinyl stearate) tablet analyzed.

Most of the research involving renormalization group is performed by computer simulation in an attempt to evaluate critical exponents.[64,65,66,67,68,69] Other applications of renormalization group involve the confirmation or denial of universality of the critical exponents,[70] which is an extremely controversial issue.

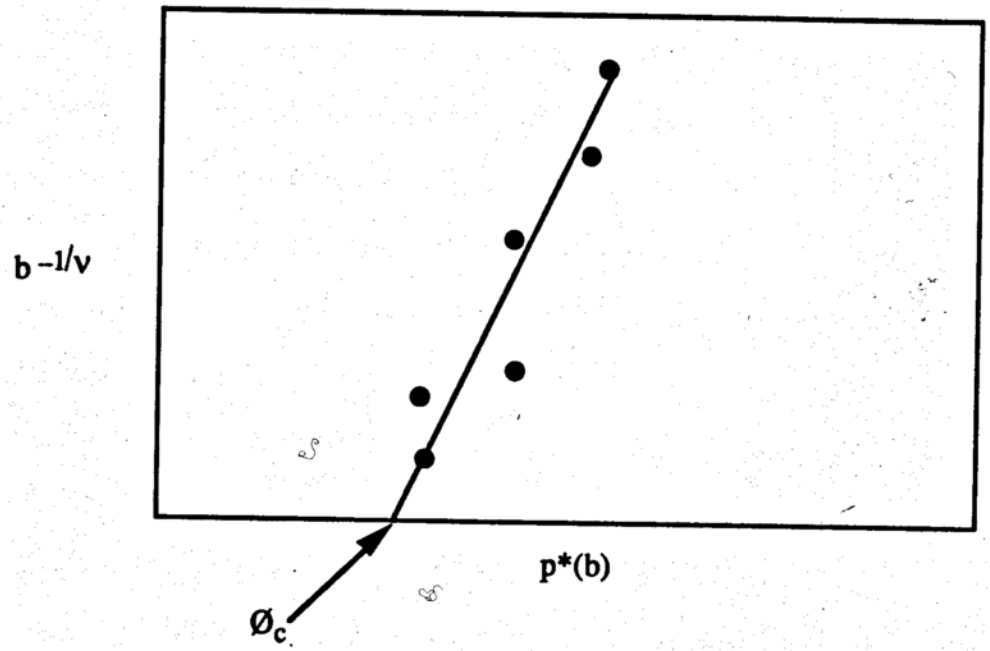


Figure 1.12 Simulated Profile of a Percolative Renormalization Group Analysis. Points represent individual scaled images, line represents the linear regression analysis. The percolation threshold of the infinite network is extrapolated from the abscissa.

F. Expected Results and Contributions

From the investigational study of the nonclassical and/or nonuniversal nature of the benzoic acid/poly(vinyl stearate) system and the determination of the effective volume fraction profile and the extension of the accessible volume fraction profile, it is the hope of this research to obtain a model which will adequately predict release rates for the system studied and answer the perplexing questions concerning threshold, coordination, and accessibility of the conducting pore space of the benzoic acid/poly(vinyl stearate) system. The model will be developed based on the principles of percolation theory and the physical and chemical properties of the two tablet components. The nonclassical nature of the system will be explained in terms of transport mechanisms which will ultimately allow the model to be based on percolation scaling laws.

The contributions of such a model will hopefully lie in its applicability to other systems. Though this research does not make any attempt to characterize other percolating polymeric systems, this logical extension may be addressed in the future.

In the field of percolation theory, as was extensively discussed, many researchers utilize computer simulations to characterize their percolating systems. The research offered here was not performed on a computer and involved a real system. The success achieved in the application of a theory to a real system determines whether or not the theory will be utilized to its potential. The contribution of this research to percolation theory lies in the fact that this real system can be characterized in terms of the concepts of classical percolation theory even though its behavior may be nonclassical or nonuniversal.

The importance of this research to the pharmaceutical field is readily evident when considering sustained or controlled release delivery devices. Percolation theory combined with simple transport equations allows the pharmaceutical scientist to predict the release characteristics and duration of release of the designed dosage form. Simultaneously, the

pharmaceutical scientist gains insight into the pore space of the matrix system from the establishment of the percolation parameters.

Manufacturing processes in the pharmaceutical industry contribute to the structure of the pore space of the dosage form. Percolation theory indicates that processing in the region close to the percolation threshold of the system may cause drastic changes in the release characteristics of the product. The percolation threshold, in the classical sense, establishes the dividing line between release and retention of the drug entity.

An extremely valuable percolation parameter to the pharmaceutical scientist is that of the accessible volume fraction. This quantity classically indicates the amount of drug which can be released from a dosage form. The counterpart of the accessible volume fraction, the isolated volume fraction, indicates how much of the drug will remain in the dosage form and is thus unavailable for transport and metabolism. Percolation theory is therefore invaluable to the pharmaceutical scientist in establishing the proper drug load for a product.

II. EXPERIMENTAL

The experimental techniques utilized in this research mainly involved the evaluation of the release rates of benzoic acid from a tablet matrix composed of micronized poly(vinyl stearate) and micronized benzoic acid in various percentages. Release profiles were generated at a pH approximately two pH units below the pK_a of benzoic acid ($pK_a = 4.03$[71]) to assure that the dominant form of the molecule was the protonated species. Samples were analyzed for benzoic acid content by high pressure liquid chromatography (HPLC) using 4-fluorobenzoic acid as an internal standard.

The nonclassical nature of the system was evaluated by monitoring the transport characteristics through pure discs and films of poly(vinyl stearate) and by monitoring the effect of osmotic pressure on the transport kinetics. The nonuniversal nature of the system was investigated via the characterization of the underlying microstructure of the porous polymer.

A. Chemicals and Reagents

Tablets were manufactured from micronized benzoic acid and micronized poly(vinyl stearate). The benzoic acid, 99+% gold label purity ACS Reagent grade, Lot # 00103JM, was obtained from Aldrich Chemical Company Inc. of Milwaukee, WI. The poly(vinyl stearate), Lot # 0902KJ; 4-Fluorobenzoic acid, 99% purity, Lot # LM01207EL; acetic acid, 99.8+% ACS reagent gold label purity, Lot # KV 00618PT; and the HPLC grade benzene, Lot # 00209BV used in this research were also purchased from Aldrich. Aerosol OT (Sodium Dioctyl Sulfosuccinate, 10% solution) was obtained from Anderson Laboratories of Fort Worth, TX, Lot # B7-11. Solvents for the HPLC system were purchased from American Burdick & Jackson Co. of Muskegon, MI and consisted of high purity HPLC grade methanol Lot # AU003. "Baker Analyzed" Reagent grade concentrated HCl Lot # 542037 from J.T. Baker Chemical Co. of Philipsburg, NJ was used to adjust the buffer

solution pH. Potassium chloride, AR, Lot # 6858 KAVY, was purchased from Mallinckrodt of Paris, KY.

The benzoic acid and poly(vinyl stearate) were micronized by the Sturtevant Mill Company of Boston, MA. Approximately one kilogram of benzoic acid was micronized at a feed rate of 2.3 kg/hr in a four inch micronizer lined with a polyurethane rubber liner. Approximately 100 grams of poly(vinyl stearate) was micronized at a feed rate of 6 grams/ min. in a two inch micronizer. The micronized materials utilized in the current research are identical to those employed in previous studies.[1]

B. Methodology

1. PREVIOUS ANALYSIS

Previous physical/chemical evaluation[1] of the two components included particle sizing of both poly(vinyl stearate) and benzoic acid and the determination of the solubility and the diffusion coefficient of the micronized benzoic acid in the dissolution medium at 37°C. Particle sizing was performed by a "dot counting logic"[72,73] technique applied to scanning electron photomicrographs of the two micronized materials. The diffusion coefficient of benzoic acid in the dissolution medium at 37°C was determined by fitting the data to a modified Levich equation.[74] Results of particle size, solubility, and diffusion coefficient determination are listed in Table 2.1. Confidence limits reflect the standard error of the mean at 95% confidence.

TABLE 2.1 PREVIOUSLY MEASURED[1] PHYSICOCHEMICAL PROPERTIES OF THE TABLET CONSTITUENTS[¥]

Material	Particle Size (μm)	Solubility (mg/ml)	Diffusion Coefficient $\times 10^5$ (cm^2/sec)
benzoic acid	12 ± 4 (n = 48)	4.6 ± 0.1 (n = 22)	1.29 ± 0.05 (n = 6)
poly(vinyl stearate)	10.3 ± 0.2 (n = 139)	n/a	n/a

[¥]Confidence interval at 95% confidence using the standard error of the mean.

2. CURRENT ANALYSIS

Current physical/chemical characterization of benzoic acid and poly(vinyl stearate) included: pycnometric density determination of both materials, melting point determination and viscosity average molecular weight of the polymer, and the evaluation of transport characteristics of benzoic acid through pure polymeric discs. The results of the density determinations for the micronized powders will be reported in this Chapter since these values are pertinent to the calculated porosities of the tablets listed in Tables 2.2a and 2.2b.

A qualitative description of the internal tablet pore structure was determined from morphological microstructural analysis of three different tablets. Methodology utilized in morphology characterization involved microtoming, light microscopy, and three-dimensional reconstruction. The methods employed in this research will be described in this Chapter.

3. RELEASE KINETICS

a) Tablet Manufacture

All materials were weighed out to the nearest 0.0001 grams on a Mettler analytical balance. Two separate sets of tablets (designated as EXP 3 and EXP 4), each composed of six tablets of varying composition, were manufactured. All twelve tablet blends containing approximately 2 grams of benzoic acid and poly(vinyl stearate) in mixtures ranging from 1.5 to 25% benzoic acid by weight were initially blended in a Wheaton glass vial sealed with a teflon-lined cap for 5 minutes, screened, transferred to a clean Wheaton glass vial, capped, and blended again for another 3 minutes. An aliquot of five hundred milligrams of material was accurately weighed and transferred to a Hastelloy die prior to compression on a Carver Press. Blending procedures were conducted with a T-Line Laboratory Stirrer manufactured by Talboys Engineering Corp. of Emerson, NJ. Hand-screening was accomplished with a U.S. Standard Sieve, manufactured according to A.S.T.M.

specifications, with 841 μm openings or the Tyler equivalent of a 20 mesh. The screen was manufactured by E.H. Sargent & Co. of Chicago, IL.

A Carver Laboratory Press, Model C, manufactured by Fred S. Carver Inc. of Menomonee Falls, WI was used to compress the micronized materials into tablets. Compressional forces were kept fairly low, at approximately 5 kN of force, during tabletting. Six Hastelloy Alloy G-3 (Corrosion Materials Inc. of Baker, LA) dies of rotating disk design and six 316 stainless steel/Hastelloy shafts were manufactured by the Physics Department machine shop of the University of Wisconsin - Madison. The Hastelloy dies, Figure 2.1, were manufactured with five 0.5 mm deep by 0.5 mm wide grooves spaced 1.5 mm apart within the die to prevent the flow of dissolution medium along the edges of the tablets during the experiments.

After compression, the residual material compressed into the exposed die grooves was carefully removed and weighed. The total tablet weight and composition were then calculated based on initial weights and losses. The radii of the dies were 0.64 cm. Tablet and die measurements were made with micrometers manufactured by Enco of Chicago, Illinois and calipers manufactured by the Mitutoyo Corporation of Japan. Tablet composition in terms of g/cm^3 was calculated from the tablet mass, initial mass composition, the respective densities of the two materials as measured by helium pycnometry, the thickness and radius measurements of the dies, and the calculated cylindrical geometry. The volume attributed to the total number of grooves covered by the tablets was also incorporated into this volume calculation based on a value of 0.0104 cm^3/groove. Porosities were calculated based on the total benzoic acid content and residual porosities determined by the difference between geometrically calculated volumes and mass-based volumes. Residual or intrinsic porosities ranged from 0.00 to 0.02. A summary of the release parameters of EXP 3 and EXP 4 are listed in Tables 2.2a and 2.2b respectively.

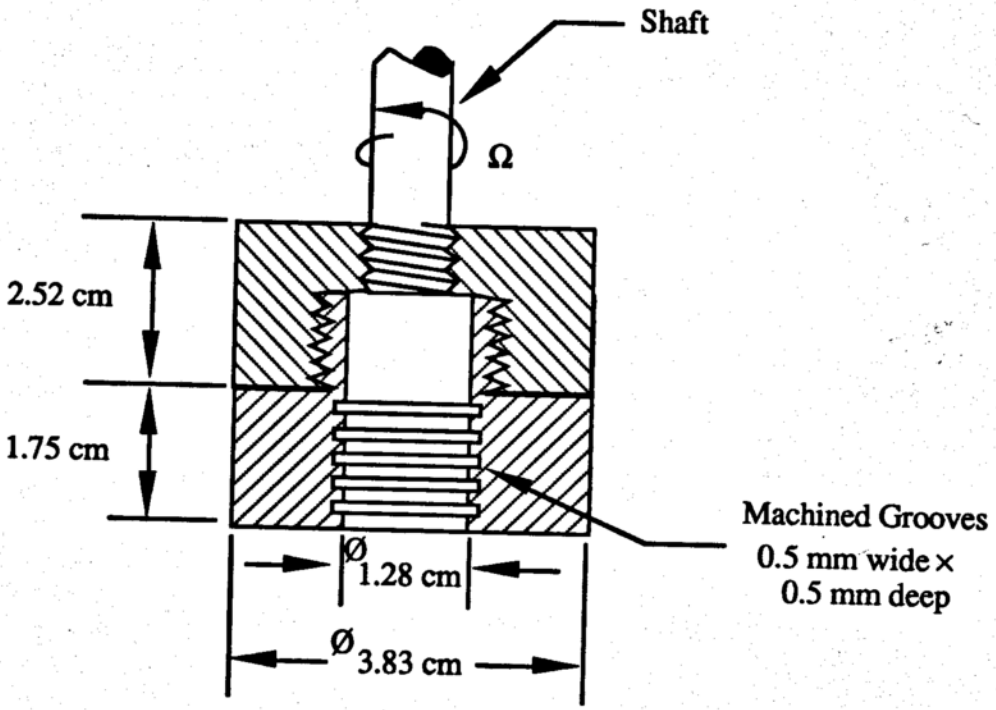


Figure 2.1 The Rotating Disk Assembly; The Hastelloy Die

TABLE 2.2A PARAMETERS FOR RELEASE EXPERIMENT 3

	Tablet Composition (% benzoic acid by weight)					
EXP 3 Parameter	5.9%	8.2%	10.6%	15.4%	20.5%	25.2%
Tablet Thickness (cm)	0.388	0.380	0.376	0.370	0.366	0.356
Tablet Volume (cm^3)	0.520	0.510	0.505	0.497	0.492	0.479
Drug Load (g)	0.294	0.0411	0.0534	0.0767	0.1027	0.1263
Drug Load (g/cm^3)	0.0565	0.0806	0.106	0.154	0.209	0.264
Volume Fraction Drug ($Ø_d$)	0.044	0.063	0.083	0.121	0.164	0.208
Inherent Volume Fraction (ε)	0.02	0.02	0.02	0.02	0.02	0.02
Porosity (Ø)	0.064	0.083	0.103	0.141	0.184	0.228

TABLE 2.2B PARAMETERS FOR RELEASE EXPERIMENT 4

	Tablet Composition (% benzoic acid by weight)					
EXP 4 Parameter	1.5%	3.3%	5.3%	7.4%	9.4%	11.1%
Tablet Thickness (cm)	0.3978	0.3907	0.3860	0.3758	0.3775	0.3835
Tablet Volume (cm^3)	0.5223	0.5132	0.5071	0.4940	0.4962	0.5039
Drug Load (g)	0.0073	0.0165	0.0261	0.0367	0.0467	0.0560
Drug Load (g/cm^3)	0.0140	0.0322	0.0515	0.0743	0.0941	0.111
Volume Fraction Drug ($\emptyset_d$)	0.011	0.025	0.041	0.059	0.074	0.088
Inherent Volume Fraction (ε)	0.01	0.01	0.01	0.00	0.02	0.00
Porosity ($\emptyset$)	0.021	0.035	0.051	0.059	0.094	0.088

b) Dissolution

Tablets compressed in rotating disk assemblies were placed in dissolution vessels containing approximately 900 ml of dissolution medium at 37°C composed of: pH 2.0 buffer adjusted with HCl, 4-fluorobenzoic acid (FBA) as the internal standard, and 0.25 mM Aerosol OT. The internal standard was added to the vessels as a 25 ml aliquot of standard FBA solution in pH 11.8 aqueous solution. Standard concentrations of FBA internal standard solutions were 2.03 mg/ml for EXP 3 and 1.01 mg/ml for EXP 4. Dissolution medium was degassed by heating to approximately 50°C prior to delivery to vessels. Heated medium was allowed to cool to 37°C before Aerosol OT and FBA solutions were added. Dies were then placed in the dissolution medium to a depth below the union of the top section of the die with the bottom in an attempt to eliminate any hydrostatic pressure buildup. The start of the experiment was coincident with the immersion.

The dissolution system used for the kinetics experiments consisted of a six spindle Distek 2000 dissolution apparatus and a Distek 3000 Autosampler manufactured by Distek Inc. of Somerset, NJ. The disk assemblies were rotated at 100 rpm and vessels lids were sealed to the tops of the dissolution vessels with vacuum grease. Lids were specially manufactured with only one sample reservoir in order to eliminate as much evaporation of the medium as possible over the duration of the kinetics experiments. A water reservoir, consisting of an on-end 6 liter Erlenmyer was suspended over the dissolution water bath at water level in order to automatically replace evaporated water and therefore maintain temperature control of the system.

Samples for EXP 3 were withdrawn by autosampler every 12 hours for the first 3 days of the experiment, then every 24 hours for the next 26 days, and finally every 48 hours for the next 20 days. The volume per sample was calibrated prior to the onset of the experiment by using the autosampler to withdraw 8 samples from each of the six vessels. The

overall mean volume per sample was determined to be 4.7 ± 0.1 ml at 95% confidence using the standard error of the mean. Volume replacement was performed after every other sample.

Samples for EXP 4 were withdrawn by autosampler every 24 hours for the first 10 days of the experiment, then every 48 hours over the next 44 days, and finally, every 72 hours until complete extraction of benzoic acid was achieved. The volume per sample was calibrated prior to the onset of the experiment by withdrawing 8 samples from each of the six vessels. The overall mean volume/sample was determined to be 4.4 ± 0.1 ml based on all 48 samples and a 95% confidence interval. Volume replacement was also performed after every other sample.

c) Analysis

Analysis of the solutions withdrawn from the dissolution apparatus was performed by HPLC. The HPLC system consisted of: a Beckman Model 160 spectrophotometer equipped with a 254 nm filter, a HPLC Model 110 Beckman pump, a Rheodyne Model 7120 injection valve, a Beckman Ultrasphere ODS (5 µm, 4.6 mm x 25 cm, S/N 9UE787) reversed phase C18 HPLC column, a Beckman Ultrasphere ODS (5 µm, 4.6 mm x 4.5 cm, S/N 7D14) matched HPLC precolumn, and a Kipp & Zonen Model BD 40 chart recorder. A 20 µl sample loop was used for EXP 3 and a 50 µl sample loop was used for EXP 4. The mobile phase consisted of 54% (v/v) methanol, 45 % (v/v) Type III water, and 1% acetic acid (v/v) pumped at 1.0 ml/min. The mobile phase was degassed by vacuum prior to use.

Standard solutions of benzoic acid were prepared by dissolving an accurately weighed amount of micronized benzoic acid in HPLC grade methanol in a 100 ml volumetric flask. Twenty five milliliters of the FBA internal standard solution was accurately transferred to

the volumetric flask prior to bringing the solution up to volume with methanol. The amount of internal standard was always identical to that delivered to the dissolution vessels in order to correlate the two solutions. A 3.0 ml aliquot of the benzoic acid stock solution was then transferred to a 25 ml volumetric flask and brought up to volume with pH 2.0 buffer solution.

Response factors, R_F, for the standards were calculated from

$$R_F = (P_F/P_B) \times C_B, \tag{2.1}$$

where P_F represents the peak height of FBA, P_B represents the peak height of the benzoic acid, and C_B represents the amount of benzoic acid in the standard. The concentration of benzoic acid in a sample was then determined by multiplying the ratio of the sample peak height of benzoic acid to FBA in the sample by the response factor.

Sample concentrations were corrected for the amount of material withdrawn from the vessel throughout the experiment based on an overall mass balance. The correction was based on the volume per sample (V_S), the ratio of the peak heights of benzoic acid in the sample (P_B) to that of the standard (P^*_B), and the benzoic acid standard concentration (C^*_B). The correction relationship is shown in Equation (2.2) below.

$$A_B = \frac{P_B}{P^*_B} \times \frac{V_S C^*_B}{1000} \tag{2.2}$$

where the factor of 1000 is used to convert micrograms to milligrams.

4. PHYSICOCHEMICAL PROPERTIES

a) Determination of the Pycnometric Densities of Benzoic Acid and Poly(vinyl stearate)

Density determinations of the two tablet constituents were made on a Quantachrome model MVP-1 Multipycnometer using the large sample cell and helium as the measurement gas. Evaluation of powder volume (V_P) was based on the ideal gas law, volume of the sample cell (V_C), volume of the reference cell (V_R), the pressure applied to the reference cell alone (P_1), and the pressure distributed throughout the sample cell and reference (P_2). The relationship utilized to calculate the powder volume was

$$V_P = V_C - V_R \cdot \left[\left(\frac{P_1}{P_2}\right) - 1\right]. \qquad (2.3)$$

The calibrated sample cell volume was 149.13 cm^3 and the calibrated reference cell volume was 72.20 cm^3. Micronized benzoic acid and poly(vinyl stearate) were accurately weighed on a Mettler balance prior to evaluation of powder volumes. Powders were charged into the large sample cell and the chamber was placed in the pycnometer. The value of P_1 was obtained by allowing gas to flow and equilibrate only into the reference cell. After equilibration was reached, a valve was turned to allow flow into the sample cell as well. The subsequent equilibration value is P_2. The powder volume was then calculated based on measured P_1 and P_2 values and calibrated V_C and V_R values. Density was determined as the quotient of the powder mass and calculated volume.

Table 2.3 lists the individual trials and results of these determinations. The density of benzoic acid obtained with this method was determined to be 1.27 ± 0.03 g/cm^3 based on three trials and 14.5846 grams of material, while the density of poly(vinyl stearate) was determined to be 0.979 ± 0.001 g/cm^3 based on four trials and 24.8580 grams of material.

TABLE 2.3 PYCNOMETRIC DENSITY DETERMINATION OF THE TABLET CONSTITUENTS

Benzoic Acid

Amount of benzoic acid weighed out: 14.5846 grams

Trial #	P_1 (psi)	P_2 (psi)	V_P (cm^3)	Density (g/cm^3)
1	16.700	5.750	11.636	1.253
2	16.207	5.576	11.476	1.271
3	16.179	5.566	11.462	1.272

Benzoic Acid Density = 1.27 ± 0.03 g/cm^3

Poly(vinyl stearate)

Amount of poly(vinyl stearate) weighed out: 24.8580 grams

Trial #	P_1 (psi)	P_2 (psi)	V_P (cm^3)	Density (g/cm^3)
1	16.154	5.952	25.376	0.9796
2	16.196	5.968	25.393	0.9789
3	16.376	6.035	25.415	0.9781
4	16.296	6.004	25.365	0.9800

Poly(vinyl stearate) Density = 0.979 ± 0.001 g/cm^3

b) Osmometry

A Vapor Pressure Osmometer, model 5500XR, manufactured by Wescor Inc. was calibrated with 1000, 295, and 100 mmol/kg standards at 37°C and used to measure the osmotic strengths of the dissolution medium with and without KCl.

The osmometer measures the vapor pressure depression of a solution within the sample chamber by utilizing a thermocouple hygrometer. A sample size of 10 µl was utilized. When the temperature of the thermocouple reaches the dew point of the solution, condensation on the thermocouple surface ceases and the thermocouple temperature stabilizes. The stabilized output is proportional to the difference between the ambient chamber temperature and the dew point temperature. The proportionality constant can be related back to the Clausius-Clapeyron equation to achieve the osmotic pressure of the solution.

The osmotic strengths were determined for a pH 2.0 solution at 37°C containing FBA and AOT in concentrations identical to those utilized in the kinetic experiments and an identical solution containing a known amount of KCl. A saturated solution of benzoic acid in water at 37°C was also analyzed for osmotic strength. A linear extrapolation to the osmotic strength of the saturated benzoic acid solution was performed in order to determine the proper concentration of KCl required to match the two solutions. This new sample of "spiked" dissolution medium was prepared and analyzed with the osmometer. Adjustments in concentrations were performed until the osmotic pressure of the two solutions matched.

c) Intrinsic Viscosity and Viscosity Average Molecular Weight of Poly(vinyl stearate)

An acid-washed Cannon 100 Q8 Ostwald Capillary viscometer was utilized in the experimental determination of the intrinsic viscosity of poly(vinyl stearate). A MGW Lauda M3 heater/water circulator was employed to maintain temperature control. Weighed aliquots of poly(vinyl stearate) were dissolved in benzene and concentrations recorded on a weight/volume basis. The "time-to-drain" was determined for four dilute solutions of polymer held at 25°C. The drain times for the prepared solutions ranged from 60 to 90 seconds. The intrinsic viscosity of the polymeric solution was determined by extrapolation. The viscosity average molecular weight was calculated based on the Mark-Houwink relationship using coefficients for poly(vinyl stearate) in benzene at 25°C[75] and the experimentally determined intrinsic viscosity of the system. The Mark-Houwink relationship, Equation (2.4), for this system is

$$[\eta] = 1.0 \times 10^{-3} \overline{M}_v^{0.65} \quad [dl/g], \tag{2.4}$$

where $[\eta]$ is the intrinsic viscosity in units of dl/g, $\overline{M}_v$ is the viscosity average molecular weight of the polymer, the Mark-Houwink coefficients "k" and "a" are 0.0010 and 0.65 respectively. The values of the Mark-Houwink coefficients depend on the nature of the polymer, the nature of the solvent, and the temperature. The molecular weight range applicable for this relationship is from 3700 to 5300 Daltons.

The viscosity average molecular weight of the polymer is defined as

$$\overline{M}_v = \left(\frac{\sum_i N_i M_i^{1+a}}{\sum_i N_i M_i} \right)^{\frac{1}{a}}, \tag{2.5}$$

where N_i is the number of polymer chains of segment length "i", M_i is the molecular weight of the polymer chain of segment length "i", and "a" is the Mark-Houwink coefficient. If a = 1, the viscosity average molecular weight equals the weight average molecular weight. Otherwise, if "a" ≠ 1,

$$\overline{M}_n < \overline{M}_v < \overline{M}_w, \tag{2.6}$$

where $\overline{M}_n$ and $\overline{M}_w$ are the number average and weight average molecular weights respectively.

The definition for the intrinsic viscosity utilized in this experiment is given in Equation (2.7) and is the limiting value of the reduced viscosity as the polymer solution concentration approaches zero.

$$[\eta] = \lim_{(c_2 \to 0)} \left[\frac{1}{c_2}\left(\frac{\eta}{\eta_o} - 1\right)\right] \tag{2.7}$$

where c_2 is the polymer solution concentration in units of g/dl, and the quantity in brackets is the reduced viscosity which has units of dl/g.

The viscosity of a dilute solution of polymer can be related to the drain time of a capillary viscometer through the Poiseuille equation,

$$Q = \frac{\pi \cdot (P_o - P_f) \cdot R^4}{8\eta L}, \tag{2.8}$$

where Q is the volume rate of flow, R is the capillary radius, L is the length of the capillary, $\mathcal{P}_o - \mathcal{P}_f$ is the pressure head (combined static pressure and gravitational force), e. g.: $\mathcal{P} = p + \rho gh$ where p is the static pressure, h is the distance upward (against gravity) from a chosen reference plane, g is the gravitational force, and ρ is density. Of course, the Poiseuille Equation only applies for systems in situations of laminar flow, incompressible flow, steady-state, Newtonian fluids, continuum fluids, no slip at the container wall, and no end effects.

Expressing Q in terms of $\Delta V/\Delta t$, where V is volume and t is time, and replacing $\mathcal{P}_o - \mathcal{P}_f$ with $\rho gL + \Delta p$,

$$\frac{\Delta V}{\Delta t} = \frac{(\rho gL + \Delta p)\cdot \pi R^4}{8\eta L}. \qquad (2.9)$$

Since the static pressure is constant, Equation (2.9) can be solved for Δt to give

$$\Delta t = \left(\frac{8\Delta V}{\pi g R^4}\right)\cdot \frac{\eta}{\rho}, \qquad (2.10)$$

where the weight of the liquid is the driving force through a capillary of constant R and L. Simplifying in terms of constants,

$$\eta = A\cdot\rho\cdot\Delta t \qquad (2.11)$$

where A is a constant equal to the reciprocal of the term in parentheses in Equation (2.10).

In terms of two solutions, 1 and 2,

$$\frac{\eta_1}{\eta_2} = \frac{\rho_1}{\rho_2} \cdot \frac{\Delta t_1}{\Delta t_2}, \tag{2.12}$$

and if dilute solutions are used, $\rho_1 \approx \rho_2$, and the relationship becomes

$$\frac{\eta_1}{\eta_2} = \frac{\Delta t_1}{\Delta t_2}. \tag{2.13}$$

Therefore, by using pure benzene as solution 2 and a solution of polymer dissolved in benzene as solution 1, the viscosity of the polymer solution relative to the benzene can be determined by measuring the drainage times of the polymer solution and the pure benzene under identical conditions. By varying polymer solution concentrations, a plot of relative viscosity as a function of concentration can be obtained. Extrapolation of the linear region to the reduced viscosity intercept gives the intrinsic viscosity of the polymer. Utilization of Equation (2.4) then allows for the determination of the viscosity average molecular weight of the polymer.

d) Melting Point and Enthalpy of Fusion of Poly(vinyl stearate)

A Perkin-Elmer Differential Scanning Calorimeter 2 (DSC 2), set at a scan rate of 20°C/min over a temperature range of – 43°C to 147°C, was used to determine the melting point and the enthalpy of fusion of poly(vinyl stearate).

The sample compartment reservoir was filled with liquid nitrogen approximately one hour before use. Calibration of the instrument baseline was performed over the range utilized in scanning. Samples were weighed out on a Mettler H51 balance and accurately

transferred to aluminum pans, sealed, and reweighed. A reference cell was also prepared at the same time. Both cells, sample and reference, were placed in their respective sample compartments and scanning was initiated. Instrument output was monitored and a final plot was issued from a Hewlett-Packard plotter.

e) Transport Through Poly(vinyl stearate) Films and Discs

The transport properties of the polymer were investigated by preparing discs and cast films of poly(vinyl stearate) and monitoring transport of benzoic acid through the monoliths. The experiment was conducted in a diaphragm cell configuration. Analysis was performed by applying Crank's[76] relationship for steady-state transport through a thin film of uniform initial distribution with surface concentrations different.

The Distek dissolution bath was utilized for this experiment. It was equipped with six stainless steel/Hastelloy dies assemblies, one of which is shown in Figure 2.2. The assemblies were arranged in a diaphragm cell configuration with the receiver solution residing outside the die assemblies and containing FBA, Aerosol OT, and pH 2.0 buffer, just as in the kinetics experiments, and the donor solution composed of the identical receiver solution spiked with benzoic acid. All solutions were maintained at 37°C and the assemblies were rotated at 100 rpm throughout the transport experiments. The donor solution contained 2.15 mg benzoic acid/ml, 1.07 μg FBA/ml and 0.25 mM Aerosol OT in pH 2.0 buffer. The receiver solution contained 1.07 μg FBA/ml and 0.25 mM Aerosol OT in pH 2.0 buffer.

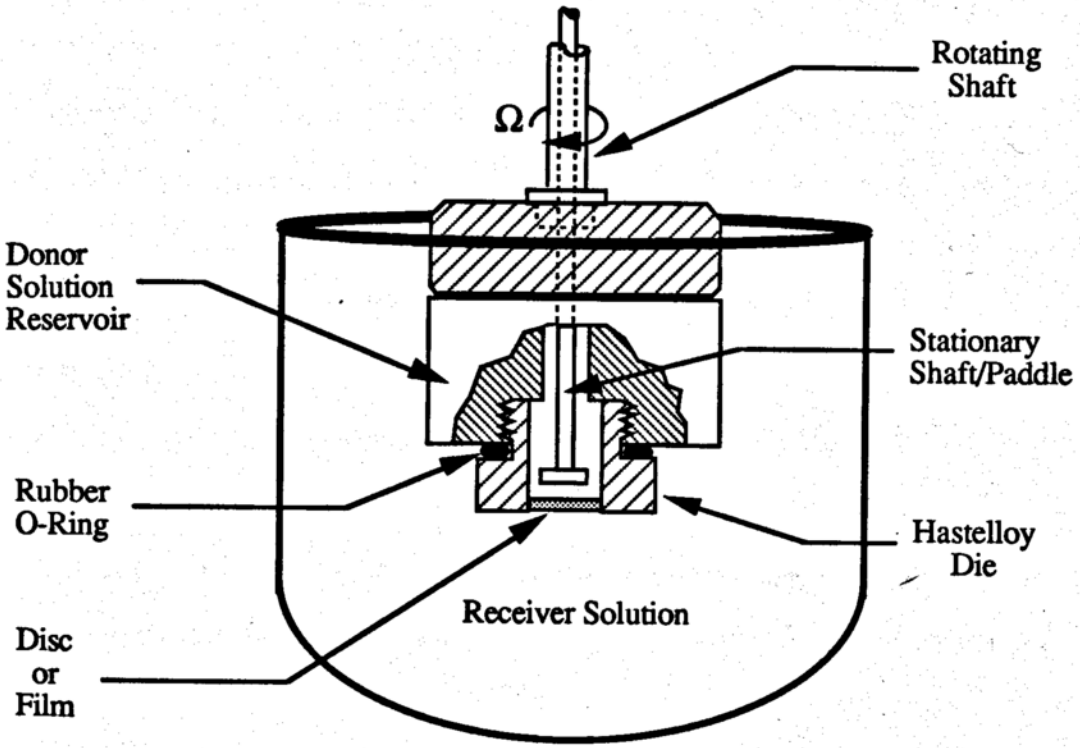


Figure 2.2 The Diffusion Cell Assembly. Pure compressed discs or cast films of polymer were manufactured directly in the lower die assembly. Transport of benzoic acid through the polymer was analyzed using this modified "diaphragm cell" method.

Three discs were prepared by compressing approximately 366 mg of micronized poly(vinyl stearate) into Hastelloy dies. Compression was performed on the Carver Press at approximately 5 kN. Disc surfaces were visually inspected for smoothness. Disc thicknesses were determined by measurements performed with micrometers.

Film preparation involved melting a small quantity of micronized poly(vinyl stearate) in a glass petri dish on a Thermodyne Stirring/Hot Plate. The melts were poured directly into a warmed Hastelloy die, which was resting on a stainless compression plate, and then placed in a Precision vacuum oven and evacuated for approximately 30 minutes at 65°C and 90 kPa vacuum to remove residual entrapped air. The molten films were then removed from the oven and allowed to solidify at room temperature. In order to assure a smooth surface for transport through the back of the film, just prior to solidification, a tablet punch was applied to the back side of the film and a slight pressure was applied by hand for approximately 2 minutes. The film was then released from the front compression plate onto which it had solidified and checked visually for cracks and surface roughness. Three films were cast and their thicknesses were evaluated with micrometers.

The densities of the donor and receiver solutions at 37°C were determined by accurately weighing 10 ml of pipetted solution on a Mettler balance. The densities of the donor and receiver solutions were identical and therefore, the overall density was determined to be 0.991 ± 0.001 based on 10 (five donor and five receiver) independent measurements and 95% confidence.

Donor and receiver solutions were degassed by heating to approximately 50°C prior to the start of the experiment. The solutions were allowed to cool to 37°C and this temperature was maintained with the use of a hot plate during the start-up phase. Approximately 700 ml or 694.3 grams of heated receiver solution were weighed accurately on a Sartorious top-loading dual range balance. Six aliquots of receiver solutions were weighed,

transferred to dissolution vessels in the dissolution bath, and covered with plexiglass lids. Approximately 65 ml or 64.5 grams of receiver solution was accurately weighed and transferred to the donor cell assembly containing either a compressed disc or cast film. All six donor cells were filled with receiver solution at 37°C. The assemblies were connected to the rotating/stationary shafts and suspended over the dissolution vessels for 24 hours. In this manner, leakage of the solution around or through the films/discs was evaluated. Rubber O-rings were placed around the threaded portion of the Hastelloy dies in order to eliminate leakage at the cell junctions. If an assembly leaked, the disc or film was discarded and another was manufactured.

When six good, nonleaking discs and films were obtained, the donor cell assemblies were disassembled and the solutions emptied. The interior of the cells were dried before heated, degassed, and weighed aliquots of donor solution were dispensed. As in the previous case, approximately 64.5 grams of donor solution were accurately weighed on the Sartorious top-loader. The filling of the donor cell assemblies was coincident with the start of the experiment. After filling, all six cells were lowered into the receiver solutions in the dissolution vessels. The solution levels outside and inside the donor sample chamber were balanced and maintained throughout the experiment in order to eliminate any pressure head. The solutions were maintained at 37°C in the dissolution bath and the cell assemblies were rotated at 100 rpm. All lids were sealed tightly to the vessels by using vacuum grease; stoppers were placed in the lid holes. Table 2.4 lists the conditions and parameters of this experiment.

Samples were withdrawn starting at day 56 to assure steady-state and then taken every 3 to 4 days for a total of 93 days.

TABLE 2.4 SAMPLE DESCRIPTIONS AND CHAMBER VOLUMES FOR TRANSPORT THROUGH POLY(VINYL STEARATE) EXPERIMENTS

	Bath Number					
	1	2	3	4	5	6
Sample Description	film unmicr.	film micr.	film micr.	disc unmicr.	disc micr.	disc micr.
Thickness (cm)	0.3075	0.3140	0.3365	0.2835	0.2805	0.2775
Start Time	11:59 am 10/10/89	11:57 am 10/10/89	11:55 am 10/10/89	11:53 am 10/10/89	11:51 am 10/10/89	11:49 am 10/10/89
Donor Soln Volume (ml)*	56.6	56.4	57.1	56.8	56.1	56.6
Receiver Soln Volume (ml)*	687.2	687.7	688.3	688.1	687.8	688.5

*Volumes are calculated based on the room temperature (23°C) solution density. Density of the donor and receiver solutions at 23°C is 0.996 ± 0.001 g/ml and density of each at 37°C is 0.991 ± 0.001 g/ml.

5. ANALYSIS OF THE MICROSTRUCTURE MORPHOLOGY

In order to evaluate the porous microstructure of the benzoic acid/poly(vinyl stearate) tablets, a series of three tablets were sectioned and photomicrographs taken. All three tablets were extracted in previous kinetics experiments prior to microtoming and represented drug loads below the percolation threshold, slightly above, and far above the threshold for the system. Three-dimensional reconstructions of the two-dimensional images were performed by hand-digitizing individual pore structures and recombining slices on a computer screen via a three-dimensional reconstruction software package. In this manner, a three-dimensional image of the porous microstructure within the tablet matrix was visualized.

a) Microtoming

An UltraCut E, Reichert-Jung microtome was utilized to slice 8.33 μm sections from the tablet surfaces. The three tablets were mounted on individual stainless steel chucks with cyanoacrylate adhesive (Figure 2.3). The tablet and chuck assembly were placed in the microtome and approximately 30 μm of material was removed prior to taking photomicrographs.

b) Microscopy

The microscope utilized for the photomicroscopy was an Olympus Model BH-2 equipped with a telescope eyepiece, square grid reticle (Figure 2.4), an X-Y micropositioner stage (Figure 2.5), and a 35 mm Olympus camera. Through-the-lens illumination was employed. Reconstructions were compiled from 50× objective images, even though images at other magnifications were taken. The square grid was imaged onto the film plane over the tablet surface and a stage micrometer with 10 μm divisions was utilized to calibrate

the grid spacing. At 50× the grid spacing was determined to be 16.7 μm. Therefore, microtoming was undertaken at thicknesses equivalent to two slices per square.

After a slice was microtomed off the tablet surface, the stainless steel chuck and tablet assembly was removed from the microtome and placed into a mounting slot on the X-Y micropositioner stage. Three positions, approximately in the midsection of each tablet, were recorded in terms of x- and y-coordinates from the micropositioner and the image at each position was focused and a photograph taken. The stainless steel chuck and tablet assembly was then removed from the positioning stage and placed back in the microtome. Great care was exercised in the realignment of the tablet surface with the microtome blade during the replacement of the tablet and chuck assembly. The alignment was important since a misalignment of the tablet plane with the microtome blade would potentially lead to an uneven slice on the next section. After realignment, another 8.33 μm was removed from the surface and the photomicrograph procedure was again repeated, taking a photograph of the same position on the tablet surface, but 8.33 μm deeper. Note that, unlike normal microtoming procedures, the photomicrographs were taken of the remaining portion of the tablet, not the 8.33 μm slice. In this method, due to the extreme brittleness and low melting point of the polymer, the microtoming procedure was completely destructive. A total of 21 slices (174.93 μm) were removed from two of the tablet surfaces and 10 slices (83.33 μm) were removed from the highest drug load tablet surface.

Images were recorded on Kodak Technical Pan 2415 135-36 Professional film at ASA 160 and an exposure adjustment of 2.00. An LBD filter was placed in the lighting tube in the position closest to the microscope objectives. The through-the-lens illumination power was set at 6 volts and the aperture on the light tube was approximately 25% open to enhance contrast.

The exposed film was developed using Kodak D-19 (1:2) developer in order to attain the highest contrast possible. Chemicals were kept at 68°F throughout the developing process. The procedure for film developing is listed in Table 2.5. This exposure setting and processing conditions, as recommended by Kodak,[77] would produce a high contrast index of 2.70.

Negatives were printed on 8 × 10 Kodak Polycontrast III Type RC FM paper using approximately F5 filtering for high contrast. Burning and dodging techniques were employed in order to eliminate shadows and flashing. Printing was done at Photo Media of the University of Wisconsin - Madison. A list of the print positions and photomicroscopy conditions is reproduced in Appendix B.

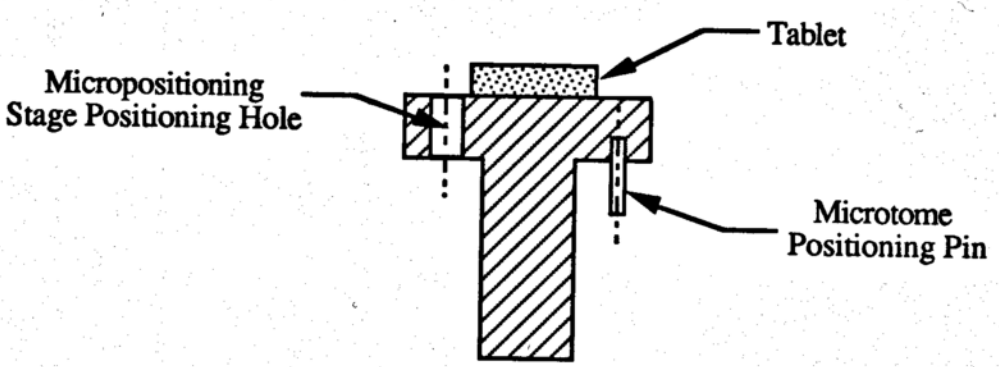


Figure 2.3 Stainless Steel Chuck and Tablet Assembly. The assembly was manufactured to be used in the microtome and the micropositioning microscope stage.

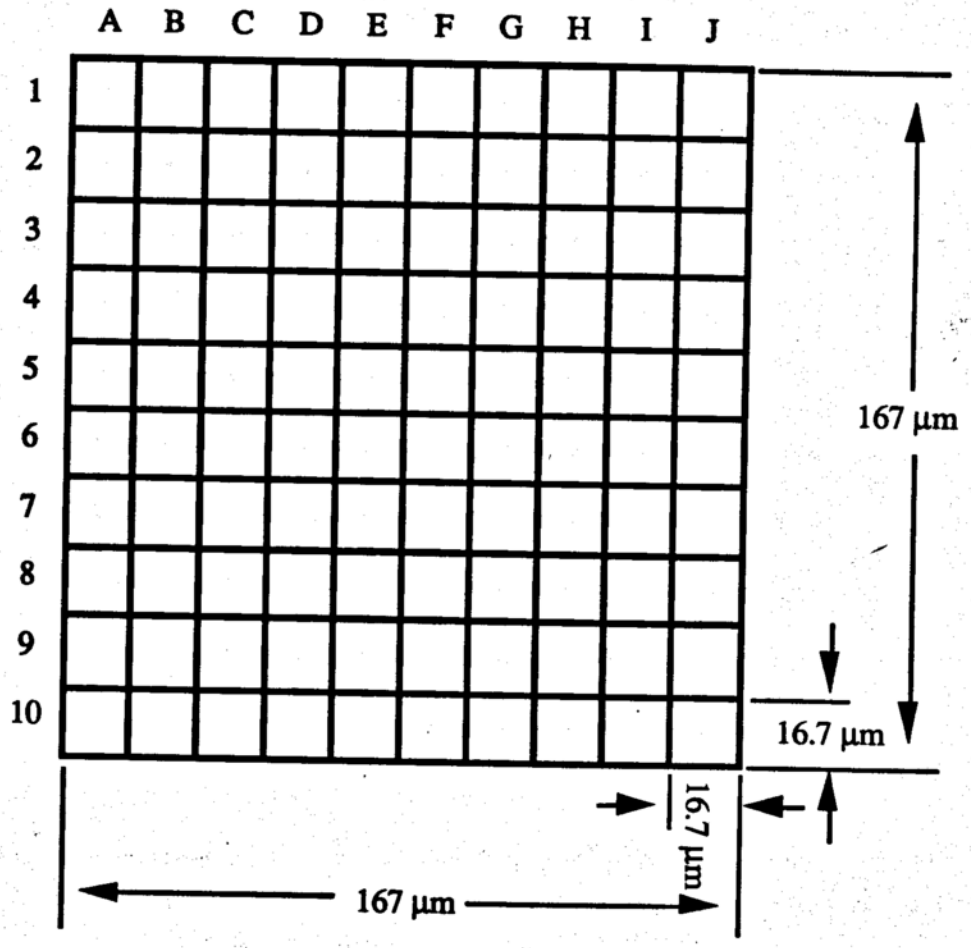


Figure 2.4 Square Grid Reticle for Photomicroscopy. Grid was placed over the tablet surface and pore structures were traced with respect to their position within the grid.

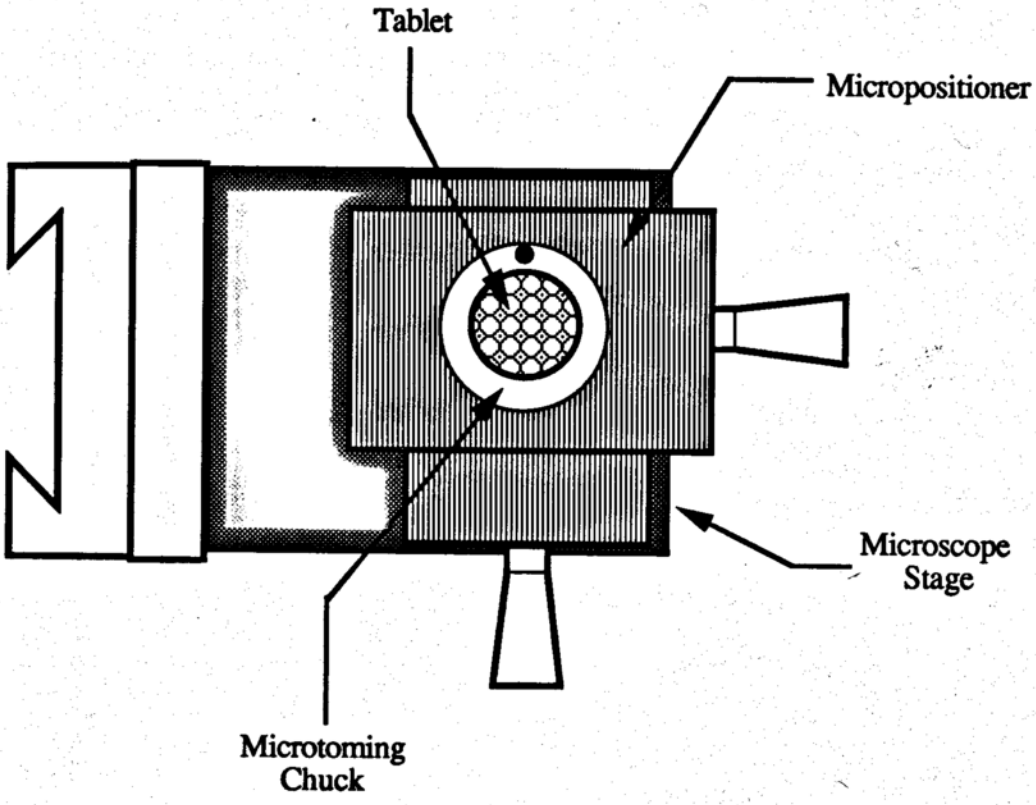


Figure 2.5 X-Y Micropositioning Stage for Photomicroscopy. Extracted tablets, mounted on the microtoming chuck, were aligned with the micropositioner after every slice. Photomicrographs were taken using the 50× objective and through-the-lens illumination.

TABLE 2.5 TECHNICAL PAN FILM PROCESSING CONDITIONS

Procedure	Agitation Conditions and Time
Wash	1 minute in tap water
Develop	7 minutes with D-19 (1:2) – agitate continuously for first 15 sec – agitate 7 sec every 30 sec – agitate continuously for last 15 sec
Rinse	with 2 to 3 tank fulls of tap water
Fix	3 minutes with Kodak Rapid Fixer – agitate continuously for first 15 sec – agitate 10 sec every 30 sec – agitate continuously for last 15 sec
Rinse	30 sec in running tap water
Rinse	with Kodak Hypoclear for 2 minutes agitate 7 sec every 30 sec
Wash	5 minutes in running tap water
Rinse	with 1 tank full of Kodak Photo Flo
Dry	in a dust free environment

c) Three-Dimensional Reconstructions

A software package, PC3D, written by and purchased from Jandel Scientific of California, was utilized to reconstruct the two-dimensional images into three-dimensional pore structures. A Numonics digitizing tablet equipped with a 16 button digitizing mouse was also purchased through Jandel and provided the means of tracing two-dimensional pore structures. All reconstructed images were obtained from 50× objective two-dimensional images.

An IBM AT 286 computer with EGA capability and color monitor was used to run the software and view the resulting images. Hard copies of the three-dimensional images were obtained on a HP 7475A Color Pro 6 pen plotter. Porosities, with respect to the traced images, were calculated with software contained within the Jandel PC3D package.

Tracing of pore structures was conducted in a grid-like format, using the square reticle grid as a guide. In this manner, the viewed tablet surface was broken down into 11 separate sections, 9 of which were 50 μm squares, 1 of which was 167 × 16.7 μm, and the last of dimensions 150 × 16.7 μm. By utilizing this method, small three-dimensional sections of the entire digitized tablet volume could be displayed on the computer screen for any one image view. In the case of complicated three-dimensional pore structures, this facilitated the viewing of images which would ultimately make the viewing screen too full and therefore too difficult to distinguish individual pore structures. Three-dimensional images were rotated 30° about the Z axis, –70° about the X axis, and + or – 3° about the Y axis for presentation in this dissertation. A two-dimensional photomicrograph of a porous section of one of the tablets is shown in Figure 2.6.

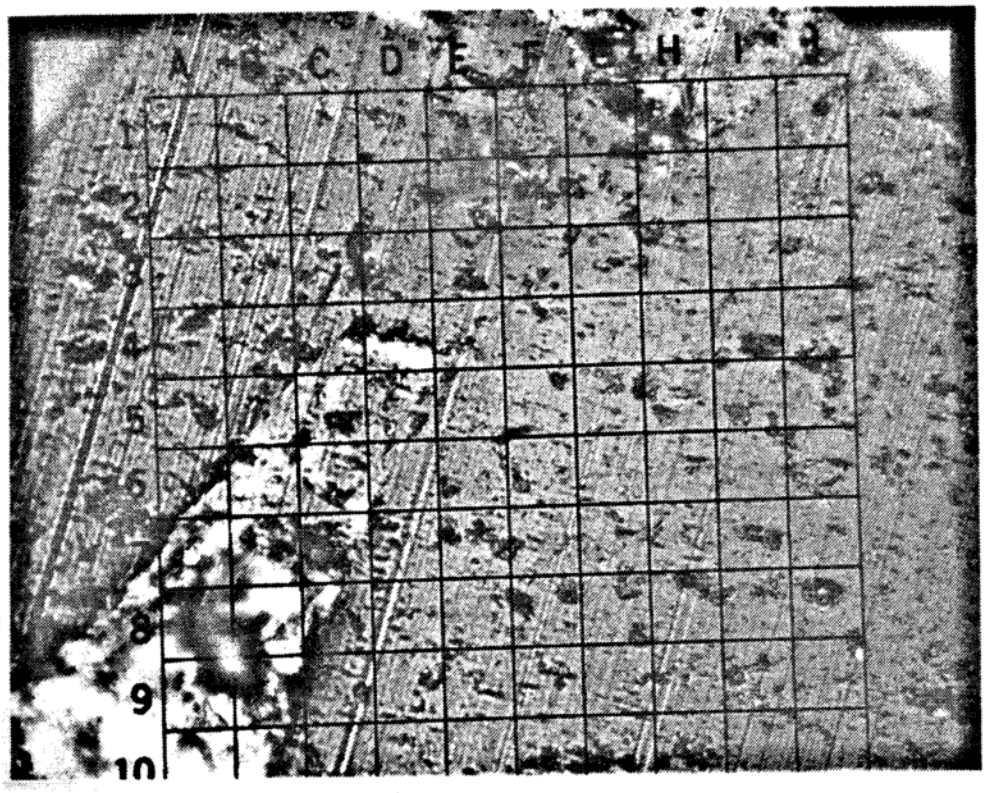


Figure 2.6 Two Dimensional Photomicrograph of the Porous Microstructure. An image of a section of the tablet $\emptyset^A = 0.141$ taken through the 50× objective and with through-the-lens illumination. Grid spacing is 16.7 μm square.

III. DATA TREATMENT AND RESULTS

In this chapter, a summary of the results obtained in terms of the transport characteristics near and below the threshold of the benzoic acid/poly(vinyl stearate) matrix and the nonclassical/nonuniversal nature of the percolating system will be presented. The conclusions drawn at the end of this Chapter will form the basis for the model developed in the Discussion Chapter which follows.

A. Percolative Transport Near and Below the Percolation Threshold

In this Section, the system is further characterized in terms of percolation parameters. Specifically, the evaluation of transport in this regime was undertaken in an attempt to determine the volume fractions effective and accessible as a function of drug load. Classically, from these results, the scaling relationships of percolation theory could be applied to evaluate the percolation threshold for the system. Subsequently, further characterization of the system in terms of its connectivity or microstructure could be elucidated via the relationship between the threshold and coordination for three-dimensional systems.

1. Data From Transport Near and Below the Percolation Threshold

As indicated in Chapter II, two sets of tablets were analyzed, EXP 3 and EXP 4; their parameters are listed in Tables 2.2a and 2.2b respectively. Data treatment for the rotating disc experiments was discussed in Chapter I and involved using a variation of Higuchi's square root of time model based on percolation theory. From the slope of the square root of time profiles obtained in these experiments, the volume fraction effective is obtained. If the experiment is allowed to go to complete extraction, as EXP 4 was, the volume fraction accessible is obtained from the plateau regions.

The square root of time results for EXP 3 and EXP 4 are given in Figures 3.1 and 3.2 respectively. The profile of EXP 3 does not plateau as observed in EXP 4 since EXP 3 was not taken to total extraction. The legend indicates the weight of benzoic acid in terms of percent of total tablet weight. The horizontal dashed lines of Figure 3.2 indicate the drug load for each of the six individual tablets.

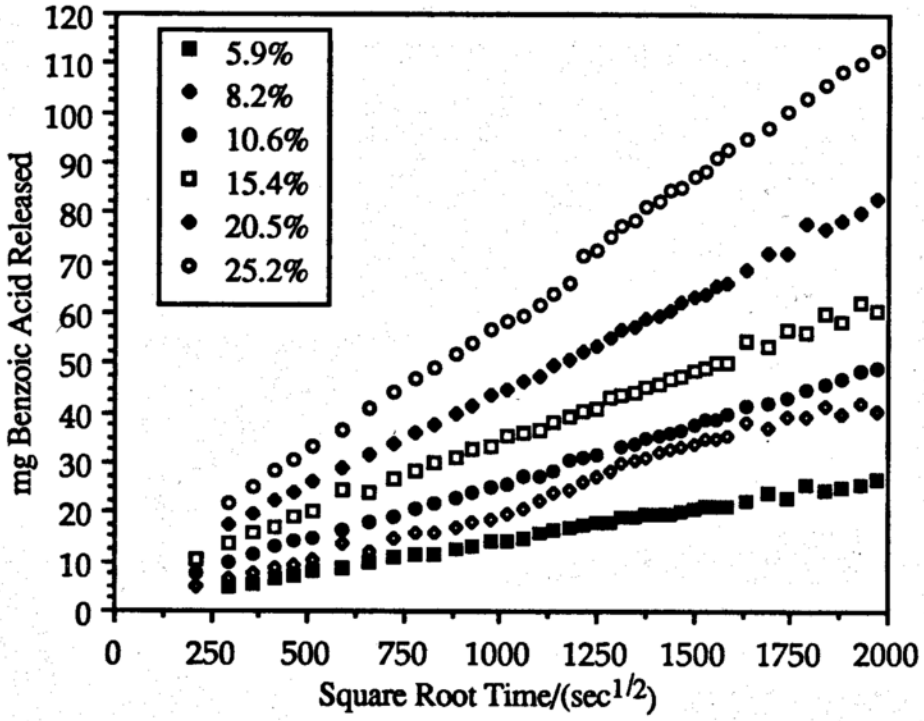


Figure 3.1 Square Root of Time Release Profile for EXP 3. Legend indicates the percentage of benzoic acid within the tablet on a weight/weight basis. Total drug load is listed in Table 2.2a. This experiment did not go to complete extraction.

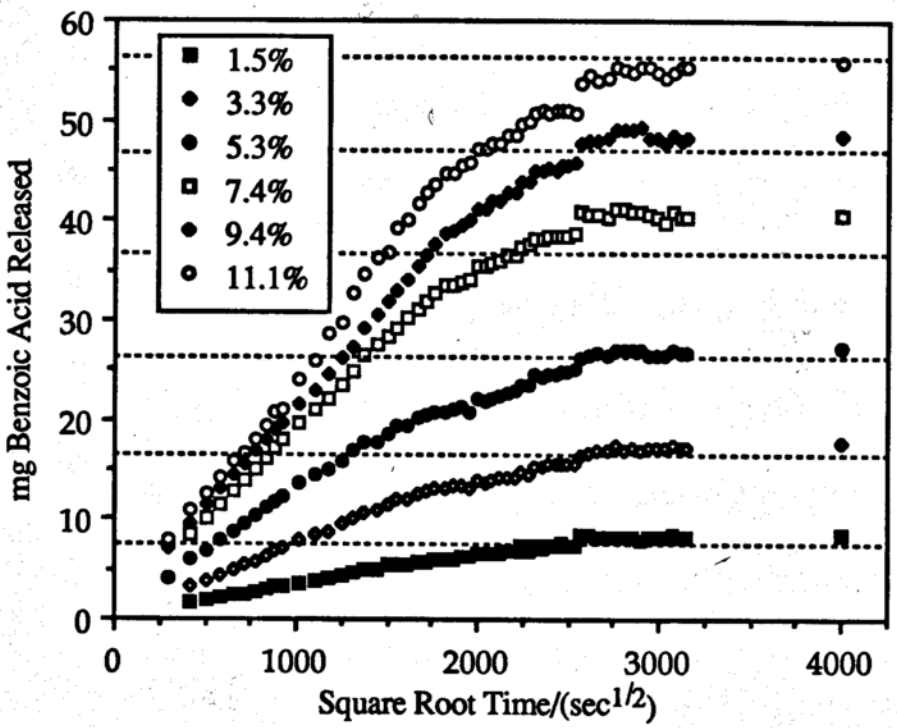


Figure 3.2 Square Root of Time Release Profile for EXP 4. Legend indicates the percentage benzoic acid within the tablet on a weight/weight basis. Dashed horizontal lines indicate drug loads for individual tablets (Table 2.2b).

2. VOLUME FRACTION ACCESSIBLE NEAR AND BELOW THE PERCOLATION THRESHOLD

As indicated in the previous section, the volume fraction accessible is obtained from the plateau region of the square root of time profiles. A summary of the accessible volume fraction results obtained in this manner is given in Table 3.1.

The tabulated data indicate that all material available for transport is accessible to transport; the volume fraction isolated is zero regardless of the drug load studied. The volume fraction isolated is therefore zero for this system in a region which would appear to be below the threshold. The existence of non zero volume fraction accessible values below the percolation threshold contradicts classical percolation theory and is an indication of non-classical behavior and/or a very complex highly coordinated microstructure. A summary of all the accessible results obtained to date (including previously reported results[1]) is listed in Table 3.2. Since the calculated accessible volume fractions based on the plateau values were not significantly different from the porosities based on drug load and inherent porosity, the matrix porosity was determined to be equivalent to its volume fraction accessible. The experimental volume fraction accessible as shown in the last column of Table 3.1, are therefore the values utilized in this research. Due to the sensitivity of the HPLC system and the method of calculating the sample volume, this assumption is reasonable.

A plot of the accessible volume fraction as a function of porosity is shown in Figure 3.3. Accessible volume fractions for other percolating systems are shown for the purpose of comparison. The current experimental results indicate that the accessible volume fraction appears to follow classical trends well above the percolation threshold, but near and below

the threshold the current system appears to deviate from the expected scaling law. From the trend of this data set it is difficult to determine whether the coordination of the benzoic acid/poly(vinyl stearate) lattice is greater than or equal to that of the face-centered cubic theoretical lattice, z = 12, or what the percolation threshold for the system actually is.

TABLE 3.1 VOLUME FRACTION ACCESSIBLE RESULTS FROM EXP 4 PLATEAU VALUES

Porosity (Ø)	Mean Plateau (mg)	Standard Deviation (mg)	Number of Observ.	Calc. Plateau $Ø^A$	Exp.§ $Ø^A$
0.021	7.9 (0.2)	0.44	24	0.022	0.021
0.035	17.1 (0.2)	0.29	15	0.036	0.035
0.051	26.7 (0.2)	0.30	15	0.051	0.051
0.059	40.6 (0.2)	0.38	15	0.065	0.059
0.094	48.4 (0.3)	0.52	15	0.097	0.094
0.088	54.9 (0.3)	0.60	15	0.086	0.088

Values in parentheses are confidence intervals calculated at 95% confidence.
§Calculated volume fraction accessible values were not significantly different from the porosity (Ø), therefore the experimental volume fraction accessible was taken as the total porosity.

TABLE 3.2 SUMMARY OF TOTAL ACCESSIBLE AND ISOLATED VOLUME FRACTION DATA OBTAINED FOR THE BENZOIC ACID/POLY(VINYL STEARATE) MATRIX

Volume Fraction Drug ($Ø_d$)	Inherent Volume Fraction (ε)	Total Porosity ($Ø$)	Volume Fraction Accessible ($Ø^A$)	Volume Fraction Isolated ($Ø^I$)
0.011	0.01	0.021	0.021	0.000
0.025	0.01	0.035	0.035	0.000
0.041	0.01	0.051	0.051	0.000
0.059	0.00	0.059	0.059	0.000
0.074	0.02	0.094	0.094	0.000
0.088	0.00	0.088	0.088	0.000
0.243	0.02	0.263	0.263	0.000
0.256	0.02	0.276	0.276	0.000
0.328	0.02	0.348	0.348	0.000
0.373	0.02	0.393	0.393	0.000
0.420	0.02	0.440	0.440	0.000
0.470	0.02	0.490	0.490	0.000

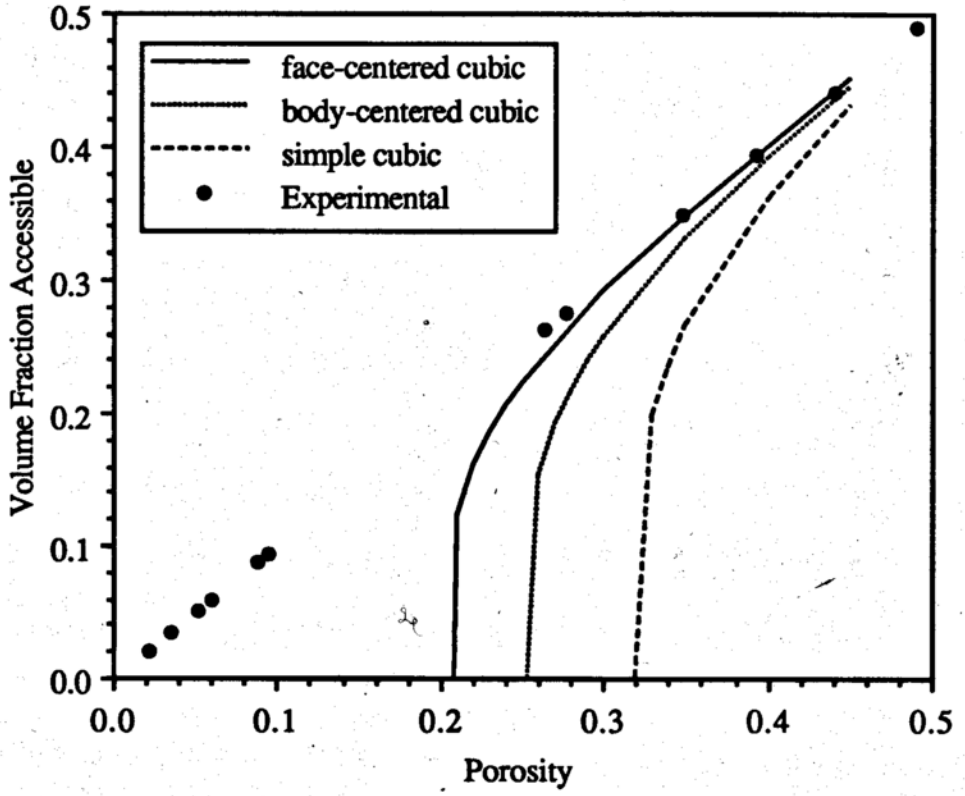


Figure 3.3 Experimental Volume Fraction Accessible Results for the Benzoic Acid/Poly(vinyl stearate) System Compared to Theory. The solid circles are experimental values. The theoretical profiles (lines) are for the face-centered cubic lattice[12] (z = 12), body-centered cubic lattice[12] (z = 8), and the simple cubic lattice[12] (z = 6). All theoretical profiles were obtained by Monte Carlo simulations.

3. VOLUME FRACTION EFFECTIVE NEAR AND BELOW THE PERCOLATION THRESHOLD

The volume fraction effective, as mentioned previously, is calculated from the slopes of the profiles of the square root of time kinetics. A statistical analysis of the linear regression results of the initial slopes of all 12 sets of data is given in Table 3.3. Confidence intervals are enclosed in parenthesis and calculated based on a 95% confidence interval. The standard error of the regression reported in Table 3.3 is equivalent to the standard deviation of the residuals for the linear regression model. It is the square root of the unexplained mean square of the residuals and is a measure of the dispersion of the experimental values about the fitted regression line.

A summary of the volume fraction effective values obtained for EXP 3 and EXP 4 are given in Table 3.4 along with a compiled list of all the volume fraction accessible and effective values, slopes, and bulk diffusion coefficients obtained from all the experiments undertaken on this system to date. Also, a complete list of release data from Experiments 1 through 4 is given in Appendix C.

A plot of the volume fraction effective as a function of porosity is shown in Figure 3.4. The experimental results are compared to three theoretical percolation lattices obtained from the literature.[13,9] Again, as with the accessible volume fraction, the system appears to follow classical percolation trends well above the threshold, but in the region near and below the threshold, anomalous or nonclassical percolative transport appears to occur. The ability for transport to occur below the "apparent" percolation threshold of the experimental system is an indication of nonclassical percolative behavior and/or nonuniversal behavior due to microscopic ordering, as stated in the accessible volume fraction section.

A comparison of the experimental and theoretical volume fraction effective profiles suggests that the lattice coordination of the benzoic acid/poly(vinyl stearate) system is greater than that of the Voronoi tessellation, lending support to the conclusion that a complex microstructure exists. However, since the experimental system does not follow classical percolative scaling laws for the effective volume fraction near the percolation threshold, it is impossible to determine the percolation threshold for this system via the classical approach.

TABLE 3.3 LINEAR REGRESSION ANALYSIS OF EXP 3 AND EXP 4 SQUARE ROOT OF TIME RELEASE PROFILES

Experiment	Ø	Slope $\times 10^5$ ($g/s^{1/2}$)	Intercept (g)	Correlation Coefficient	Std. Error of Regression	Number of Observ.
EXP 3	0.064	1.30	0.0013	0.997	0.00041	39
		(0.03)	(0.0004)			
	0.083	1.9	0.001	0.98	0.00076	11
		(0.3)	(0.001)			
	0.103	2.34	0.0026	0.9994	0.00038	39
		(0.03)	(0.003)			
	0.141	2.88	0.0056	0.998	0.00079	40
		(0.05)	(0.0007)			
	0.184	3.87	0.0057	0.9991	0.00076	39
		(0.05)	(0.0007)			
	0.228	5.51	0.004	0.998	0.00126	39
		(0.09)	(0.001)			
EXP 4	0.021	0.335	0.0002	0.998	0.00008	21
		(0.009)	(0.0001)			
	0.035	0.761	0.0000	0.9994	0.00010	19
		(0.013)	(0.0001)			
	0.051	1.19	0.0010	0.998	0.00024	19
		(0.03)	(0.0003)			
	0.059	1.81	0.0010	0.9997	0.00018	23
		(0.02)	(0.0002)			
	0.094	2.07	0.0007	0.9994	0.00032	25
		(0.03)	(0.0004)			
	0.088	2.49	-0.0006	0.997	0.00083	26
		(0.07)	(0.0009)			

Values in parentheses are confidence intervals calculated at 95% confidence.

TABLE 3.4 SUMMARY OF ALL PERCOLATION PARAMETERS OBTAINED FROM EXPERIMENTAL RESULTS

Experiment	$\emptyset_d$	ε	$\emptyset^A$	Slope x 10^5 ($g/s^{1/2}$)	D_B x 10^6 (cm^2/s)	$\emptyset^E$ (exp)
EXP 4	0.011	0.01	0.021	0.34	0.053	0.004
EXP 4	0.025	0.01	0.035	0.76	0.120	0.009
EXP 4†	0.041	0.01	0.051	1.19	0.179	0.014
EXP 3	0.044	0.02	0.064	1.30	0.200	0.015
EXP 4	0.059	0.00	0.059	1.81	0.289	0.022
EXP 3	0.063	0.02	0.083	1.88	0.292	0.023
EXP 4	0.074	0.02	0.094	2.07	0.301	0.023
EXP 4	0.088	0.00	0.088	2.49	0.367	0.028
EXP 3	0.083	0.02	0.103	2.34	0.343	0.027
EXP 3†	0.121	0.02	0.141	2.88	0.356	0.028
EXP 3	0.164	0.02	0.184	3.87	0.474	0.037
EXP 3	0.208	0.02	0.228	5.51	0.758	0.059
EXP 1†	0.243	0.02	0.263	7.32	1.14	0.089
EXP 1	0.256	0.02	0.276	7.56	1.16	0.090
EXP 2	0.287	0.02	0.307	9.77	1.73	0.134
EXP 2	0.301	0.02	0.321	9.92	1.70	0.132
EXP 1	0.328	0.02	0.348	11.82	2.21	0.171
EXP 2	0.346	0.02	0.366	14.15	3.00	0.233
EXP 1	0.373	0.02	0.393	15.30	3.26	0.253
EXP 2	0.382	0.02	0.402	15.98	3.47	0.269
EXP 1	0.420	0.02	0.440	18.56	4.26	0.330
EXP 2	0.455	0.02	0.475	21.11	5.09	0.394
EXP 1	0.470	0.02	0.490	21.33	5.03	0.390
EXP 2	0.502	0.02	0.522	24.42	6.17	0.478

†Indicates tablets used in analysis of microstructure experiments.

By definition:

$$\emptyset = \emptyset_d + \varepsilon = \emptyset^A + \emptyset^I = \emptyset_d^A + \varepsilon + \emptyset^I$$

for $\emptyset^I = 0$:

$$\emptyset = \emptyset_d + \varepsilon = \emptyset_d^A + \varepsilon = \emptyset^A$$

and since ε is a constant: $\emptyset_d = \emptyset_d^A$.

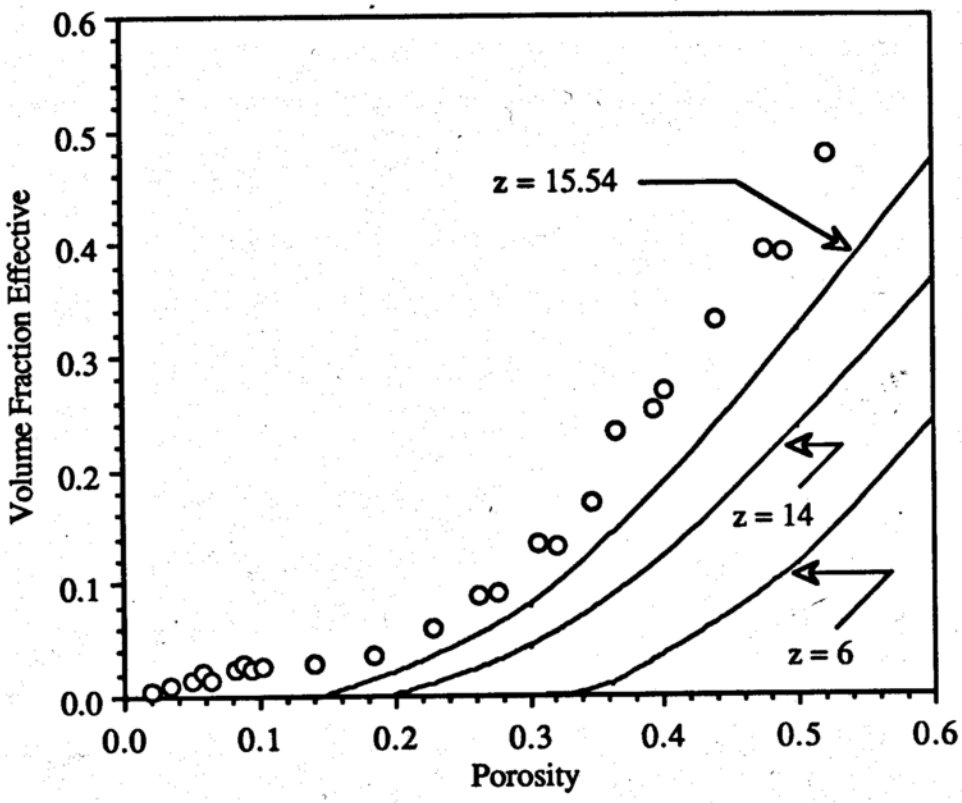


Figure 3.4 Experimental Volume Fraction Effective Results for the Benzoic Acid/Poly(vinyl stearate) System Compared to Theory. Open circles are experimental data points. All three lines are simulations, the Voronoi tessellation (z = 15.54),[9] the Tetrakaidecanoic tessellation (z = 14),[9] and the simple cubic lattice (z = 6).[13]

B. Analysis of Nonclassical Percolating Systems

The results of Section A of this Chapter indicate that the benzoic acid/poly(vinyl stearate) system exhibits nonclassical percolative transport near and below the apparent threshold of the system. Also, unlike classical percolating systems, the benzoic acid/poly(vinyl stearate) system does not follow the expected percolation scaling laws near the threshold; this makes it virtually impossible to determine the threshold based on classical accessible and/or effective scaling laws.

This Section will address the issue of applicable nonclassical percolating systems. The experiments conducted in this Section will elucidate the mechanisms for the observed nonclassical behavior and will provide support for the model developed in Chapter IV.

1. CHANGING MICROSTRUCTURE

a) Contribution of Osmotic Pressure to Transport

An analysis of the effect of osmotic pressure resulting from the dissolution of benzoic acid entrapped within the poly(vinyl stearate) tablet matrix is undertaken in this section. In the context of nonclassical percolative transport, the increased pressure associated with the dissolution of the conducting material within the matrix could hypothetically alter the microstructure by rupturing membranes of poly(vinyl stearate) separating benzoic acid particles. The resulting experimental observation, in terms of transport, would be an enhancement of transport through the matrix caused by artificially induced conducting pathways. The incidence of enhanced transport would be most evident in the region close to the percolation threshold. In the region slightly above the threshold, a large fraction of the conducting particles exist in a continuous, highly tortuous pathway spanning the lattice. All other conducting sites exist as isolated clusters of material. Slightly below the threshold, the sample spanning pathway theoretically does not exist, but a small change in the volume

fraction conducting in the direction of the threshold would result in the appearance of a sample spanning pathway through which transport could occur.

As indicated in Chapter II, the osmotic pressure of a saturated solution of benzoic acid was matched with that of the dissolution medium by adding KCl. Table 3.5 shows the resulting measured osmotic pressures.

After obtaining isosmotic solutions of saturated benzoic acid and dissolution medium, kinetic release rates were measured in osmotically matched and unmatched solutions. Benzoic acid/poly(vinyl stearate) tablets with compositions of 25, 30, 35, 40, and 45% benzoic acid by weight were evaluated. The 35% by weight tablet release kinetics were analyzed under two conditions, isosmotic dissolution medium and nonisosmotic dissolution medium. The extent of variation of the slopes of the resulting square root of time release profiles were utilized as an indicator of the extent of osmotic pressure effect on the release characteristics of the benzoic acid/poly(vinyl stearate) system. Results are listed in Table 3.6.

The experimental results indicate that the osmotic pressure produced by a saturated solution of benzoic acid does not alter the release profiles. It can therefore be concluded that these experimental conditions do not change the internal porous microstructure of the tablets. The coordination of the benzoic acid/poly(vinyl stearate) system remains a constant throughout the duration of release.

TABLE 3.5 ISOSMOTIC SOLUTION PREPARATION

Solution	Osmotic Pressure (mmol/kg)	Conc. KCl (g/L)
Saturated Benzoic Acid Solution	101.0	n/a
Dissolution Medium without KCl	37	0
Dissolution Medium with KCl	101.0	2.82

TABLE 3.6 COMPARISON OF BENZOIC ACID RELEASE RATES INTO OSMOTICALLY MATCHED AND UNMATCHED BUFFER SOLUTIONS[9]

	Slope Of Mass Released versus Square Root Of Time ($g/s^{1/2} \times 10^5$)	
Drug Load ($Ø_d$)	Unmatched Solution (pH 2 buffer)	Isosmotic Solution (pH 2 buffer + KCl)
0.21	5.5 ± 0.1	5.6 ± 0.1
0.26	7.6 ± 0.5	7.5 ± 0.2
0.30	9.9 ± 0.7	9.8 ± 0.2
0.38	16 ± 1	12.7 ± 0.3

[9]The buffer solution is considered matched if it is isosmotic with a saturated solution of benzoic acid.

Confidence interval calculated at 95% confidence.

2. CHARACTERIZATION OF BIPHASIC CONDUCTING SYSTEMS

a) Viscosity Average Molecular Weight of Poly(vinyl stearate)

Based on the method described in Chapter II, solutions of poly(vinyl stearate) dissolved in benzene were prepared and their "time-to-drain" values were measured with respect to that of pure benzene. Table 3.7 lists the solution concentrations utilized and the resulting drain times, relative drain times, and reduced viscosities.

A plot of the reduced viscosity as a function of concentration (Figure 3.5) has an intercept on the reduced viscosity axis of 0.1340 dl/g which is the intrinsic viscosity (Equation (2.7)). This translates to a viscosity average molecular weight of 1,870 Daltons using the Mark-Houwink relationship stated in Chapter II. For the repeat unit of poly(vinyl stearate), $(C_{20}H_{38}O_2)_n$, using a calculated molecular weight per repeat unit of 310.4 Daltons, this translates to an average chain length of 6 repeat units. The term "polymer" should therefore not be used with poly(vinyl stearate), but rather, the term "oligomer" is more appropriate.

TABLE 3.7 REDUCED VISCOSITIES FOR POLY(VINYL STEARATE)/BENZENE SOLUTIONS AT 25°C

Solution Concentration (g/dl)	Drain Time (sec)	Relative Drain Time (sec)	Reduced Viscosity (dl/g)
0.000 (pure benzene)	60.1 (0.2)	1.000	n/a
0.409	63.5 (0.1)	1.057	0.1394
0.900	67.9 (0.1)	1.130	0.1444
1.993	78.7 (0.1)	1.309	0.1550
2.961	90.2 (0.1)	1.501	0.1692

Values in parenthesis are standard deviations based on five evaluations.

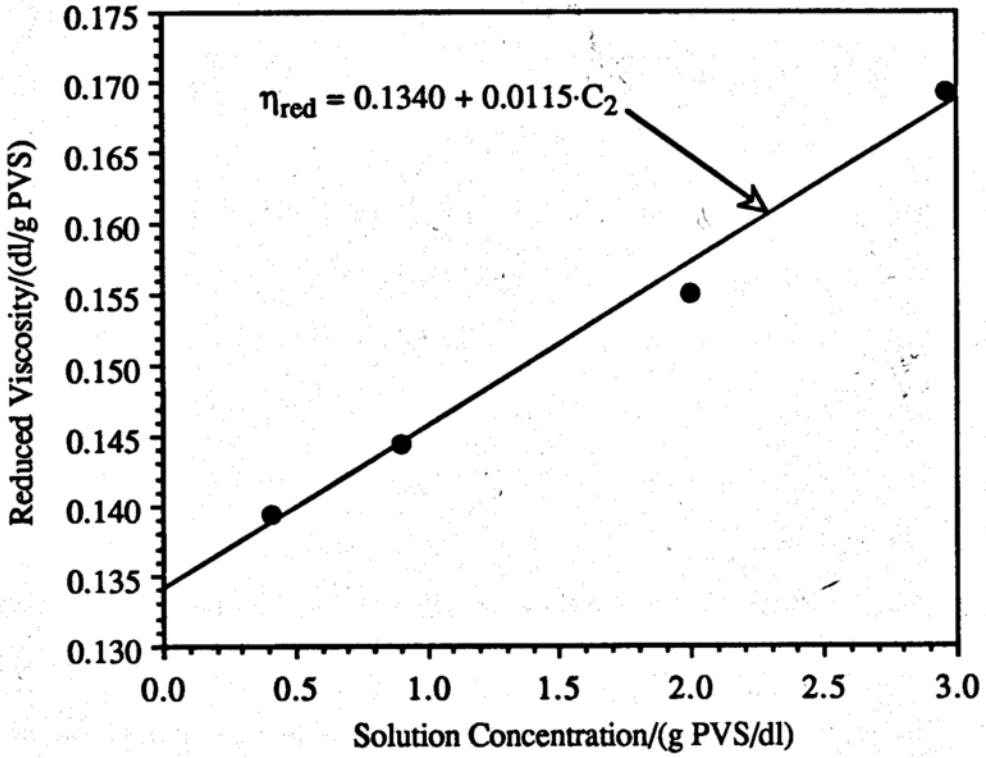


Figure 3.5 Determination of the Intrinsic Viscosity of Poly(vinyl stearate) Based on Reduced Viscosity Results. Solid circles are experimental data, solid line is the linear regression line for the four points.

b) Melting Point and Heat of Fusion of Poly(vinyl stearate)

The results from the DSC scans taken of pure polymer indicated a first order phase transition at 49.37°C with an onset temperature of 41.93°C. The peak spanned a temperature range of 37.37 to 60.28°C and from the area under the curve, the ΔH_{fus} was calculated to be 23.02 cal/gram. Scan rate was 20 degrees per minute over a temperature range of –13°C to 127°C. Poly(vinyl stearate) sample weight was 11.33 mg of pure, unpurified powder.

Literature values[78] for purified poly(vinyl stearate) indicate a first order phase transition at 51.7°C from refractive index measurements and a range of 50.5 to 51.2°C from polarizing light microscopy when evaluated under heating conditions. The authors of this work indicated the presence of a hysteresis effect in either method of evaluation. The cooling first order phase transitions showed lower melting temperatures; 45.6°C from refractive index work, and a range of 44.0 to 46.5°C from polarizing light microscopy. These scientists remarked on the relatively low molecular weights obtained in the synthesis of polymers obtained from vinyl esters of long-chain fatty acids. The poly(vinyl stearate) sample synthesized and analyzed in their research was polymerized in bulk at 75°C using benzoyl peroxide as an initiator.

c) Biphasic Conductivity

The aspect of biphasic conduction as a nonclassical contribution is addressed here. The ability of poly(vinyl stearate) to act as a conducting phase to the benzoic acid is investigated through permeability experiments. The transport model will be discussed and the results presented.

The analysis of the transport of benzoic acid through the polymer was conducted as outlined in Chapter II. The overall numerical value of the permeability constant is not important to this research, only the ability or inability of benzoic acid to transport through a disc or film of poly(vinyl stearate) is crucial. If benzoic acid does have the ability to transport through pure polymer, the percolating system will be nonclassical and biphasic in nature. This experiment will therefore confirm whether or not the isolated and dead end clusters have the ability to contribute to transport.

(i) PERMEABILITY MODEL:

Transport through the polymer was modeled as transport through a thin film of uniform initial concentration with surface concentrations different. The model reproduced here is discussed by Crank[76] in his text entitled The Mathematics of Diffusion. The relationship describing transport through a film where the initial membrane concentration is zero and the receiver cell concentration is maintained at essentially zero throughout the experiment is

$$\frac{Q_t}{lC_1} = \frac{D_B t}{l^2} - \frac{1}{6} - \frac{2}{\pi^2}\sum_{1}^{\infty}\frac{(-1)^2}{n^2}\exp\left(\frac{D_B n^2 \pi^2 t}{l^2}\right), \qquad (3.1)$$

where Q_t represents the total amount of diffusing substance which has passed through the membrane in time t, l is the membrane thickness, C_1 is the concentration of the donor compartment, and D_B is the bulk diffusion coefficient.

In terms of partitioning, Equation (3.1) becomes

$$\frac{Q_t}{lC_1} = \frac{Pt}{l} - \frac{1}{6} - \frac{2}{\pi^2}\sum_{1}^{\infty}\frac{(-1)^2}{n^2}\exp\left(-\frac{Pn^2\pi^2 t}{l}\right), \tag{3.2}$$

where P is the permeability and is equal to the product of the bulk diffusion coefficient and the partition coefficient divided by the membrane thickness as shown in Equation (3.3).

$$P = \frac{D_B \cdot K}{l} \tag{3.3}$$

where K is the partition coefficient.

For the steady-state situation, Equation (3.2) reduces to

$$Q_t = PC_1 \cdot \left(t - \frac{1}{6P}\right). \tag{3.4}$$

From Equation (3.4), a plot of Q_t versus t has an intercept L_t on the t-axis as given by

$$L_t = \frac{1}{6P}, \tag{3.5}$$

from which the permeability, P, can be obtained.

Assumptions associated with this derivation are: (1) C_1 is a constant, (2) the amount of benzoic acid originally in the membrane is zero, (3) the concentration in the receiver cell is dilute compared to C_1, (4) the volume of both compartments remains constant, and (5) the diffusion coefficient is a constant.

(ii) PERMEABILITY RESULTS:

Results obtained from the experiment outlined in Chapter II, are shown in Figure 3.6. The discs composed of poly(vinyl stearate) showed a very wide variability in release characteristics. This variability is more than likely due to the production of shear planes during compression of the pure polymer discs. The shear planes are essentially cracks within the ideally nonporous disc and would ultimately produce a greater degree of transport than that of the cast films. The waxy nature of the polymer material lends itself to the ability to form these fissures. Photomicrographs taken of a pure compressed poly(vinyl stearate) disc show large cracks or fissures resembling shear planes (Figure 3.7).

Due to the high degree of variability of the discs, the cast film data were utilized to calculate the permeability. Based on three samples, the permeability, P, was calculated as $4 \pm 2 \times 10^{-7}$ cm/sec at 95% confidence. Table 3.8 gives results for all six experiments.

From these results, it can be concluded that transport of benzoic acid through the pure polymer or "oligomer" is possible. A more detailed discussion of this matter will be presented in the next Section.

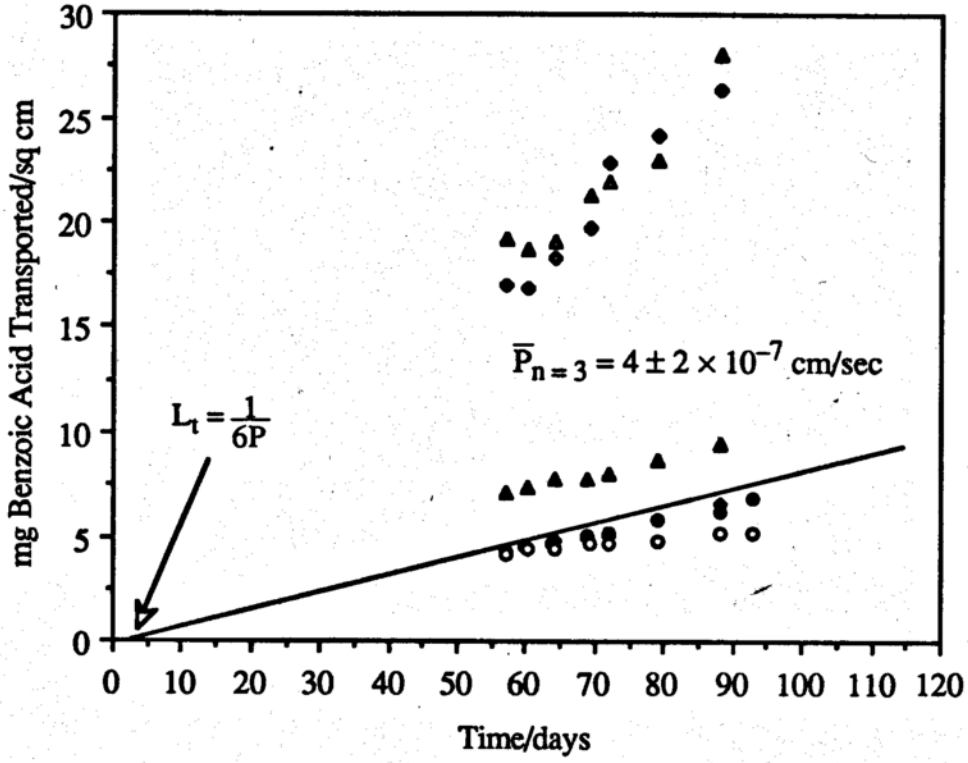


Figure 3.6 Permeability of Poly(vinyl stearate) Discs and Films to Benzoic Acid. Open symbols represent data from compressed discs while closed symbols represent data from cast films. Calculated profile (solid line) is based on Equation (3.4) using the shown average permeability and thickness calculated from all three cast films.

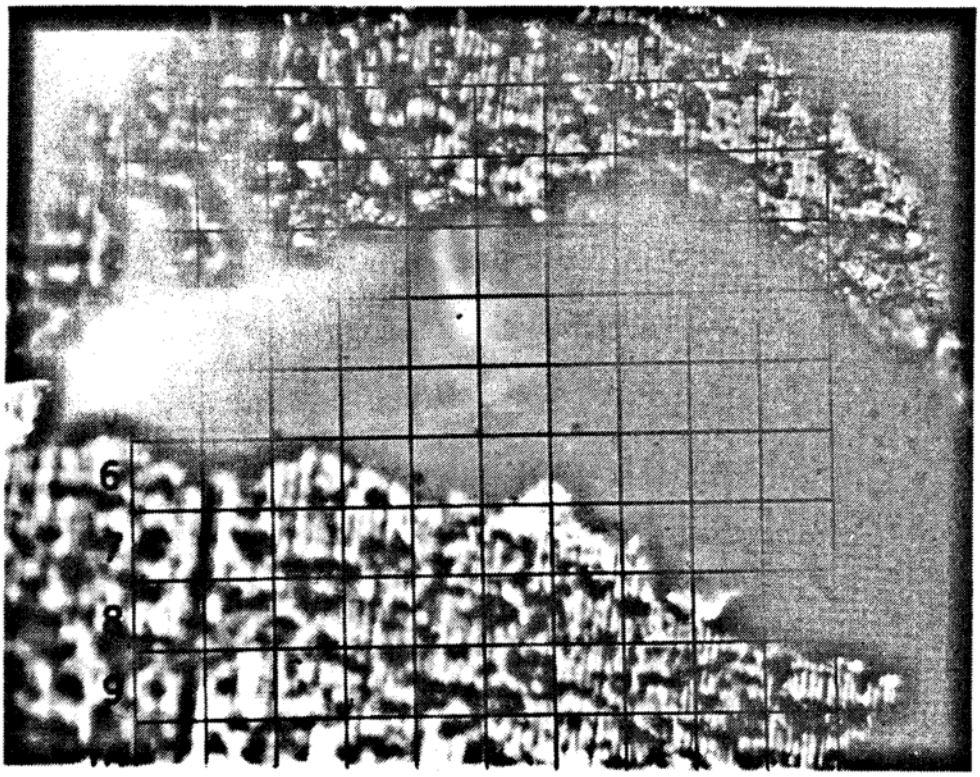


Figure 3.7 Photomicrograph of Compressed Disc of Poly(vinyl stearate) Surface. Scale: Each individual square with the matrix is 16.7 μm. The total grid size is 167 × 167 μm.

TABLE 3.8 PERMEABILITY RESULTS FROM POLY(VINYL STEARATE) CAST FILMS AND COMPRESSED DISCS

Bath	1	2	3	4	5	6
Sample	Film	Film	Film	Disc	Disc	Disc
$P \times 10^7$	4.04	3.5	5.9	3.49	16.5	17.4
(cm/sec)	(0.03)	(0.3)	(0.2)	(0.09)	(0.2)	(0.4)
Average Permeability of Films				$4 \pm 2 \times 10^{-7}$ cm/sec		

Values in parenthesis are confidence intervals calculated at 95% confidence.

3. CHARACTERIZATION OF THE POROUS MICROSTRUCTURE

Three tablets were characterized in terms of their porous microstructure. They had volume fractions accessible of 0.051, 0.141, and 0.263. These tablets were chosen since they theoretically would be below the percolation threshold, near and above the threshold, and far above the threshold. Therefore, in the tablet below the threshold, only isolated clusters of material would be present. Similarly, for the sample near and above the threshold, a sample spanning cluster should be present along with isolated clusters of material. For the tablet far above the threshold, the pore structure should be very well defined and hardly any isolated clusters should be apparent.

Color illustrations of the reconstructions are presented in the following subsection along with color stereo images for viewing with three-dimensional stereo glasses. Porosities calculated by the three-dimensional reconstruction program will be compared and contrasted with those based on drug load and inherent porosity.

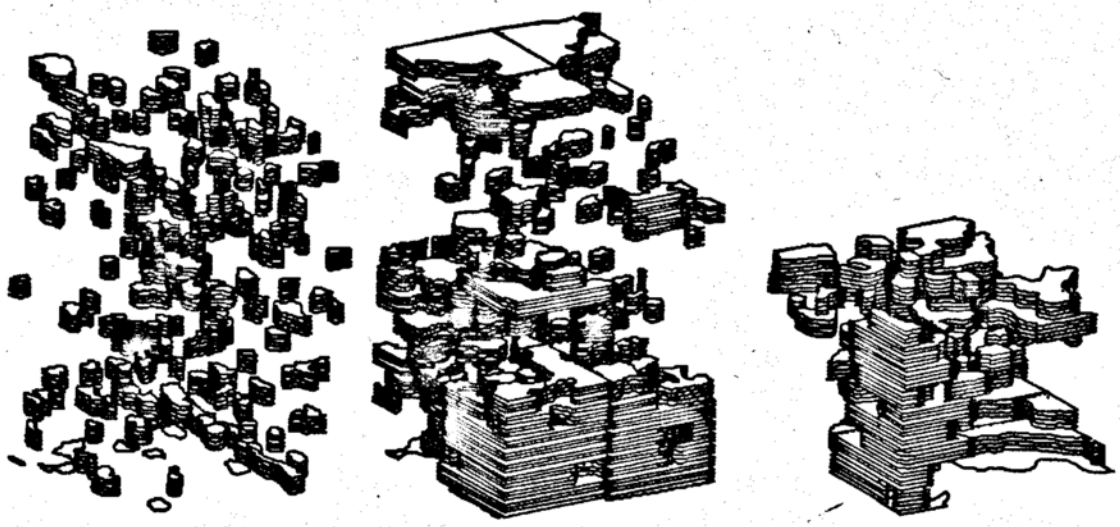
a) Three-Dimensional Reconstructions

Twenty one 8.33 μm thick slices of $\emptyset^A = 0.051$ and 0.141 were taken and reconstructions were done on one position of the tablet surface. Ten 8.33 μm thick slices of $\emptyset^A = 0.263$ were taken and reconstructed into a three-dimensional images of a portion of the tablet surface.

Figure 3.8 shows a comparison of the three tablets at dimensions of $100 \times 100 \times 167$ μm for $\emptyset^A = 0.051$ and 0.141; $\emptyset^A = 0.263$ has dimensions of $100 \times 100 \times 83$ μm. The back section ($100 \times 50 \times 167$ or 83 μm) of each one of the reconstructions is blue while the front section ($100 \times 50 \times 167$ or 83 μm) is red. Figure 3.9 shows the same sections of the three tablets as Figure 3.8, but with the back blue section removed.

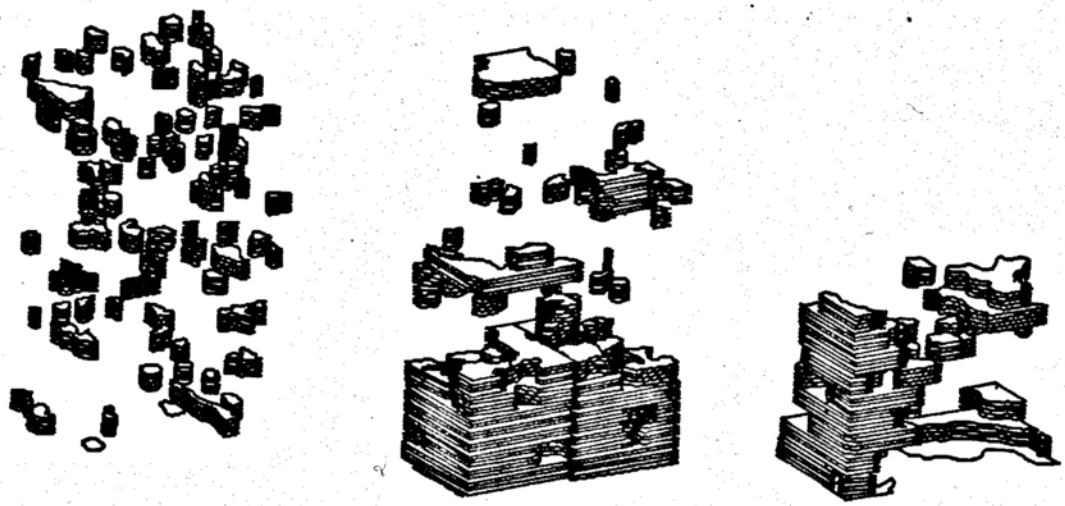
Figures 3.10 - 3.13 are stereo images of $\emptyset^A$ = 0.051, 0.141, and 0.263 respectively. They offer the same views as shown in Figure 3.8 but in a three-dimensional format offset of +3° and –3° from the y-axis for viewing with stereo glasses.

From these three-dimensional reconstructions, it can be concluded that the micropositioner methodology allowed for precise alignment of the two-dimensional images. The pore structures reproduced from this extensively labor intensive method depict a complex underlying microstructure. The porous microstructure, with respect to the drug loads analyzed and the apparent percolation threshold, follow the expected structural trend of complexity and arrangement. As the drug load increases to values above the percolation threshold, the sample spanning cluster becomes the dominant structure with the matrices. Below the percolation threshold, the isolated clusters appear to dominate, and near and above the threshold, the isolated clusters and sample spanning cluster both exist. A more detailed discussion will be offered in the next Section.



(a) (b) (c)

Figure 3.8 Three Dimensional Reconstructions of the Pore Structure. Dimensions of 100 μm × 100 μm × 167 μm or 83 μm. $\emptyset^A$ = 0.051 (a), 0.141 (b), and 0.263 (c). Back section of all three figures is blue while front section is red. Blue and red sections have dimensions of 100 μm × 50 μm × 167 μm or 83 μm. This illustration is a "color original" and therefore some loss of detail may occur in copies.



(a) (b) (c)

Figure 3.9 Three Dimensional Reconstructions of the Pore Structure. Dimensions of 100 μm × 50 μm × 167 μm or 83 μm. $\emptyset^A$ = 0.051 (a), 0.141 (b), and 0.263 (c). This figure is drawn in red. Same figure as shown on previous page without the back section. This illustration is a "color original" and therefore some loss of detail may occur in copies.

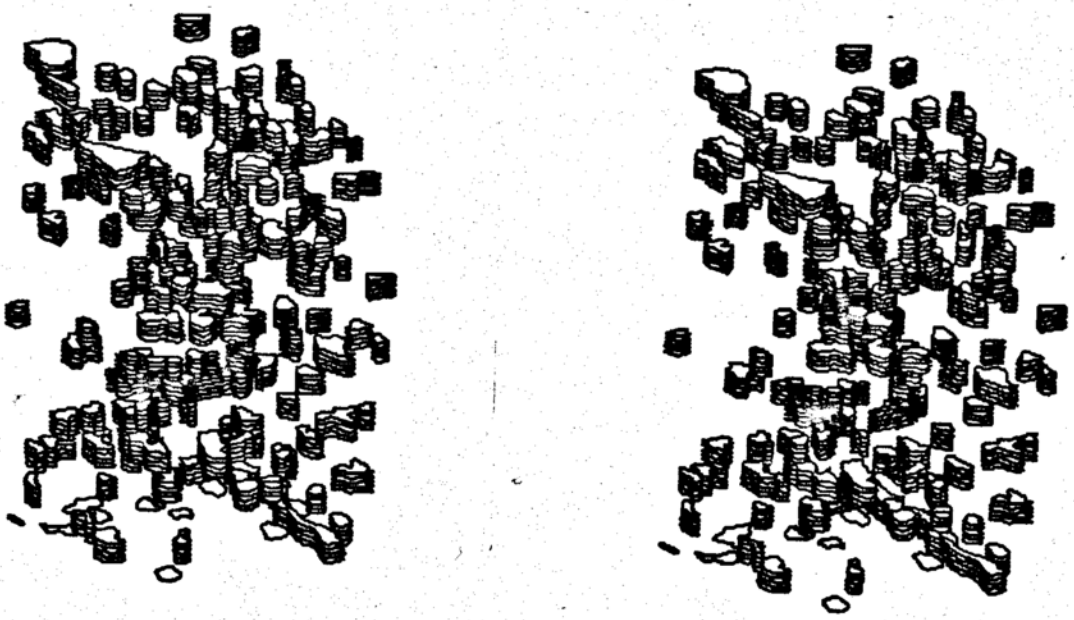


Figure 3.10 Three Dimensional Reconstruction For Stereo Viewing, Total Porosity = 0.051. Dimensions of figures shown are 100 μm × 100 μm × 167 μm. Back sections of both figures are blue while front sections are red. Blue and red sections have dimensions of 100 μm × 50 μm × 167 μm. Right and left images are offset by ±3° from the y-axis. Strong evidence of isolated clusters are apparent; this tablet is below the threshold. This illustration is a "color original" and therefore some loss of detail may occur in copies.

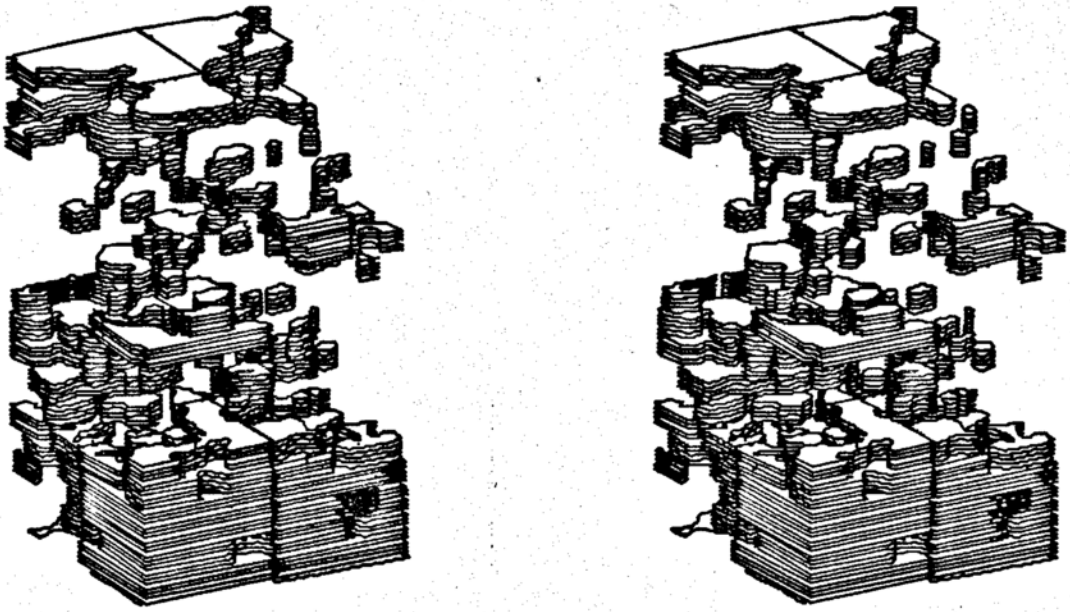


Figure 3.11 Three Dimensional Reconstruction For Stereo Viewing, Total Porosity = 0.141. Dimensions of figure shown are 100 μm × 100 μm × 167 μm. Back sections of both figures are blue while front sections are red. Blue and red sections have dimensions of 100 μm × 50 μm × 167 μm. Right and left images are offset by ±3° from the y-axis. This tablet is near and above the threshold. Isolated clusters and the sample spanning cluster are both present. This illustration is a "color original" and therefore some loss of detail may occur in copies.

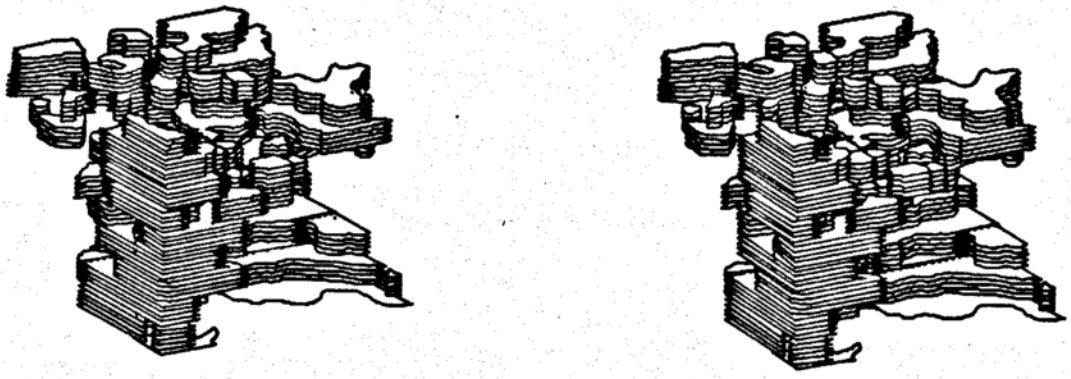


Figure 3.12 Three Dimensional Reconstruction For Stereo Viewing, Total Porosity = 0.263. Dimensions of figures shown are 100 μm × 100 μm × 83 μm. Back sections of both figures are blue while front sections are red. Blue and red sections have dimensions of 100 μm × 50 μm × 83 μm. Right and left images are offset by ±3° from the y-axis. Strong pore structure exists throughout the matrix. This tablet is far above the percolation threshold. This illustration is a "color original" and therefore some loss of detail may occur in copies.

b) Estimation of Porosity Based on Reconstructions

The PC3D software package contained a module through which the total volume of the traced polygons (pores) could be calculated. This volume divided by the total volume of the cube traced, is the porosity of the section. If the porosity calculated by the PC3D software matched the porosities of the individual tablets based on drug load and inherent porosity, then the pore structure of the sample section is assumed characteristic of the entire tablet. Results of this study are given in Table 3.9.

From Table 3.9, the reconstruction porosities compare fairly well with the experimentally determined porosities, indicating that the analyzed microstructure is representative of the entire tablet microstructure. The largest deviation appears near and above the theoretical percolation threshold of the system. This is expected since this is the concentration region in which the pore structure is changing most rapidly.

TABLE 3.9 COMPARISON OF EXPERIMENTAL POROSITIES TO PC3D CALCULATED VALUES FOR THE MICROTOMED TABLETS

$Ø^A$	PC3D Calculations			Experimental Ø
	Volume of Polygons (μm^3)	Total Sectioned Volume (μm^3)	Reconstruction Ø	
0.051	2.866×10^5	4.879×10^6	0.059	0.051
0.141	8.765×10^5	4.879×10^6	0.180	0.141
0.263	5.662×10^5	2.323×10^6	0.244	0.263

C. Overall System Results

1. OSMOTIC PRESSURE RESULTS

The results from the osmotic pressure studies indicate that osmotic pressure does not enhance release rates of benzoic acid from poly(vinyl stearate) matrices. The slopes of the matched and unmatched kinetic profiles at low drug loads are not significantly different from each other as shown in Table 3.6. It can therefore be concluded that the coordination of the benzoic acid/poly(vinyl stearate) matrix does not change with release of benzoic acid.

2. TRANSPORT THROUGH POLY(VINYL STEARATE) RESULTS

Based on the results from this section, benzoic acid has the ability to transport through pure poly(vinyl stearate), either in the form of cast films or compressed discs. Taking the other physical properties measured in this section into consideration (listed in Table 3.10), the low melting point and low molecular weight, along with the method of micronization utilized to reduce the particle size of the polymer, transport is most likely due to a combination of polymer chain "wiggling" and water uptake by the amorphous regions of the polymer.

A more amorphous nature may have been imparted to the polymer during the micronization procedure. Amorphous regions are known to have a much greater affinity for water than hydrophobic crystalline regions[79] and the transport of benzoic acid would be imminent due to an enhanced free volume caused by the water. The water enhanced solubility causes a free volume change within the matrix. Therefore, the amorphous nature of the polymer and the low number of repeat units per polymer chain both contribute to chain motion within the solid matrix and subsequently both enhance the partitioning of benzoic acid through the poly(vinyl stearate).

TABLE 3.10 SUMMARY OF POLY(VINYL STEARATE) MATERIAL PROPERTIES

Property	Result	Method
$\overline{M}_v$	1,870 Daltons	Intrinsic Viscosity
	~6 repeat units	
T_m	49.4°C	DSC
ΔH_{fus}	23.02 cal/g	DSC
P†	4×10^{-7} cm/s	Diaphragm Cell

†permeability constant.

In terms of classical percolation theory, benzoic acid, as the "conducting" material, has the ability to diffuse through pores as well as through the polymer itself. There are systems which exhibit such behavior in percolation theory. The percolation scientists have described this transport in terms of "termites".[53,54] A termite has the ability to diffuse slowly (or chew) through the nonconducting phase. When the termite encounters a pore, it rapidly traverses the void (or skates) until it hits the other side. The termite then continues on its way by again slowly making its way through the classically nonconducting phase. This model has been invoked in bond percolation systems which have superconducting as well as normal metallic bonds.[53,54]

The ability of benzoic acid to transport through the polymer also brings up some interesting points about the nontransporting clusters within the matrix. In general, since isolated clusters and dead end clusters do not contribute to transport, they do not enter the transport relationship. In this nonclassical system which allows diffusion through the pure classically "nonconducting" phase, however, both isolated and dead end clusters must be accounted for in the bulk transport relationships. This inclusion of morphological properties with transport properties will be addressed in the Discussion Chapter to follow.

3. MICROSTRUCTURE MORPHOLOGY RESULTS

The complex microstructure evident at all levels of drug load is readily apparent from Figures 3.8 - 3.12. The more complex the microstructure of a system, the lower the percolation threshold. The inherently complex nature of the underlying microstructure of the benzoic acid/poly(vinyl stearate) system therefore results in a naturally low percolation threshold.

Literature references of low threshold percolating systems have been discussed previously[55,56] for systems composed of aluminum oxide fleece and aerogels. The low threshold values of these systems are generally attributed to oriented microstructures. Even though it is difficult to discern whether or not any definite orientation or bias exists in the three-dimensional reconstructions for the benzoic acid/poly(vinyl stearate) matrix system discussed in this research, very fine chain-like structures appear to exist in the lowest drug load reconstruction (Figures 3.8 and 3.10). Chain-like structures have been observed in this research during the evaluation of the particle size of benzoic acid. Samples of pure benzoic acid powder, when observed under the scanning electron microscope, exhibited definite self-associating tendencies (Figure 3.13). If there is an orientation of the benzoic acid particles, the transport would be characterized as nonuniversal. Since this characterization is beyond the scope of this research, the system will be treated mathematically as universal with an understanding that the tendencies of the transport could be interpreted as nonuniversal.

Unfortunately, the methodology utilized to evaluate the benzoic acid/poly(vinyl stearate) tablet morphological microstructure allowed only for a qualitative analysis of the underlying pore structure. Therefore the actual value of the percolation threshold and the coordination of the benzoic acid/poly(vinyl stearate) matrix cannot be calculated directly by this method.

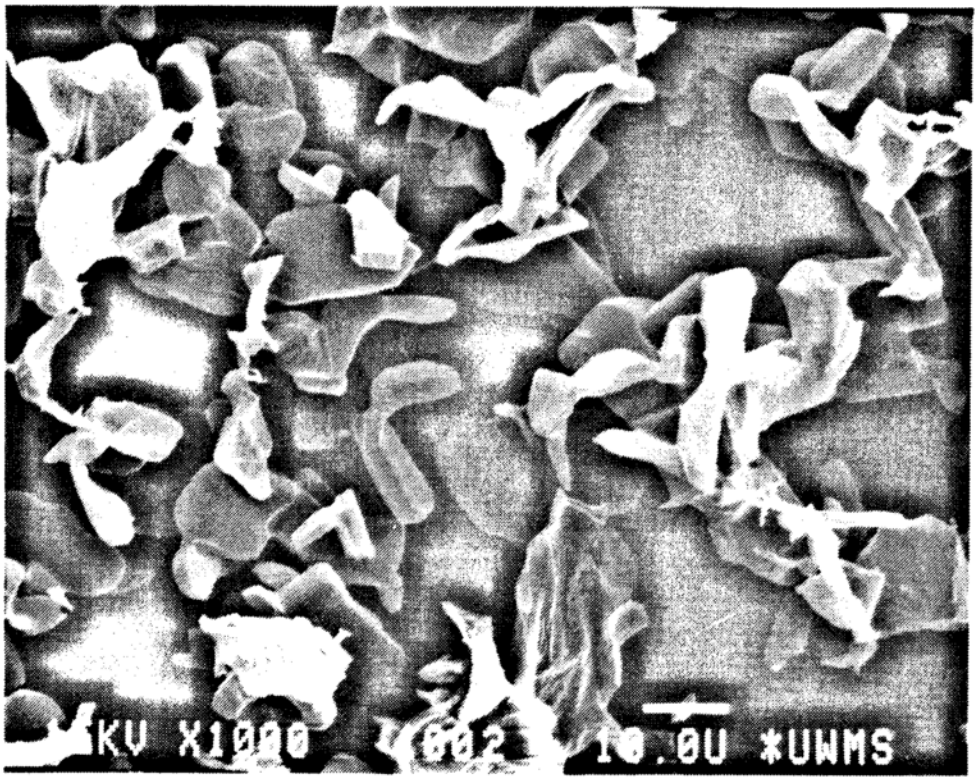


Figure 3.13 Scanning Electron Photomicrograph of Micronized Particles of Pure Benzoic Acid Powder. Chain-like structures of benzoic acid particles indicate possible self-associating tendencies of the pure powder.

4. CONCLUSIONS

The conclusions which can be made from the experimental results discussed in this Chapter are first, that the system is nonclassical in terms of percolative transport. Second, this nonclassical behavior is basically due to the ability of the nonconducting phase to act as a conducting phase. The nonclassical system is therefore a biphasic percolating system. Third, the complex microstructure of the system results in an inherently low percolation threshold for the system. This complex microstructure may be oriented in space, in which case the transport would be classified as nonuniversal as well as nonclassical. Due to the difficulty in characterizing the orientation of the underlying microstructure, the system will be mathematically treated as a nonclassical percolating system.

The evaluation of the percolation threshold of this system as well as the nonclassical transport model will be addressed in Chapter IV.

IV. DISCUSSION

Results discussed in Chapter III indicated that the system composed of benzoic acid and poly(vinyl stearate) is a nonclassical percolating system. The nonclassical nature was concluded to be attributed to the ability of the "nonconducting" phase to act as a conducting phase.

In the first Section of this Chapter, a nonclassical percolative transport and cluster diffusion model will be derived based on the experimental observations of the previous Chapter. The second Section of this Chapter addresses the evaluation of the nonclassical model. The model will be evaluated based on comparison to experimental bulk diffusivities, comparison to scaling theory, and contributions to bulk transport.

A. Development of the Nonclassical Percolative Transport Model

In this Section a model will be developed based on classical and nonclassical percolative transport scaling parameters. The model, which is an unusual combination of morphological properties and percolative transport properties, will be evaluated in terms of the experimentally determined bulk diffusivities. Three parameters will be fitted to twenty four sets of experimental data by using multiple nonlinear regression analysis.

After the model is discussed and developed, the percolation threshold of the system will be assessed. The definition of the percolation threshold for this nonclassical system will still be based on a continuous sample spanning cluster of conducting sites spanning the lattice in the direction of transport. The conducting sites, in this system, will be the benzoic acid particles plus the inherent porosity of the matrix. The percolation threshold is, therefore, that volume fraction of benzoic acid plus inherent porosity which first spans the tablet in the direction of transport; this is a definition that does not differ from the classical theory.

The use of bulk diffusivity will be utilized throughout the duration of this dissertation to describe transport through the polymer discs. In classical percolation theory, the volume fraction effective is calculated relative to transport in a system where the volume fraction conducting is equal to one. In the nonclassical system discussed here, both phases are conducting medium for the benzoic acid. Therefore, there are two reference states to normalize the transport properties; pH 2 dissolution medium and poly(vinyl stearate). To eliminate the confusion associated with this situation, the observed bulk transport will not be normalized and the bulk diffusivity of benzoic acid through the porous polymer system will be utilized in modeling procedures. All percolative scaling laws can be applied to the bulk diffusivity as well as the volume fraction effective and identical trends will be observed in either case. Fitting of the transport model will be performed in terms of $D_B \times 10^6$ since the statistics program utilized would not provided accurate results for values as small as 10^{-6}. All graphs and equations will reflect this factor.

1. THE SYSTEM

a) Transport Near and Above the Percolation Threshold

As discussed in the previous chapter, the isolated and dead end clusters must be accounted for in the transport relationship of the benzoic acid/poly(vinyl stearate) system. These morphological properties don't normally contribute to transport, but in the situation where the classically "nonconducting" phase is a slowly conducting one, they must be taken into consideration. Therefore, contrary to classical percolation theory, which describes transport only in terms of the volume fraction effective, the relationship for bulk transport or bulk diffusivity of benzoic acid through the porous polymer near and above the percolation threshold is given as a linear combination of morphological and kinetic percolation parameters

$$D_B \propto \emptyset^E + \alpha \cdot (\emptyset^D + \emptyset^I), \qquad \emptyset > \emptyset_c, \tag{4.1}$$

where the transport relationship is composed of the classical percolative transport property, $\emptyset^E$, and the nonclassical percolation morphological properties, $\emptyset^D$ and $\emptyset^I$. The different proportionality constant preceding $\emptyset^D$ and $\emptyset^I$ reflects the transition from a morphological property to a transport property.

From percolation theory, it is known that the accessible volume fraction can be broken down into the dead end clusters and the backbone volume fraction. Also, the total porosity of the matrix, by mass balance, includes all the accessible volume fraction and all the isolated volume fraction. These two relationships can be written in the following forms

$$\emptyset^D = \emptyset^A - \emptyset^B \tag{4.2}$$

$$\emptyset^I = \emptyset - \emptyset^A. \tag{4.3}$$

Substitution of Equations (4.2) and (4.3) into Equation (4.1) yields the relationship describing transport near and above the percolation threshold

$$D_B \propto \emptyset^E + \alpha \cdot (\emptyset^A - \emptyset^B + \emptyset - \emptyset^A) \tag{4.4}$$

which, upon simplification, yields

$$D_B \propto \emptyset^E + \alpha \cdot (\emptyset - \emptyset^B). \tag{4.5}$$

The scaling laws for the volume fraction effective and the backbone volume fraction are known from percolation theory to be

$$\emptyset^E \propto (\emptyset - \emptyset_c)^{\mu}, \qquad \emptyset > \emptyset_c \tag{4.6}$$

$$\emptyset^B \propto (\emptyset - \emptyset_c)^{\gamma_b}, \qquad \emptyset > \emptyset_c \tag{4.7}$$

where in three dimensions the values of the universal exponents μ and γ_b are 2.0 and 0.9 respectively.[16,17] Substitution of Equations (4.6) and (4.7) into Equation (4.5), and eliminating the proportionality constant, yields

$$D_B = \varepsilon \cdot (\emptyset - \emptyset_c)^{\mu} + \alpha \cdot \emptyset - \vartheta \cdot (\emptyset - \emptyset_c)^{\gamma_b}, \tag{4.8}$$

for $\emptyset > \emptyset_c$.

Equation (4.8) is the nonclassical percolative transport relationship which describes transport of benzoic acid through porous poly(vinyl stearate) near and above the percolation threshold for the system. It is a relationship which contains the classical percolative transport property of the matrix with the nonclassical morphological properties of the system. This modified percolative transport equation therefore takes into account the nonclassical transport of benzoic acid through pure poly(vinyl stearate).

b) Transport Below the Percolation Threshold

The anomalous diffusion observed below the percolation threshold of the system is attributed to the transport of benzoic acid directly through poly(vinyl stearate). In a percolating system below its threshold, conducting material exists in isolated clusters only; the sample spanning cluster is absent and transport across the matrix is theoretically impossible. Therefore, below the percolation threshold

$$\emptyset^A = \emptyset^E = 0, \quad \emptyset < \emptyset_c, \tag{4.9}$$

since the sample spanning cluster is absent. It is important to note that since the accessible volume fraction equals zero, so do the backbone volume fraction and the dead end clusters. Also, since $\emptyset^A = 0$, the porosity, $\emptyset$, is equal to the isolated volume fraction

$$\emptyset = \emptyset^I, \emptyset < \emptyset_c. \tag{4.10}$$

The bulk diffusivity below the percolation threshold for the benzoic acid/poly(vinyl stearate) system is therefore given by

$$D_B \propto \emptyset, \quad \emptyset < \emptyset_c, \tag{4.11}$$

which can be derived directly from Equations (4.1) and (4.9). Eliminating the proportionality constant

$$D_B = \alpha \cdot \emptyset, \ \emptyset < \emptyset_c . \tag{4.12}$$

Equation (4.12) describes transport below the percolation threshold of a nonclassical percolating system. In the classical system, transport below the threshold is not possible due to the absence of the sample spanning cluster. The proportionality constant for porosity is assumed to be identical below and above the threshold.

2. DETERMINATION OF THE PERCOLATION THRESHOLD

Before the analysis of the model discussed in the previous section can be addressed, the percolation threshold of the benzoic acid/poly(vinyl stearate) system must be evaluated. The difficulty in determining the threshold from the experimental transport data lies in the lack of classical percolative transport scaling behavior near the threshold. The experimental volume fraction effective profile does not approach zero as the porosity approaches the percolation threshold of the system in the well-defined manner dictated by the universal scaling exponent and the pre-exponential factor.

From the scaling relationships discussed previously, it is readily evident that a ln-ln plot of the scaling laws will yield a straight line with the slope equal to the universal exponent. If a plot of ln $\emptyset^E$ versus ln $\emptyset$ is evaluated, the resulting plot will also be linear, indicating that a scaling relationship is evident.

A break in a ln $\emptyset^E$ versus ln $\emptyset$ plot would indicate a transition to another scaling law: transition to another dominating mechanism of transport. Transport mechanisms above and below the percolation threshold of the benzoic acid/poly(vinyl stearate) system will be different as is evident in the developed model. Below the percolation threshold, the dominant form of transport is through poly(vinyl stearate) via cluster diffusion. Far above the percolation threshold, the dominant form of transport is through the porous channels. In the region close to, but above, the percolation threshold, the transport mechanism consists of a combination of cluster diffusion (isolated and dead end clusters allowing transport from cluster to cluster as well as from cluster to sample spanning cluster) and percolative transport (transport on the sample spanning cluster). The ability of the benzoic acid particles to diffuse from an isolated cluster to a sample spanning cluster or through pure polymer into pockets of pores in a "nonskate"/"skate" manner would be a primary mechanism of transport in this transition region.

The resulting ln-ln plot of the bulk diffusivity data obtained from the kinetics experiments versus the system porosity is shown in Figure 4.1. This plot of the experimental data shows three distinct regions. The first region is indicative of scaling below the threshold (isolated cluster diffusion), the third region is scaling above the threshold (percolative transport dominating, but cluster diffusion in terms of isolated and dead ends still evident). The second region is a transition region between these two where the "skating" on clusters and diffusion through poly(vinyl stearate) as well as diffusion on the sample spanning cluster occurs to the same degree. The first break in the ln-ln plot is therefore the percolation threshold of the system.

Linear regression analysis on the three regions was performed and the results are given in Table 4.1. The intersection point of region I and II, and therefore the percolation threshold, was determined by simultaneously solving the first two linear relationships for the intersecting porosity value. At 95% confidence, the intersection point was determined to be 0.09 ± 0.02, which is slightly higher than the threshold originally calculated for this system.[1]

The low percolation threshold obtained for this system is, therefore, a quantity reflecting the complexity of the underlying porous microstructure. Regardless of the transport characteristics of the pure polymer, the experimentally determined threshold is still lower than the thresholds of the other fairly complex percolating lattice types such as the Voronoi and the tetrakaidecanoic tessellations.

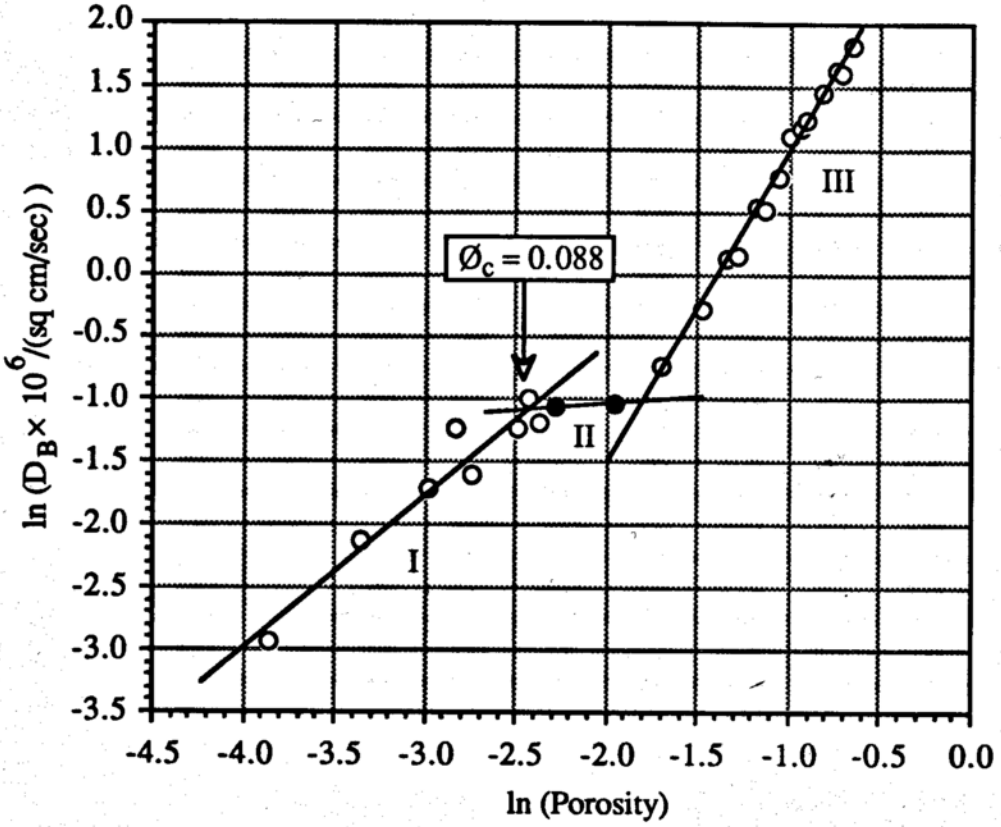


Figure 4.1 Estimation of the Percolation Threshold of the Benzoic Acid/ Poly(vinyl stearate) Tablet Matrix. A ln-ln plot of the experimentally determined bulk diffusivities versus the total matrix porosity. The individual points are experimental data. The solid lines are regression lines for each region as indicated by the Roman numerals. The intersection of the first two regions is taken to be the threshold of the system. The percolation threshold was evaluated to be 0.09 ± 0.02 at 95% confidence.

TABLE 4.1 LINEAR REGRESSION ANALYSIS FOR THE PERCOLATION THRESHOLD ESTIMATION OF THE BENZOIC ACID/POLY(VINYL STEARATE) SYSTEM

Region	Slope	Intercept	Correlation Coefficient	Std. Error of Regression	Number of Observations
I	1.2	1.8	0.96	0.18	8
	(0.3)	(0.9)			
II	0.12	-0.81	1.00	n/a	2
	(n/a)	(n/a)			
III	2.5	3.50	0.996	0.07	14
	(0.1)	(0.1)			
I/II	intersecting $\emptyset = 0.09 \pm 0.02$				

Values in parenthesis are confidence intervals calculated at 95% confidence.

3. NONLINEAR REGRESSION ANALYSIS

With the determination of the experimental percolation threshold of the system, evaluation of the nonclassical percolative transport model parameters can be undertaken. Nonlinear multiple regression analysis was carried out on the bulk diffusivity kinetic data by using a statistical software package (SYSTAT, Inc., Evanston, IL). Only three parameters were fit and the total number of data points was twenty four. A table of the statistical results for both above and below the threshold is given in Table 4.2. Residuals are plotted separately. Fits are compared to the experimental bulk diffusivity values in the next Section.

a) Estimation of the Nonclassical Percolative Transport Model Parameters Below the Percolation Threshold

From subsection 1 of this Section, Equation (4.12) was derived to describe transport below the percolation threshold of the system. By fitting Equation (4.12) with seven sets of experimental bulk diffusivity versus porosity data, the following result is achieved

$$D_B = 3.8 \times 10^{-6} \cdot \emptyset, \tag{4.13}$$

which is applicable for $\emptyset < \emptyset_c$.

The value of α was determined to be $3.8 \pm 0.6 \times 10^{-6}$ at 95% confidence using the standard error of the estimate, as reflected in Equation (4.13). Table 4.2 lists all three parameters obtained for the model above and below the threshold and an error analysis. A plot of the residuals for the model fit of Equation (4.13) is shown in Figure 4.2.

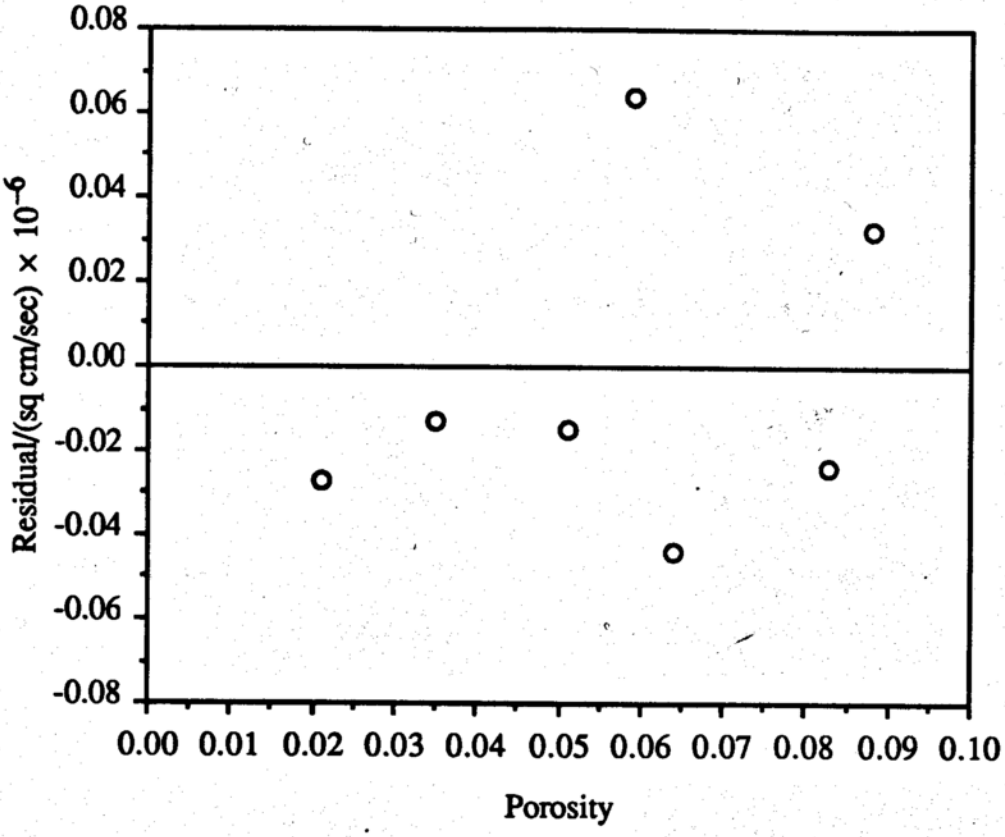


Figure 4.2 Residuals Plotted as a Function of Porosity for Transport Below the Percolation Threshold. Residuals are calculated as the difference between the model estimate of bulk diffusivity and the experimentally measured value of the bulk diffusivity.

b) Estimation of the Nonclassical Percolative Transport Model Parameters Near and Above the Percolation Threshold

The relationship derived for nonclassical percolative transport near and above the percolation threshold was given in Equation (4.8). Using $\emptyset_c = 0.09$ and $\alpha = 3.8 \times 10^{-6}$, Equation (4.8) becomes

$$D_B = \varepsilon \cdot (\emptyset - 0.09)^{2.0} + 3.8 \times 10^{-6} \cdot \emptyset - \vartheta \cdot (\emptyset - 0.09)^{0.9}, \qquad (4.14)$$

where the universal exponents for conductivity and backbone in three dimensions have also been substituted.

Fitting the remaining 17 sets of data, the two variables, ε and ϑ, were determined to be $33 \pm 2 \times 10^{-6}$ and $3.9 \pm 0.7 \times 10^{-6}$ respectively, based on the standard error of the estimate and a 95% confidence interval. The resulting relationship for nonclassical percolative transport near and above the percolation threshold is therefore

$$D_B \times 10^6 = 33 \cdot (\emptyset - 0.09)^{2.0} + 3.8 \cdot \emptyset - 3.9 \cdot (\emptyset - 0.09)^{0.9}. \qquad (4.15)$$

The residuals for this system are plotted as a function of porosity in Figure 4.3 and an error analysis is tabulated in Table 4.2.

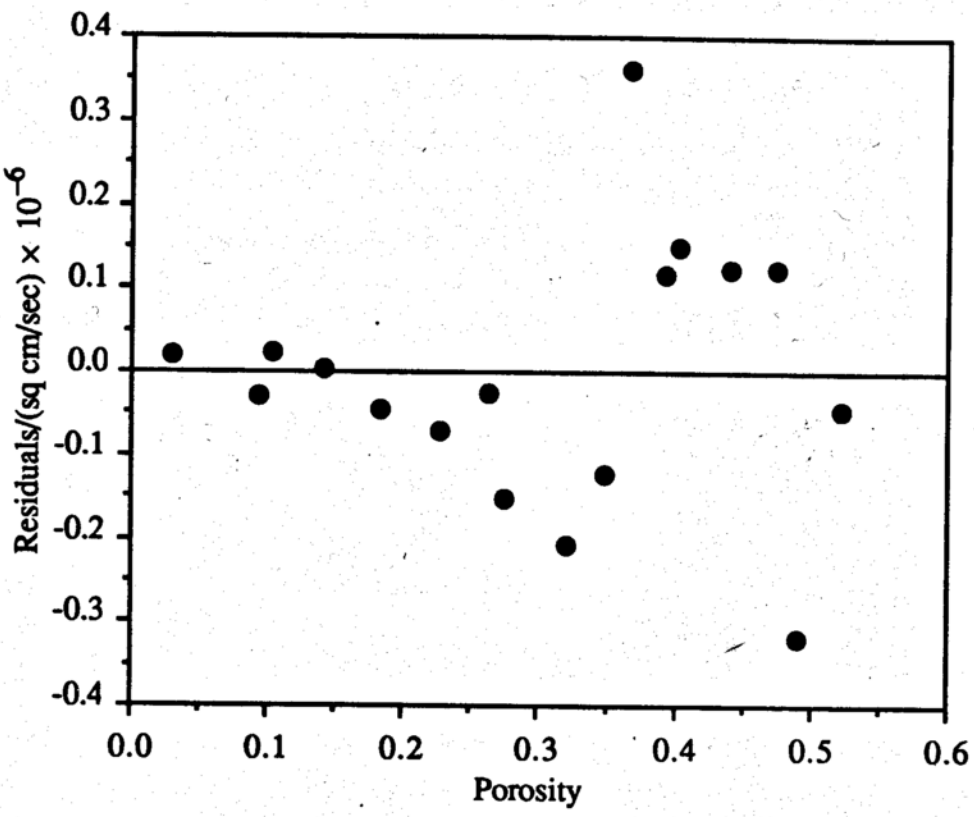


Figure 4.3 Residuals Plotted as a Function of Porosity for Transport Near and Above the Percolation Threshold. Residuals are calculated as the difference between the model estimate of the bulk diffusivity and the experimentally measured value of the bulk diffusivity.

TABLE 4.2 STATISTICAL EVALUATION OF THE NONCLASSICAL PERCOLATIVE TRANSPORT MODEL PARAMETER ESTIMATES

Model Region	Fitted Parameter	Model Estimate $\times 10^6$	Std. Error of the Estimate $\times 10^6$	Number of Observations
Near and Above $\emptyset_c$	ε	33 (2)	0.90	17
	ϑ	3.9 (0.7)	0.35	17
Below $\emptyset_c$	α	3.8 (0.6)	0.23	7

Values in parenthesis are 95% confidence intervals.

B. Evaluation of the Nonclassical Percolative Transport Model

In this Section, the model developed in Section A will be assessed. The calculated bulk diffusivity data obtained from the percolative transport cluster diffusion model will be compared to the experimental bulk diffusivity data obtained from the kinetics experiments. Assessment of the model in terms of scaling will be undertaken by comparison of ln-ln profiles. First, a comparison of the predicted ln-ln profile to the experimental ln-ln profile shown in Figure 4.1 will be tested to evaluate the effectiveness of the method utilized to obtain the percolation threshold. Also, the correlation of the predicted scaling profiles to the classical scaling relationships of percolation theory will be explored via a ln D_B versus ln $(\emptyset - \emptyset_c)$ plot.

Finally, the last section of this Chapter deals with the percolative parameter contributions to the bulk diffusivity profile. The calculated profile will be broken down into morphological and transport contributions. A change from the nonclassical to the classical realm will be sought, essentially the transition to a region where the dominating transport is through porous channels within the matrices.

1. Comparison to Experimental Bulk Diffusivities

From the kinetic data listed in Table 3.4 a plot of the experimental bulk diffusivities and the predicted bulk diffusivities dictated by the model against the porosity of the system was made (Figure 4.4). The excellent agreement is readily apparent.

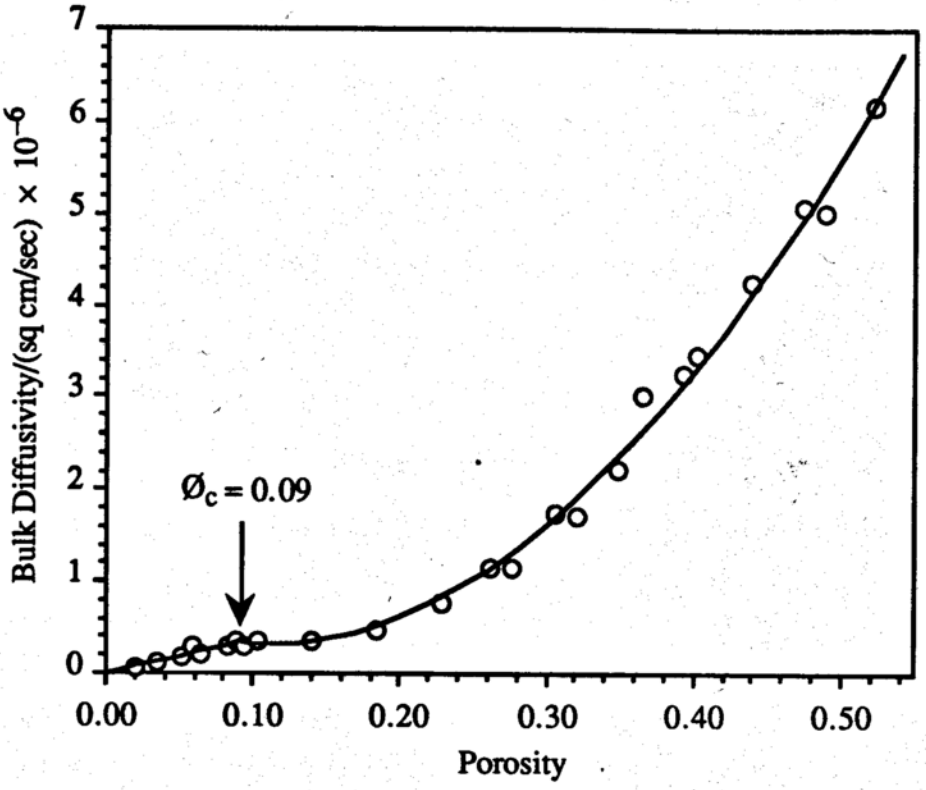


Figure 4.4 Comparison of Experimental Results to Percolative Transport and Cluster Diffusion Model. Open circles are experimental bulk diffusivities, the solid line is the calculated profile based on the percolative transport and cluster diffusion model (Equations (4.13) and (4.15)). The threshold was evaluated to be 0.09 ± 0.02. By using Equation (4.16), the coordination of this system was determined to be 28 ± 7.

By using the percolation threshold value of 0.09 previously determined for this system, the coordination for the benzoic acid/poly(vinyl stearate) matrix can be determined from Equation (4.16) (Equation (1.1) of Chapter I)

$$\emptyset_c = \frac{1}{1 + 0.356 \cdot z} . \qquad (4.16)$$

The coordination obtained in this manner was determined to be 28 ± 7 based on a 95% confidence interval.

The high coordination calculated for this system is supported by the experimentally derived three-dimensional reconstructions shown in Chapter III. The highly complex pore structure apparent in these reconstructions indicates an inherently high coordination, as discussed earlier. The calculated coordination of 28 therefore is consistent with what one might expect from the experimental results even though the actual coordination cannot be obtained from the reconstruction data.

2. Comparison to Scaling Theory

a) The Percolation Threshold

The method used to obtain the percolation threshold for the benzoic acid/poly(vinyl stearate) system is not a general method utilized by percolation scientists. The method will therefore be scrutinized more closely in terms of the predicted profile obtained for the bulk diffusivity. A comparison of the experimental ln D_B versus ln Ø profile to the predicted ln D_B versus ln Ø profile is shown in Figure 4.5. The deviation at the lowest drug load below the percolation threshold is readily apparent; however, the variation over the majority of the profile is minimal. The implications of the deviation at low drug load is a problem associated with percolation theory and will be addressed in Chapter V.

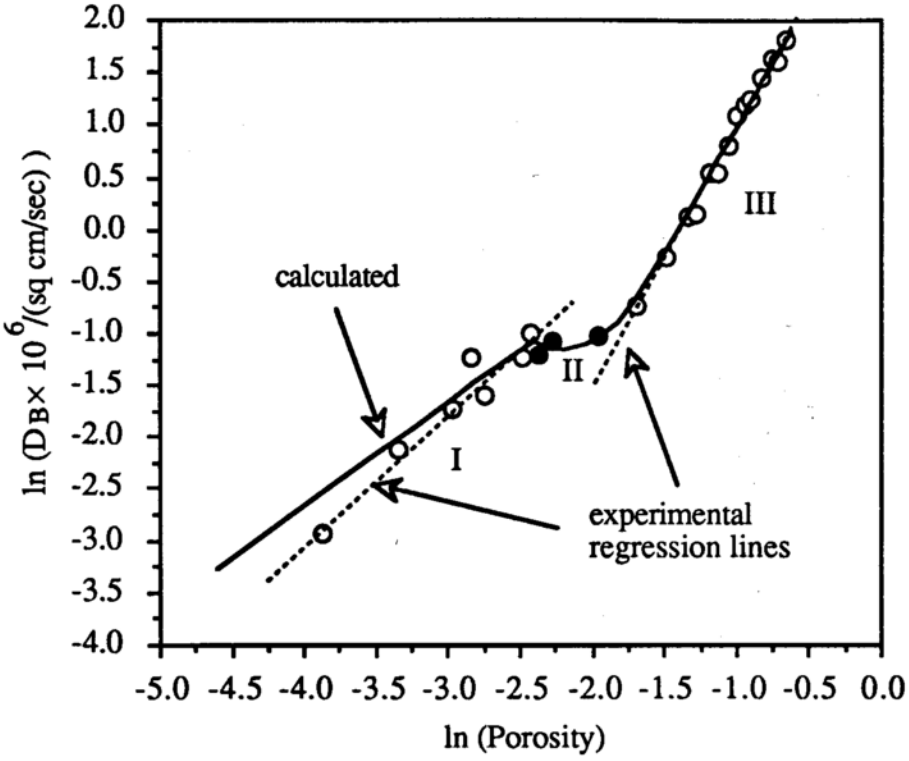


Figure 4.5 Assessment of the Percolation Threshold Estimation Method. Solid line is the calculated profile based on the percolative transport/cluster diffusion model. The dashed lines are regression lines both below and above the percolation threshold (I and III of Figure 4.2). The open and closed circles are experimental data.

b) Percolative Scaling

In classical percolation theory, many scientists have evaluated the universal exponents by examining the slopes of ln $\emptyset^i$ versus ln($\emptyset - \emptyset_c$) profiles of the scaled percolative variable, $\emptyset^i$. A knowledge of the percolation threshold of the system must be known a priori in order to derive such a profile. In this research, the percolation threshold was not known a priori and therefore such an assessment wasn't possible. Figure 4.6 is a ln D_B versus ln($\emptyset - \emptyset_c$) plot of the calculated profile based on the derived percolative transport and cluster diffusion model compared to the experimental bulk diffusivities.

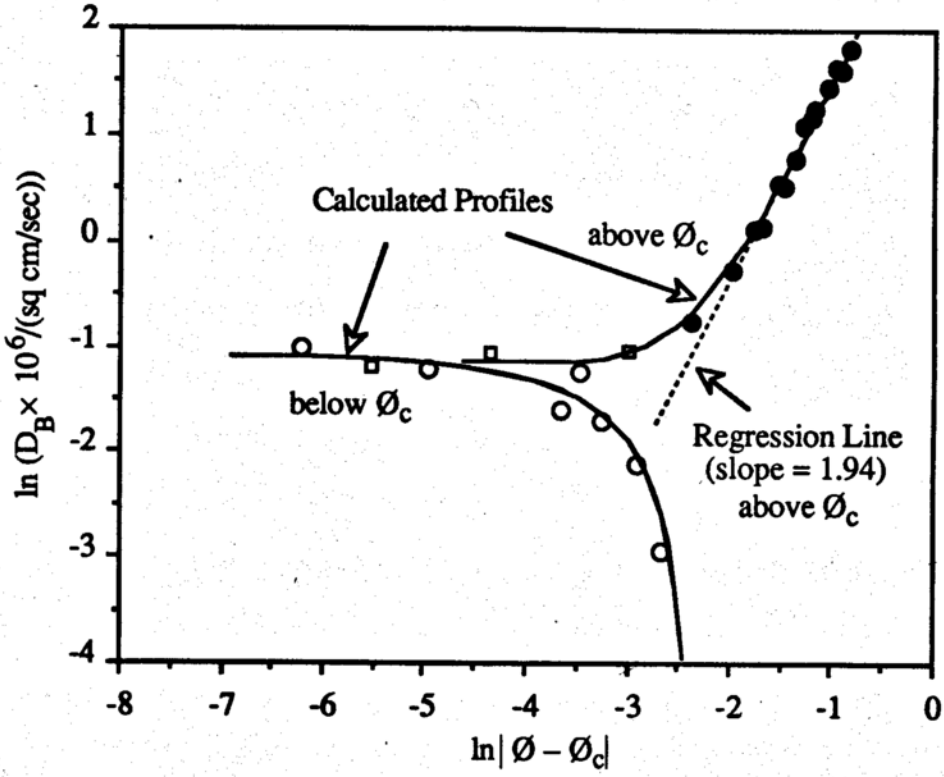


Figure 4.6 Scaling Relationship for the Calculated Profile. Solid lines are calculated profiles labelled as above or below threshold. Regression line (dashes) for above threshold as labelled. Points are experimental data values, open circles below the threshold, closed circles above the threshold, and open squares are transition region data (region II) not used in the scaling assessment. Slope above threshold indicates scaling due to effective volume fraction. Scaling below threshold is not strong enough to indicate classical scaling.

From Figure 4.6, regression analysis on the results above the threshold gives a slope of 1.94 as indicated on the graph. The linear regression relationship is given by

$$\ln\left(D_B \times 10^6\right) = 3.47 + 1.94 \cdot \ln|\emptyset - 0.09| \,. \tag{4.17}$$

The correlation coefficient was 0.974 with only the last 9 sets of kinetics data used. The limited data set allowed for evaluation of the classical nature of the system in a realm where the dominating transport would theoretically be along the sample spanning cluster. In the instance where the sample spanning cluster dominated transport, the slope in this region would be 2.0. The slope value of 1.94 indicates that scaling in this region is indeed dominated by transport through pores.

The slope visibly changes as the threshold is approached from above. The regression line for the first 7 sets of data above the threshold (referring to closed circles in Figure 4.6) is not shown in Figure 4.6, but the relationship is

$$\ln\left(D_B \times 10^6\right) = 2.81 + 1.53 \cdot \ln|\emptyset - 0.09|, \tag{4.18}$$

with a correlation coefficient of 0.985. This change in slope (1.94 to 1.53) either indicates that the cluster diffusion mechanism is operating in addition to the percolative transport mechanism in this region or that nonuniversal scaling is occurring. Since it is not possible in this research to evaluate the nonuniversal nature of this system, no direct conclusions can be made in terms of nonuniversal scaling.

Below the threshold, the data are scattered over the entire profile so that it is difficult to determine a universal scaling exponent. This is to be expected, since below the threshold, the model is proportional to porosity alone. Therefore, below the threshold, scaling in the

classical sense does not exist while above the threshold scaling of a classical/nonclassical nature exists. Anomalous diffusion occurs below the threshold from isolated clusters of benzoic acid and this diffusion as well as diffusion from back bone clusters and along sample spanning clusters also contributes to transport above the threshold.

The next section will address the issue of how strongly the isolated and dead end clusters contribute to the overall transport profile and over what concentration range their effects are apparent.

3. Contributions to Bulk Transport

Since the previous Section alluded to the possibility that the mechanism of transport appears to change over the concentration range investigated, this Section will attempt to separate the dominating mechanisms as a function of porosity into their individual contributions to the observed bulk transport.

Figure 4.7 is a graph of the contributions to transport resulting from the morphological cluster parameters of isolated and dead end clusters, and the classical percolative transport parameter of volume fraction effective. The profile is only broken up into its contributing fractions above the threshold, since below the threshold, the transport is due to a single mechanism: isolated cluster diffusion.

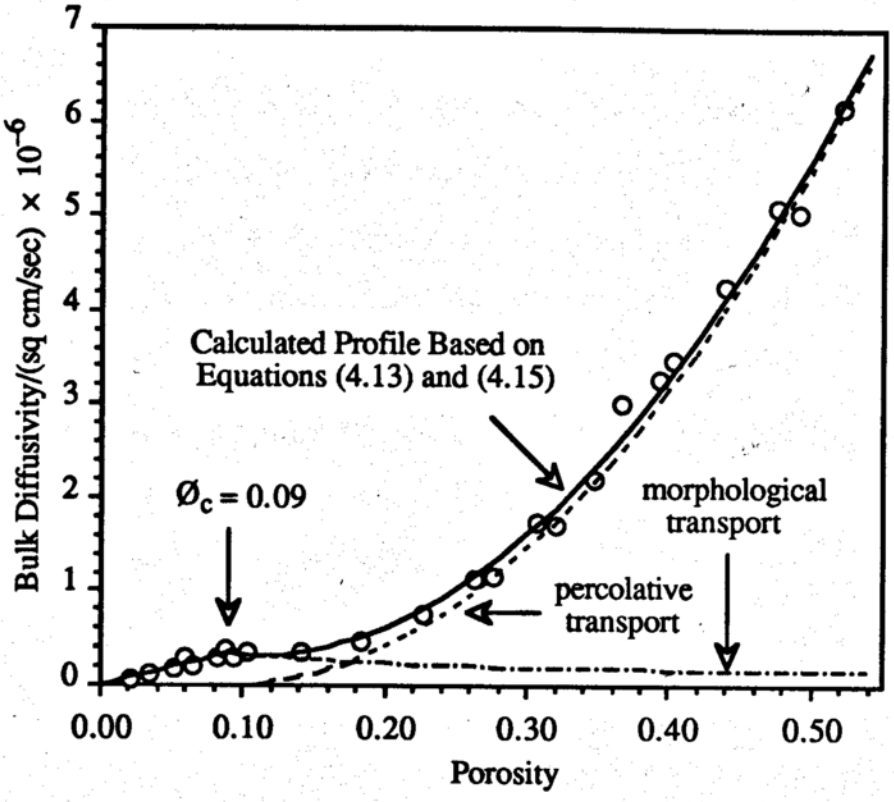


Figure 4.7 Cluster and Percolative Contributions to Bulk Diffusion. Solid line is the calculated profile. Dashed lines are the contributions of the percolative transport parameter (volume fraction effective) and the percolative morphological parameters (isolated clusters and dead end clusters).

From Figure 4.7, the morphological contribution to transport assumes a weakly exponential decrease which is indicative of classical cluster size distribution and dead end cluster size behavior above the percolation threshold. The percolative transport mechanism is a dominating contributor to transport above the threshold as the morphological parameter values wane. At regions well above the threshold it appears that the dominating mechanism of transport is diffusion along the sample spanning cluster, as was stated in the previous section. The slight deviation of the percolative transport mechanism from the total calculated profile is presumably real and is due to the ability of benzoic acid molecules to jump across poly(vinyl stearate) junctions through thin polymer membranes separating pore channels. In this manner, the "skate"/"nonskate" mechanism[53,54] is still operating. The morphological cluster diffusion most strongly influences transport in the region nearest the percolation threshold, as can be concluded from the graph.

4. THE KINETICS MODEL

The modified Higuchi square root of time model employed in the evaluation of the release profiles, as described in Chapters I and III and shown in Equation (1.40), is based on drug release from heterogeneous matrices along interstitial channels or pores. The benzoic acid/poly(vinyl stearate) matrix is a porous matrix, but due to the ability of benzoic acid to diffuse through the poly(vinyl stearate), the matrix can be viewed as homogeneous. The model describing release from a homogeneous polymer matrix assumes that the drug is dissolved in the polymer and that diffusion occurs through the polymer only. This is not exactly the format of transport from the benzoic acid/poly(vinyl stearate) system, but certainly in the low drug load regime below the percolation threshold, this mechanism would apply. The relationship shown in Equation (4.19) was also derived by T. Higuchi[32] and describes the release of drug from a homogeneous dosage form.

$$Q = \sqrt{D \cdot (2A - C_s) \cdot C_s t} \qquad (4.19)$$

where C_s is the solubility of the drug in the polymer matrix, D is the diffusion coefficient of the drug through the matrix material, and the other variables are as described previously for Higuchi's heterogeneous matrix transport relationship,[31] Equation (1.36).

The difference between Equations (1.36) and (4.19), homogeneous versus heterogeneous matrix system, is simply the porosity term, Ø, in Equation (1.36) and the D_e term versus the D transport term in Equation (4.19). The porosity term in Equation (1.36) corrects for the amount of drug dissolved in the pores and its absence in Equation (4.19) signifies the absence of porous transport channels. In the context of percolation theory, ignoring the D versus D_e scenario, Equation (4.19) can be written as

$$Q = \sqrt{D_B C_s \cdot (2\emptyset_d^A \rho - C_s) \cdot t}\,. \qquad (4.20)$$

The bulk diffusion coefficient, D_B, is identical to the diffusion coefficient, D, used by Higuchi; namely the value of the diffusion coefficient of the drug through the matrix.

Both Equations, (4.19) and (4.20), exhibit linear amount released versus square root of time profiles. Diffusion coefficients are obtained from the slope knowing pertinent material and system properties. Again, Equation (4.20) is similar to Equation (1.40) except for the absence of the porosity term in Equation (4.20).

For drug loads much higher than the solubility of the drug in its respective medium, both Equations (4.20) and (1.40) collapse to

$$Q = \sqrt{2\emptyset_d^A \rho D_B C_s t}\,, \qquad (4.21)$$

which is obviously the case for homogeneous diffusion in the system of interest since the solubility of benzoic acid in the poly(vinyl stearate) would at least be one to two orders of magnitude lower than the solubility of benzoic acid in the dissolution medium and therefore at least two to three orders of magnitude smaller than the $2 \times \emptyset_d^A \times \rho$ term. In the heterogeneous case, for the lowest drug load investigated, the porosity × solubility term is three orders of magnitudes smaller than the $2 \times \emptyset_d^A \times \rho$ term and therefore justifies the use of the release kinetics equation in the form shown in Equation (4.21).

As is evident from the above discussion, both situations, diffusion in a heterogeneous system or diffusion in a homogeneous system, can be modeled by the same relationship at high drug loads relative to the solubility of the drug in the respective medium. A re-analysis of the release data obtained to date indicate that dropping the $\emptyset \times C_s$ term doesn't alter the reported results over the drug load range investigated.

V. SUMMARY AND CONCLUSIONS

The overall purpose of this research was to develop a quantitative transport model which described the release of a drug entity from a porous hydrophobic polymeric delivery device. The delivery device consisted of a directly compressed tablet composed of benzoic acid and poly(vinyl stearate). The proposed model was based on the concepts of classical and nonclassical percolation theory and bulk transport through porous matrices. The model adequately described the transport as a function of composition.

The percolation threshold of the benzoic acid/poly(vinyl stearate) system was determined to be 0.09 ± 0.02, which corresponded to a coordination of 28 ± 7. The nonclassical aspect of the percolative transport and cluster diffusion model was concluded to stem from the ability of benzoic acid to transport through poly(vinyl stearate). The low percolation threshold and subsequently high coordination was concluded to be a function of the complex underlying microstructure of the porous matrix and could possibly indicate nonuniversal behavior.

A. Analysis and Characterization of the System

Release kinetic data were obtained for a series of tablets ranging in concentrations from 1 to 55% benzoic acid by weight. The release kinetics were obtained from a rotating disc apparatus and were monitored by analysis of benzoic acid on a reversed phase HPLC apparatus. From the linear square root of time profiles, the bulk diffusivities were obtained as a function of drug load. The compiled data set was ultimately fit to the nonclassical percolative transport and cluster diffusion model in two divisions; below the percolation threshold and near and above the percolation threshold.

The material properties of benzoic acid and poly(vinyl stearate) were characterized in terms of viscosity average molecular weight of the polymer, transport of benzoic acid through pure polymer melts and discs, melting point and enthalpy of formation of the polymer, density of both materials, solubility of the benzoic acid in the dissolution medium, and the diffusion coefficient of benzoic acid in the dissolution medium. Results of the transport experiments through pure poly(vinyl stearate) indicated that the polymer acted as a conducting medium for the benzoic acid. Therefore, release of benzoic acid from the tablet matrices did not occur only through the porous channels produced by drug dissolution and diffusion, as originally expected and dictated by classical percolation theory. Release also occurred directly through the polymer.

1. The Percolative Transport and Cluster Diffusion Model

The biphasic conducting nature of the tablet matrix promoted another mechanism of transport and projected the system into the realm of "nonclassical" percolative transport. Nonclassical behavior is defined as a deviation from classical contributions to scaling. In classical percolation theory, there is only one contribution to transport, the volume fraction effective. The volume fraction effective is dependent on the volume fraction of the conducting phase of the matrix. A classical percolating system is, by definition, composed of phases which can be classified strictly as conducting and nonconducting. The ability of both phases, benzoic acid and poly(vinyl stearate), to act as conducting entities, with no nonconducting phase present, therefore resulted in nonclassical contributions to transport in the form of the morphological parameters of isolated and dead end clusters.

The complication produced by the ability of the poly(vinyl stearate) to allow transport of benzoic acid resulted in a nontraditional approach to the determination of the percolation threshold of the system. From ln-ln plots of the experimental bulk diffusivities versus the

porosities of all the matrices analyzed, the percolation threshold was taken as the break between two linear regions. Justification of this method lies in the relationship observed between the scaled property and the gap exponent of percolation theory. From this method, the percolation threshold was determined to be 0.09 ± 0.02, which corresponded to a coordination of 28 ± 7 for the benzoic acid/poly(vinyl stearate) system.

The evaluation of the model involved fitting pre-exponential factors of the nonclassical model. Only three parameters, one below and two above the percolation threshold, were fit for twenty four sets of experimental data. The mechanisms associated with the observed transport were a combination of classical percolative transport, or transport along the porous sample spanning cluster, and nonclassical cluster diffusion, transport from cluster to cluster though poly(vinyl stearate) branches. The cluster diffusion is described in terms of morphological characteristics of the matrix not normally attributed to transport; isolated and dead end clusters. Far above the percolation threshold, within the concentration range evaluated, the model appeared to collapse to the classical percolative transport scheme except for a slight deviation in the direction of increased transport. This slight deviation is assumed real and is due to the nonclassical enhanced transport caused by jumping from one section of the sample spanning cluster to another indicative of transport through the polymer.

The low threshold and subsequently high coordination of the benzoic acid/poly(vinyl stearate) matrix were determined to be inherent properties of the system. Three-dimensional reconstructions of the underlying porous microstructure corroborated this conclusion. The percolation threshold of the system was determined to be between 0.051 and 0.141 based on the three-dimensional reconstructions. The results of these reconstruction experiments therefore support the calculated percolation threshold of 0.09.

The three-dimensional images, by themselves, were insufficient to definitively confirm or deny the existence of microscopic ordering of the porous structure. However, if the underlying microstructure were ordered in a biased manner, the resulting transport would be nonuniversal. Since the nonuniversal nature of the benzoic acid/poly(vinyl stearate) system could neither be confirmed nor denied, the model derived in this research only treated the aspect of nonclassical transport contributions. The aspect of nonuniversality and its implications are discussed in Section B of this Chapter.

2. The Mechanism of Transport Through the Polymer

In order to clarify the mechanism of transport through the polymer, physical/chemical properties of the polymer were investigated and interpreted. The evaluation of the polymer's molecular weight, its melting point, heat of fusion, and the method of particle size reduction all supported the experimental observation of transport of uncharged, fairly water soluble molecules of benzoic acid through the hydrophobic polymer.

The low molecular weight of the "polymer", dictating an average chain length of only six repeat units, along with the low melt temperature of this waxy "oligomer" supported an argument for high polymer chain mobility. This mobility may allow passage of the solubilized benzoic acid through the polymer structure. The structure of solid poly(vinyl stearate) alone, with a 17 carbon chain attached to the backbone of the polymer, allows one to envision chain entanglement and mobility. The fact that the polymer itself cannot be synthesized to a high degree of polymerization[78] indicates that steric effects may be imposed by the long carbon chain.

The temperature at which the release experiments were performed was within 5° of the onset temperature observed in the melting point determination of the polymer. The argument of chain mobility is most definitely compounded by this condition. So, under the

conditions employed in the release experiments and the solid state properties of the "polymer", transport thorough pure poly(vinyl stearate) was not an unexpected result.

The processing procedure utilized to reduce the particle size of the poly(vinyl stearate) and the benzoic acid employed a micronizer. A micronizer is an air impact mill which forces particles against one another and the sides of the mill to reduce the particle size of a material. The crystallinity of the polymer may have been reduced with this procedure and therefore a more amorphous nature may have been imparted to the polymer. A reduction of the crystalline structure of the polymer would result in an increase in the number and/or concentration of amorphous regions within the polymer structure. The water uptake associated with the amorphous regions of a polymer is well documented[79] and in the benzoic acid/poly(vinyl stearate) system these regions would provide a pathway of transport for the water soluble benzoic acid through the polymer. If the amorphous nature of the polymer was such that it formed "sample spanning clusters" spanning the matrix, the benzoic acid could be transported freely either through polymer or pore space in a "skate"/"nonskate" manner. The amorphous clusters would not even have to be sample spanning, if they were large enough to link various section of the porous sample spanning clusters or even finite pore clusters to produce a "concerted sample spanning cluster" transport would be enhanced.

B. Deviation From Classical and Universal Percolating Systems

The ability of the poly(vinyl stearate) to act as a conducting phase in concert with the conducting pore space produced by the benzoic acid dissolution simulates another system in percolation theory, that of the diffusing termite.[53,54] The ability of the benzoic acid/poly(vinyl stearate) system to exhibit this similar mechanism is due to the physicochemical properties of the polymer and the benzoic acid. Systems which are composed of only biphasic conducting materials exhibit nonclassical transport tendencies.

The high coordination and low threshold values obtained for the benzoic acid/poly(vinyl stearate) system were determined to be indicative of the system due to a complex underlying microstructure. Systems which also exhibit low thresholds, around 3%, are aerogels[55] and aluminum oxide fleece.[56] The low thresholds observed for these two systems were attributed to microscopic ordering.

1. Biphasic Conductivity and Nonclassical Behavior

It was concluded that the benzoic acid/poly(vinyl stearate) system was a biphasic conducting system based on the experimental results. The biphasic nature of the system indicates that the pore structure produced by the dissolution and the diffusion of the benzoic acid and the polymeric material or portions thereof form a "concerted sample spanning cluster". This sample spanning cluster produces anomalous diffusion below the percolation threshold and constitutes the basis of the proposed nonclassical transport model. In terms of percolation parameters, the observed transport was concluded to be derived from classical percolative transport and morphological cluster diffusion. The morphological parameters of isolated and dead end clusters, which do not classically contribute to transport, in this system, support transport. The literature corroborates these results with systems such as the diffusing "termite."[53,54] The systems currently characterized by this mode of

transport are superconductors which exhibit a phase transition at the percolation threshold associated with termites below the threshold and ants above the threshold.

2. Microscopic Ordering and Nonuniversal Behavior

In systems which exhibit microscopic ordering, like the aerogels[55] and aluminum oxide fleece[56] discussed earlier, the percolation threshold of the system is low and the resulting coordination is high. The transport through such systems is biased, and is said to exhibit nonuniversal behavior.[59,80,81,82,83] The nonuniversal behavior is manifested in the form of a different or variable universal exponent value and a lower than expected percolation threshold.

From the limited microstructural data, it was not possible to conclude that microscopic ordering occurred. Therefore, the derived model does not reflect any aspect of microscopic ordering or structural bias. Instead, the low percolation threshold and subsequently high coordination is stated to be a property inherent to the system studied, which is a valid conclusion based on the three-dimensional reconstructions of the pore structure. In order to determine whether a structural bias did exist, the three-dimensional reconstructions of the tablet matrices could be fitted with a statistical autocorrelation function to assess the degree of randomness of the pore structure. The conductivity through the matrix could then be evaluated by a separate technique, such as electrical conductivity, to determine the extent of nonuniversal behavior expressed in the conductivity exponent.

From the transport data, in the region far above the percolation threshold of the system, the conductivity exponent was determined to be 1.94, which is consistent with the universal value of 2.0. This experimental evidence, though by no means conclusive, supports an unbiased transport and therefore universal behavior.

C. Difficulties and Limitations of This Research

This Section is concerned with some of the physical and theoretical limitations of the systems utilized to study the percolative aspects of the benzoic acid/poly(vinyl stearate) system. The discussion offered here will present some questions brought about by the success of the nonclassical percolation model as well as some possible solutions to mechanistic concerns. Answers to the questions posed here were not investigated in this research and are only offered as conjecture.

1. The Kinetics Model

With the success of the nonclassical model, questions about the applicability of the modified Higuchi square root of time model for heterogeneous systems used to obtain kinetic release data arose. The benzoic acid/poly(vinyl stearate) system, because of its ability to allow transport via two mechanisms can be thought of as a homogeneous system since transport through the polymer occurs. It was found, however, that both the heterogeneous and homogeneous models collapsed to the same relationship. The collapsed equation was justified for use in both situations based on order of magnitude estimates. The new relationship, Equation (4.21), did not effect the outcome of the calculated results obtained from the old relationship, Equation (1.40).

2. LIMITATIONS OF THE MODEL

a) Cluster Size Far Below the Percolation Threshold

Limitations of the nonclassical model appeared in the very low drug load regime, below the percolation threshold. Percolation scaling relationships are only applicable for large clusters.[16] In the realm where the clusters of pore structures are small, the model showed some deviation. This deviation was assumed to be real based on cluster size arguments.

b) Morphological versus Percolative Contributions to Transport

In an attempt to separate the contributions to transport, it was shown that the nonclassical percolative model above the percolation threshold approached a realm where the transport was almost totally dominated by the classical sample spanning cluster. This dominating mechanism is physically due to the increased interconnectedness of the porous microstructure as more benzoic acid is incorporated into the matrix.

The direct, independent contribution to transport produced by the volume fraction effective was not able to be distinguished from the morphological parameter contributions. The pre-exponential factors of the volume fraction effective and the backbone volume fraction scaling relationships were fit simultaneously. An independent method of examining the contributions to transport brought about by the percolative transport and morphological parameters would add strength to the nonclassical model and the transport mechanism it predicts. In this manner, the classical versus nonclassical contributions to transport would be elucidated.

D. Questions

1. Volume Fraction Effective From Conductivity Measurements

A question brought up by the separation of contribution analysis summarized above, deals with the characterization of the effective volume fraction profile. Much of percolation theory has been tested on conducting networks in order to analyze the behavior associated with the volume fraction effective.[46,60,84] It is therefore feasible to envision that an electrical conductivity experiment undertaken on extracted tablets from the benzoic acid/poly(vinyl stearate) studies would yield information about only the classical percolative transport properties of the matrices. Fitting the scaling law for the effective volume fraction to the observed experimental percolation profile would yield a value for the percolation threshold of the system as well as the pre-exponential factor for the effective volume fraction. Also, the nonuniversality issue could be addressed with this experimental approach.

In this manner, the more "nontraditional" method utilized to obtain the percolation threshold could be discarded and one fitted parameter would be eliminated in the nonclassical percolative transport model analysis. The exact contribution of the classical transport parameter can be incorporated into the nonclassical model to support or contradict the mechanistic model proposed in this research. Of course, the conductivity measurements assume that only transport occurs through the pore structure and that the ion transport properties are indicative of the transport properties of benzoic acid.

2. Meaning of Pre-Exponential Factors

Another question brought to mind from the modeling performed in this research involves the pre-exponential factors. It appears from percolation theory, that pre-exponential factors have some predetermined significance from scaling theory, but they are definitely influenced by the system composition as well. Therefore, what factors of the percolating

system dictate the nature of the pre-exponential factors?

Speculation on this question can begin with the nonclassical percolative model developed here. The two pre-exponential factors of the morphological contributions to transport were fit one below the percolation threshold for the isolated clusters, and one above the percolation threshold for the dead end clusters. Both fitted values were not significantly different from each other. Does this indicate that the isolated and dead end clusters contribute to transport via the same mechanism or that both have the same structural characteristics within the benzoic acid/poly(vinyl stearate) system? The thoughts associated with the development of the nonclassical model support the conclusion that the isolated and dead end clusters are mechanistically similar with respect to their transport contributions, and percolation theory dictates that there is an underlying structural similarity at all length scales. This last concept has been discussed in the context of the inter-relationship of fractal geometry and percolation theory.[21,85]

If the pre-exponential factor of the morphological properties is indicative of the "termite" transport mechanism of benzoic acid is the pre-exponential factor of the volume fraction effective indicative of transport through the porous network? Comparative studies between similar transport studies in percolating ceramic discs using benzoic acid as the transported entity,[86,87] indicate that there may be a connection.

In summary, it is proposed that the pre-exponential factor may provide some information to the nature of the diffusing species as well as the mechanism of transport. Only further experiments conducted in this light will provide more insight.

3. Evaluation of Coordination

Is there a method to corroborate coordination of a matrix? The only method utilized in this research was the inter-relationship found between the coordination number and the threshold. The method of three-dimensional reconstruction utilized in this research only hinted at the value of the percolation threshold of the system, not the coordination. The underlying microstructure was much too complex to identify a coordination

The most obvious method of characterizing coordination in a percolating system is by initially dictating a coordination by using spheres or cubes to simulate of the classical lattices. If this is feasible, can the coordination of a system be dictated so that a percolation threshold is delegated? What effect does particle size have on the coordination? If the particles size is changed but the geometry of the particles is unchanged, will the threshold change? Experimental evaluation of such concepts is difficult due to the task of constructing particles of known size and geometry and then manufacturing discs of these materials without changing their shape.

4. Testing the Model

The proposed model adequately describes transport in a benzoic acid/poly(vinyl stearate) matrix as manufactured in this research. The next phase of the research in terms of applicability of the model would involve testing other matrix systems. If a system is composed of a truly nonconducting polymer and benzoic acid, would the nonclassical effect be eliminated? Or in this situation, would the nonuniversal aspect become more apparent? Testing of the model would also include a system which exhibited a different degree of permeability to the diffusing entity. Would the pre-exponential factors of the nonclassical model change with these different systems?

Testing the model in this manner would establish the overall applicability and usefulness of the model to the pharmaceutical scientist. Dosage forms are composed of many polymeric materials and manufactured by many methods. The absolute test of the derived nonclassical model would be in the description of transport in other percolating systems, classical, nonclassical, or nonuniversal.

E. Applications

The applicability of the model derived in this research could be wide-spread in pharmacy. Pharmaceutical scientists are always endeavoring to predict the release characteristics of a dosage form. With the developed model, as derived, transport through a porous conducting medium which is permeable to the transported drug entity can be predicted. Though the direct proof of this is still presumptuous, the current research presented here at the least establishes feasibility.

The mechanistic aspect of the proposed model also provides insight into the structure of the dosage form studied. Not only is the connectivity established from the percolation threshold determination, but the complexity of the pore structure is revealed. This important physical picture allows the formulator to diagnose complications arising from manufacturing procedures and the resulting delivery profiles.

In summary, the applicability of this model just to sustained or controlled release delivery system is short-sighted; any disordered system, whether the disordered phase be porous channels or microemulsions,[88] can at least be partially understood based on the principles and concepts of percolation theory.

VI. REFERENCES

[1]J. E. Hastedt, "Diffusional Release From a Porous Polymeric Matrix - A Model Based on Percolation Theory," M.S. Thesis, University of Wisconsin - Madison (1987).

[2](a) P. J. Flory, "Molecular Size Distribution in Three Dimensional Polymers. I. Gelation," *J. Am. Chem. Soc.* **63** (1941): 3083-3090.

(b) P. J. Flory, "Molecular Size Distribution in Three Dimensional Polymers. II. Trifunctional Branching Units," *J. Am. Chem. Soc.* **63** (1941): 3091-3096.

(c) P. J. Flory, "Molecular Size Distribution in Three Dimensional Polymers. III. Tetrafunctional Branching Units," *J. Am. Chem. Soc.* **63** (1941): 3096-3100.

[3]S. R. Broadbent and J. M. Hammersley, "Percolation Processes, Crystals and Mazes," *Proc. Camb. Phil. Soc.* **53** (1957): 629-641.

[4]L. S. Schulman and P. E. Seiden, "Percolation and Galaxies," *Science* **233** (1986): 425-431.

[5]G. MacKay and N. Jan, "Forest Fires as Critical Phenomena," *J. Phys. A: Math. Gen.* **17** (1984): L757-L763.

[6]B. J. Last and D. J. Thouless, "Percolation Theory and Electrical Conductivity," *Phys. Rev. Letters* **27** (1971): 1719-1721.

[7]S. Reyes and K. F. Jensen, "Estimation of Effective Transport Coefficients in Porous Solids Based on Percolation Concepts," *Chem. Eng. Sci.* **40** (1985): 1723-1734.

[8]J. E. Hastedt and J. L.Wright; "Diffusion in Porous Materials Above the Percolation Threshold," *Pharm. Research* in press (1990).

[9]P. H. Winterfeld, "Percolation and Conduction Phenomena in Disordered Composite Media," Ph.D. Thesis, University of Minnesota, Minneapolis (1981).

[10]J. L. Meijering, "Interface Area, Edge Length, and Number of Vertices in Crystal Aggregates with Random Nucleation," *Philips Res. Rep.* **8** (1953): 270-290.

[11]C. Domb and N. W. Dalton, "Crystal Statistics with Long-Range Forces I. The Equivalent Neighbour Model," *Proc. Phys. Soc.* **89** (1966): 859-871.

[12]P. Dean and N. F. Bird, Monte Carlo Studies of the Percolation Properties of Two- and Three-Dimensional Lattices, National Physics Lab. Math Div. Ma61, Teddington, Middlesex, England (1966).

[13]S. Kirkpatrick, "Percolation and Conduction," *Rev. of Mod. Phys.* **45** (1973): 574-588.

[14]S. Reyes and K. F. Jensen, "Percolation Concepts in Modelling of Gas-Solid Reactions-I. Application to Char Gasification in the Kinetic Regime," *Chem. Eng. Sci.* **41** (1986): 333-343.

[15]K. K. Mohanty, J. M. Ottino, and H. T. Davis, "Reaction and Transport in Disordered Composite Media: Introduction of Percolation Concepts," *Chem. Eng. Sci.* **37** (1982): 905-924.

[16]D. Stauffer, Introduction to Percolation Theory, Taylor & Francis, Philadelphia (1985).

[17]S. Kirkpatrick, AIP Conf. Proc., ed. J. C. Garland and D. B. Tanner, No. 40, Am. Inst. of Physics, New York (1978).

[18]D. Stauffer, "Scaling Theory of Percolation Clusters," *Phys. Reports* **54** (1979): 1-74.

[19]C. D. Mitescu and J. Roussenq, Annals of the Israel Physical Society Vol. 5 "Percolation Structures and Processes," eds. G. Deutscher, R. Zallen, and J. Adler, Israel Physical Society (1983): Chap. 4: "Diffusion on Percolation Clusters."

[20]Y. Gefen, A. Aharony, S. Alexander, "Anomalous Diffusion on Percolating Clusters," *Phys. Rev. Letters* **50** (1983): 77-80.

[21]H. E. Stanley and A. Coniglio, Annals of the Israel Physical Society Vol. 5 "Percolation Structures and Processes," eds. G. Deutscher, R. Zallen, and J. Adler, Israel Physical Society (1983): Chap. 5: "Fractal Structure of the Incipient Infinite Cluster in Percolation."

[22]S. Havlin, D. Ben-Avraham, and H. Sompolinsky, "Scaling Behavior of Diffusion on Percolation Clusters," *Phys. Rev. A* **27** (1983): 1730-1733.

[23]D. Stauffer, S. Wilke, Y. Gefen, V. Ilkovic, and A. Aharony, "Diffusion on Random Clusters and the Parasite Problem," *J. Phys. A: Math. Gen.* **17** (1984): 647-656.

[24]M. E. Fisher, "The Theory of Condensation and the Critical Point," *Physics* **3** (1967): 255-283.

[25]M. E. Fisher and J. W. Essam, "Some Cluster Size and Percolation Problems," *J. Math. Phys.* **2** (1961): 609-619.

[26]R. B. Stinchcombe, "Conductivity and Spin-Wave Stiffness in Disordered Systems - An Exactly Soluble Model," *J. Phys. C: Solid State Phys.* **7** (1974): 179-203.

[27]S. Reyes and K. F. Jensen, "Percolation Concepts in Modelling of Gas-Solid Reactions-II. Application to Char Gasification in the Diffusion Regime," *Chem. Eng. Sci.* **41** (1986): 345-354.

[28]S. Reyes and K. F. Jensen, "Percolation Concepts in Modelling of Gas-Solid Reactions-III. Application to Sulphation of Calcined Limestone," *Chem. Eng. Sci.* **42** (1987): 565-574.

[29]J. Heinrichs and N. Kumar, "Simple Exact Treatment of Conductance in a Random Bethe Lattice," *J. Phys. C: Solid State Phys.* **8** (1975): L510-L516.

[30]R. G. Larson and H. T. Davis, "Conducting Backbone in Percolating Bethe Lattices," *J. Phys. Chem. Solid State Phys.* **15** (1982): 2327-2331.

[31]T. Higuchi, "Mechanism of Sustained-Action Medication: Theoretical Analysis of Rate of Release of Solid Drugs Dispersed in Solid Matrices," *J. Pharm. Sci.* **52** (1963): 1145-1149.

[32]T. Higuchi, "Rate of Release of Medicaments From Ointment Bases Containing Drugs in Suspension," *J. Pharm. Sci.* **50** (1961): 874-875.

[33]D. R. Paul and S. K. McSpadden, "Diffusional Release of a Solute From a Polymer Matrix," *J. Memb. Sci.* **1** (1976): 33-48.

[34]P. I. Lee, "Diffusional Release of a Solute From a Polymeric Matrix - Approximate Analytical Solutions," *J. Memb. Sci.* **7** (1980): 255-275.

[35]J. B. Schwartz, A. P. Simonelli, and W. I. Higuchi, "Drug Release From Wax Matrices I. Analysis of Data with First-Order Kinetics and with the Diffusion-Controlled Model," *J. Pharm. Sci.* **57** (1968): 274-277.

[36]J. B. Schwartz, A. P. Simonelli, and W. I. Higuchi, "Drug Release From Wax Matrices II. Application of a Mixture Theory to the Sulfanilamide-Wax System," *J. Pharm. Sci.* **57** (1968): 278-282.

[37]H. Fessi, J. -P. Marty, F. Puisieux, and J. T. Carstensen, "The Higuchi Square Root Equation Applied to Matrices with High Content of Soluble Drug Substance," *Int. J. Pharm.* **1** (1978): 265-274.

[38]N. A. Peppas, "A Model of Dissolution-Controlled Solute Release From Porous Drug Delivery Polymeric Systems," *J. Biomed. Mat. Res.* **17** (1983): 1079-1087.

[39]R. Gurny, E. Doelker, and N. A. Peppas, "Modelling of Sustained Release of Water Soluble Drugs From Porous, Hydrophobic Polymers," *Biomaterials* **3** (1982): 27-32.

[40]R. A. Siegel and R. Langer, "A New Monte Carlo Approach to Diffusion in Constricted Porous Geometries," *J. Colloid and Interface Sci.* **109** (1986): 426-440.

[41]W. M. Saltzman, S. H. Pasternak, and R. Langer, "Microstructural Models for Diffusive Transport in Porous Polymers," *ACS Symp. Ser.* **348** (Controlled Release Technol.: Pharm. Appl.) (1987): 16-33.

[42]R. A. Siegel, Controlled Release of Drugs: Polymers and Aggregate Systems, ed. M. Rosoff, VCH Publishers, New York (1989): Chap. 1: "Modeling of Drug Release From Porous Polymers."

[43]J. P. Straley, "The Ant In the Labyrinth: Diffusion In Random Networks Near the Percolation Threshold," *J. Phys. C: Solid St. Phys.* **13** (1980): 2991-3002.

[44]R. Mehr, T. Grossman, N. Kristianpoller, and Y. Gefen, "Simple Percolation Experiment in Two Dimensions," *Am. J. Phys.* **54** (1986): 271-273.

[45]D. M. Smith and D. L. Stermer "Mercury Porosimetry: Theoretical and Experimental Characterization of Random Microsphere Packings," *J. Colloid and Interface Sci.* **111** (1986): 160-166.

[46]Y. Song, T. W. Noh, S. -I. Lee, and J. R. Gaines, "Experimental Study of the Three-Dimensional ac Conductivity and Dielectric Constant of a Conductor-Insulator Composite Near the Percolation Threshold," *Phys. Rev. B.* **33** (1986): 904-908.

[47]Z. -Y. Yan, S. Weinbaum, and R. Pfeffer, "On the Fine Structure of Osmosis Including Three-Dimensional Pore Entrance and Exit Behaviour," *J. Fluid Mech.* **162** (1986): 415-438.

[48]M. Yanuka, F. A. L. Dullien, and D. E. Elrick, "Percolation Processes and Porous Media I. Geometrical and Topological Model of Porous Media Using a Three-Dimensional Joint Pore Size Distribution," *J. Colloid and Interface Sci.* **112** (1986): 24-41.

[49]M. Yanuka, "Percolation Processes and Porous Media II. Computer Calculations of Percolation Probabilities and Cluster Formation," *J. Colloid and Interface Sci.* **127** (1989): 35-47.

[50]M. Yanuka, "Percolation Processes and Porous Media III. Prediction of the Capillary Hysteresis Loop from Geometrical and Topological Information of Pore Space," *J. Colloid and Interface Sci.* **127** (1989): 48-58.

[51]H. Domes, R. Leyrer, D. Haarer, and A. Blumen, "Percolative Aspects In Photo-conductivity," *Phys. Rev. B.* **36** (1987): 4522-4524.

[52]A. R. Kerstein and B. F. Edwards, "Percolation Model for Simulation of Char Oxidation and Fragmentation Time-Histories," *Chem. Eng. Sci.* **42** (1987): 1629-1634.

[53]J. Adler, A. Aharony, and D. Stauffer, "First Exit Time of Termites and Random Super-Normal Conductor Networks," *J. Phys. A: Math. Gen.* **18** (1985): L129-L136.

[54]A. Bunde, A. Coniglio, D. C. Hong, and H. E. Stanley, "Transport in a Two-Component Randomly Composite Material: Scaling Theory and Computer Simulations of Termite Diffusion Near the Superconducting Limit," *J. Phys. A: Math. Gen.* **18** (1985): L137-L144.

[55]J. Ricke and G. Reichenauer, "Structural Investigation of SiO_2 - Aerogels," *J. Non-Crystalline Solids* **95 & 96** (1987): 1135-1142.

[56]D. Büttner, F. Löffler, R. Caps, and J. Fricke, "Investigation of Solid Thermal Conduction in Evacuated Load-Bearing Fibrous Insulations," *High Temperature-High Pressures* **18** (1986): 537-543.

[57]S. S. Manna, D. Stauffer, and D. W. Heermann, "Simulation of Three-Dimensional Bootstrap Percolation," *Physica A* **162** (1989): 20-26.

[58]H. O. Mártin, E. V. Albano, and A. L.Maltz, "Percolation with Diffusion of Particles with Attractive Interactions," *J. Phys. A: Math. Gen.* **20** (1987): 1531-1542.

[59]A. K. Sarychev and A. P. Vinogradoff, "Percolation In Anisotropic Systems and Structure of the Infinite Cluster," *J. Phys. C: Solid State Phys.* **12** (1979): L681-L683.

[60]C. D. Mitescu, M. Allain, E. Guyon and J. P. Clerc, "Electrical Conductivity of Finite-Size Percolation Networks," *J. Phys. A: Math. Gen.* **15** (1982): 2523-2531.

[61]G. G. Jerauld, L. E. Scriven, and H. T. Davis, "Percolation and Conduction on the 3D Voronoi and Regular Networks: A Second Case Study in Topological Disorder," *J. Phys. C: Solid State Phys.* **17** (1984): 3429-3439.

[62]A. L. Efros, Physics and Geometry of Disorder - Percolation Theory, Mir Publishers, Moscow, USSR (1986).

[63]K. G. Wilson, "Problems in Physics with Many Scales of Length," *Scientific American* **Aug.** (1979): 158-179.

[64]P. J. Reynolds, J. E. Stanley, and W. Klein, "Large-Cell Monte Carlo Renormalization Group for Percolation," *Phys. Rev. B* **21** (1980): 1223-1245.

[65]M. J. Kolb, "A Monte Carlo Renormalisation Group for Aggregation Processes," *Phys. A: Math. Gen.* **20** (1987): L285-L289.

[66]Y. Yuge and M. Hori, "Monte Carlo Renormalisation Group Approach to Critical Percolation Behaviour in Three Dimensions: Simple Cubic Lattice," *J. Phys. A: Math. Gen.* **20** (1987): 3523-3531.

[67]P. J. Reynolds, W. Klein, and H. E. Stanley, "A Real-Space Renormalization Group for Site and Bond Percolation," *J. Phys. C: Solid State Phys.* **10** (1977): L167-L172.

[68]A. P. Young and R. B. Stinchcombe "A Renormalization Group Theory for Percolation Problems," *J. Phys. C: Solid State Phys.* **8** (1975): L535-L540.

[69]A. B. Harris, T. C. Lubensky, W. K. Holcomb, and C. Dasgupta, "Renormalization-Group Approach to Percolation Problems," *Phys. Rev. Letters* **35** (1975): 327-330.

[70]T. Vicsek and J. Kertész, "Monte Carlo Renormalisation-Group Approach to Percolation on a Continuum: Test of Universality," *J. Phys. A: Math. Gen.* **14** (1981): L31-L37.

[71]K. G. Mooney, M. A. Mintun, K. J. Himmelstein, and V. J. Stella, "Dissolution Kinetics of Carboxylic Acids I: Effect of pH under Unbuffered Conditions," *J. Pharm. Sci.* **70** (1981): 13-22.

[72]B. H. Kaye, "Some Aspects of the Efficiency of Statistical Methods of Particle Size Analysis," *Powder Technology* **2** (1968/69): 97-110.

[73]B. H. Kaye and R. Murphy, "Size Distribution Estimation Using Dot Counting Logic," *Powder Technology* **4** (1970/71): 203-213.

[74]J. Newman, "Schmidt Number Correction for the Rotating Disk," *J. Phys. Chem.* **70** (1966): 1327-1328.

[75]W. J. Burlant and A. Adicoff, "Polymerization of Vinyl Stearate by High Energy Electrons," *J. Poly. Sci.* **27** (1958): 269-274.

[76]J. Crank, The Mathematics of Diffusion, 2nd ed., Oxford University Press, New York (1975).

[77]KODAK Technical Pan Film 2415/6415 Information, KODAK Publication No. **P-255**, M6A068 Minor Rev. 2-86-BX, Eastman KODAK Co., Rochester, New York (1985).

[78]W. S. Port, J. E. Hansen, E. F. Jordan Jr., T. J. Dietz, and D. Swern, "Polymerizable Derivatives of Long-Chain Fatty Acids. IV. Vinyl Esters," *J. Poly. Sci.* **VII** (1946): 207-220.

[79]C. A. Oksanen and G. Zografi, "The Relationship Between the Glass Transition Temperature and Water Vapor Absorption by Poly(vinylpyrrolidone)," *Pharm. Research* **7** (1990): 654-657.

[80]D. Stauffer, "Monte Carlo Study of Biased Diffusion at the Percolation Threshold," *J. Phys. A: Math. Gen.* **18** (1985): 1827-1829.

[81]S. Havlin, A. Bunde, H. E. Stanley, and D. Movshovitz, "Diffusion on Percolation Clusters with a Bias in Topological Space: Non-Universal Behavior," *J. Phys. A: Math. Gen.* **19** (1986): L693-L698.

[82]P. M. Kogut and J. P. Straley, "Distribution-Induced Non-Universality of the Percolation Conductivity Exponents," *J. Phys. C: Solid State Phys.* **12** (1979): 2151-2159.

[83]S. -I. Lee, Y. Song, T. W. Noh, X. -D. Chen, and J. R. Gaines, "Experimental Observation of Nonuniversal Behavior of the Conductivity Exponent for Three-Dimensional Continuum Percolation Systems," *Phys. Rev. B.* **34** (1986): 6719-6724.

[84]B. Abeles, H. L. Pinch, and J. I. Gittleman, "Percolation Conductivity in W-Al_2O_3 Granular Metal Films," *Phys. Rev. Letters* **35** (1975): 247-250.

[85]B. B. Mandelbrot, Annals of the Israel Physical Society Vol. 5 "Percolation Structures and Processes," eds. G. Deutscher, R. Zallen, and J. Adler, Israel Physical Society (1983): Chap. 3: "An Explicit Fractal Model of Percolation Clusters."

[86]R. D. Skwierczynski, "Characterization of Porous Hydroxyapatite and β-Whitlockite Ceramic Disks: An Application of Percolation Theory," M.S. Thesis, University of Wisconsin - Madison (1990).

[87]S. R. Ellis, "Porous Alumina Ceramics in Drug Delivery: Processing Concerns and Percolation Models," Ph.D. Thesis, University of Wisconsin - Madison (1990).

[88]J. Peyrelasse and C. Boned, "Conductivity, Dielectric Relaxation, and Viscosity of Ternary Microemulsions: The Role of the Experimental Path and the Point of View of Percolation Theory," *Phys. Rev. A* **41** (1990): 938-953.

VII. APPENDIX

Appendix A: Derivation of the Release Kinetics Model

The model derived here will follow the format used by Higuchi[31,32] in his 1961 and 1963 publications. Modifications will be made in terms of percolation theory and reference is made to the schematic shown in Figure 7.1. The assumptions of this derivation are: (1) the diffusion coefficient is a constant, (2) pseudosteady-state conditions hold, (3) the drug load is greater than the drug solubility, and (4) sink conditions hold.

Fick's first law states that

$$J_B = \frac{dM_t}{Sdt} = \frac{dQ}{dt} = -D_B \frac{dC}{dx} = \frac{D_B C_s}{x}, \qquad (7.1)$$

where J_B is the steady-state flux through a unit surface area of the bulk material, C is the concentration of the solute in the water-filled pores, M_t is the amount of drug released at time t, S is the surface area of release, D_B is the bulk diffusion coefficient of the solute through the bulk porous material at steady-state, C_s is the drug solubility in the dissolution medium, x is distance, and Q is the amount released per unit area.

From Figure 7.1, the mass balance between the amount released, dQ, and the amount remaining in the matrix can be written as

$$dQ = \varnothing_d^A \rho dx - \frac{1}{2} \varnothing C_s dx, \qquad (7.2)$$

where ρ is the solid state density of benzoic acid. The density of benzoic acid enters this relationship because the volume fraction accessible due to drug is calculated as the quotient of the drug load in grams per unit volume of tablet and the density of benzoic acid.

Equation (7.2) can then be substituted into Equation (7.1) to give

$$\varnothing_d^A \rho dx - \frac{1}{2}\varnothing C_s dx = \frac{D_B C_s}{x} dt . \qquad (7.3)$$

Equation (7.3) can be rearranged to

$$\frac{\left(\varnothing_d^A \rho - \frac{1}{2}\varnothing C_s\right)}{D_B C_s} \cdot x dx = dt \qquad (7.4)$$

which, when integrated with the boundary conditions

$$\text{At } x = 0, t = 0 \qquad (7.5a)$$

$$\text{At } x = x, t = t , \qquad (7.5b)$$

results in

$$t = \frac{\varnothing_d^A \rho - \frac{1}{2}\varnothing C_s}{2 D_B C_s} \cdot x^2 . \qquad (7.6)$$

Solving for x,

$$x = \left(\frac{2 D_B C_s}{\varnothing_d^A \rho - \frac{1}{2}\varnothing C_s} \cdot t\right)^{1/2} . \qquad (7.7)$$

From integrating Equation (7.2) over the interval where Q goes from zero to Q and x goes from 0 to x, the result is

$$Q = \varnothing_d^A \rho x - \frac{1}{2}\varnothing C_s x . \qquad (7.8)$$

Equation (7.8) can be rearranged to show that

$$Q = \left(\emptyset_d^A \rho - \frac{1}{2}\emptyset C_s\right) \cdot x \ . \tag{7.9}$$

Substituting Equation (7.7) into (7.9), the result is

$$Q = \left(\emptyset_d^A \rho - \frac{1}{2}\emptyset C_s\right) \cdot \left(\frac{2D_B C_s}{\emptyset_d^A \rho - \frac{1}{2}\emptyset C_s} t\right)^{1/2}. \tag{7.10}$$

Equation (7.10) can now be simplified to

$$Q = \sqrt{2D_B C_s\left(\emptyset_d^A \rho - \frac{1}{2}\emptyset C_s\right) \cdot t} \ . \tag{7.11}$$

This relationship can also be written in the familiar form

$$Q = \sqrt{D_B C_s \left(2\emptyset_d^A \rho - \left(\emptyset_d^A + \varepsilon\right) C_s\right) t}, \tag{7.12}$$

which is identical to Equation (1.40) discussed earlier knowing that

$$\emptyset = \emptyset_d^A + \varepsilon \, , \tag{7.13}$$

where ε is the inherent porosity of the matrix.

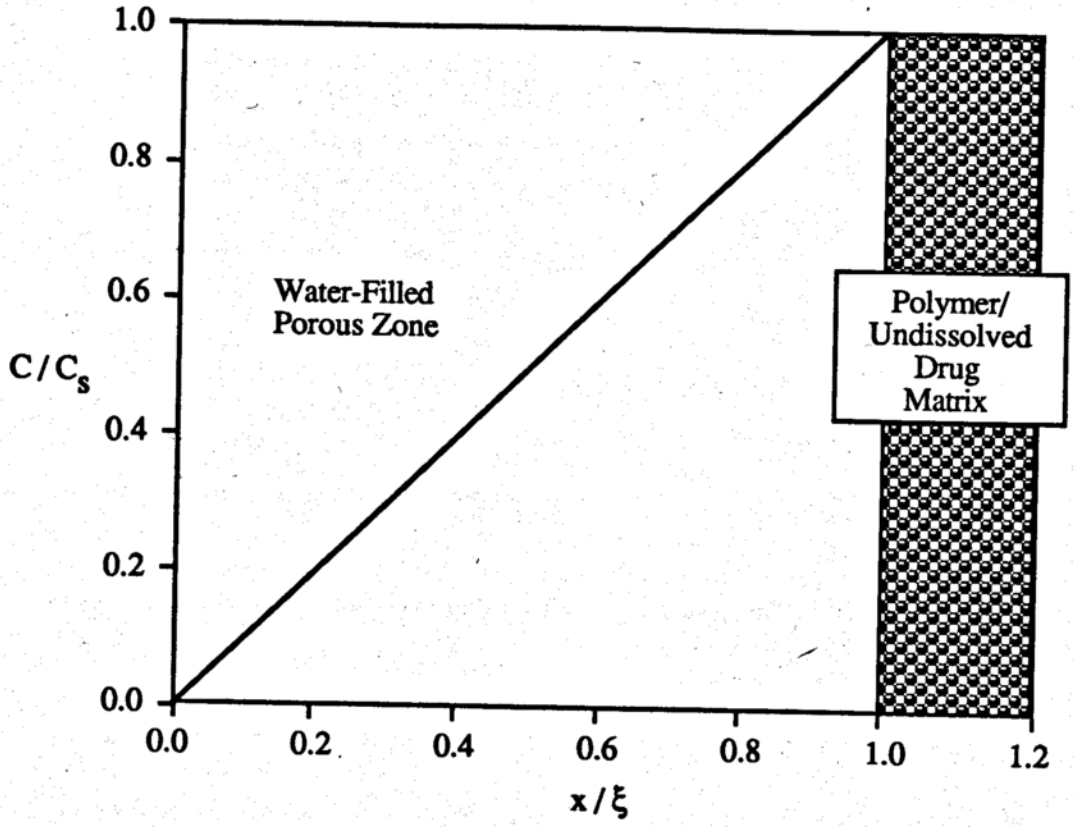


Figure 7.1 Schematic Diagram of the Pseudosteady-State Diffusion Problem for the Benzoic Acid/Poly(vinyl stearate) Matrix System.

Appendix B: Photomicrograph Data for Three-Dimensional Reconstructions

Microtoming Data:

I. Tablet EXP 4C:

$Ø^A = 0.051$, Region I.
Slices taken at 8.33 μm intervals. Approximately 30 μm sliced off surface before starting.
Magnifications of 50X, 20X, and 5X used; 20X and 5X alternating slices.

EXP 4C	Position 1	Position 2	Position 3	Zero (50X)
x	4.40	4.34	4.26	8.74
y	8.10	7.46	6.50	8.57

II. Tablet EXP 3D:

$Ø^A = 0.141$, Region II.
Slices taken at 8.33 μm intervals. Approximately 30 μm sliced off surface before starting.
Magnifications of 50X, 20X, and 5X used; 20X and 5X alternating slices.

EXP 3D	Position 1	Position 2	Position 3	Zero (50X)
x	0.70	1.30	1.20	8.58
y	9.10	7.50	6.5	8.12

III. PVS Disc:

$Ø^A = 0.000$
Approximately 30 μm taken off surface before taking pictures.
Magnifications of 50X, 20X, and 5X used.

	Position 1	Position 2	Position 3	Zero (20X)
x	1.38	3.14	0.60	9.54
y	6.5	6.6	4.78	8.33

NEGATIVES PRINTED AS 8 X 10'S

Picture #	Roll #	Exp. #	Position	Description
1	1	2	1	EXP 4C "surface", 50X
2	1	3	2	EXP 4C "surface", 50X
3	1	4	3	EXP 4C "surface", 50X
4	1	5	3	EXP 4C "surface", 20X
5	1	6	3	EXP 4C 8.33 µm, 5X
6	1	7	3	EXP 4C 8.33 µm, 50X
7	1	8	2	EXP 4C 8.33 µm, 50X
8	1	9	1	EXP 4C 8.33 µm, 50X
9	1	10	1	EXP 4C 16.66 µm, 50X
10	1	11	2	EXP 4C 16.66 µm, 50X
11	1	12	3	EXP 4C 16.66 µm, 50X
12	1	13	3	EXP 4C 16.66 µm, 20X
13	1	14	3	EXP 4C 24.99 µm, 5X
14	1	15	3	EXP 4C 24.99 µm, 50X
15	1	16	2	EXP 4C 24.99 µm, 50X
16	1	17	1	EXP 4C 24.99 µm, 50X
17	1	18	1	EXP 4C 33.32 µm, 50X
18	1	19	2	EXP 4C 33.32 µm, 50X
19	1	20	3	EXP 4C 33.32 µm, 50X
20	1	21	3	EXP 4C 33.32 µm, 20X
21	1	22	3	EXP 4C 41.65 µm, 5X
22	1	23	3	EXP 4C 41.65 µm, 50X
23	1	24	2	EXP 4C 41.65 µm, 50X
24	1	25	1	EXP 4C 41.65 µm, 50X
25	1	26	1	EXP 4C 49.98 µm, 50X
26	1	27	2	EXP 4C 49.98 µm, 50X
27	1	28	3	EXP 4C 49.98 µm, 50X
28	1	29	3	EXP 4C 49.98 µm, 20X
29	1	30	3	EXP 4C 58.31 µm, 5X
30	1	31	3	EXP 4C 58.31 µm, 50X
31	1	32	2	EXP 4C 58.31 µm, 50X
32	1	33	1	EXP 4C 58.31 µm, 50X
33	1	34	1	EXP 4C 66.64 µm, 50X
34	1	35	2	EXP 4C 66.64 µm, 50X
35	1	36	3	EXP 4C 66.64 µm, 50X
36	2	1	3	EXP 4C 66.64 µm, 20X
37	2	2	3	EXP 4C 74.97 µm, 5X
38	2	3	3	EXP 4C 74.97 µm, 50X
39	2	4	2	EXP 4C 74.97 µm, 50X

Picture #	Roll #	Exp. #	Position	Description
40	2	5	1	EXP 4C 74.97 µm, 50X
41	2	6	1	EXP 4C 83.30 µm, 50X
41	2	7	2	EXP 4C 83.30 µm, 50X
42	2	8	3	EXP 4C 83.30 µm, 50X
43	2	9	3	EXP 4C 83.30 µm, 20X
44	2	10	3	EXP 4C 91.63 µm, 5X
45	2	11	3	EXP 4C 91.63 µm, 50X
46	2	12	2	EXP 4C 91.63 µm, 50X
47	2	13	1	EXP 4C 91.63 µm, 50X
48	2	14	1	EXP 4C 99.96 µm, 50X
49	2	15	2	EXP 4C 99.96 µm, 50X
50	2	16	3	EXP 4C 99.96 µm, 50X
51	2	17	3	EXP 4C 99.96 µm, 20X
52	2	18	3	EXP 4C 108.29 µm, 5X
53	2	19	3	EXP 4C 108.29 µm, 50X
54	2	20	2	EXP 4C 108.29 µm, 50X
55	2	21	1	EXP 4C 108.29 µm, 50X
56	2	22	1	EXP 4C 116.62 µm, 50X
57	2	23	2	EXP 4C 116.62 µm, 50X
58	2	26	3	EXP 4C 116.62 µm, 50X
59	2	27	3	EXP 4C 116.62 µm, 20X
60	2	28	3	EXP 4C 124.95 µm, 5X
61	2	29	3	EXP 4C 124.95 µm, 50X
62	2	30	2	EXP 4C 124.95 µm, 50X
63	2	31	1	EXP 4C 124.95 µm, 50X
64	3	1	1	EXP 4C 133.28 µm, 50X
65	3	2	2	EXP 4C 133.28 µm, 50X
66	3	3	3	EXP 4C 133.28 µm, 50X
67	3	4	3	EXP 4C 133.28 µm, 20X
68	3	5	1	EXP 3D “surface”, 50X
69	3	6	2	EXP 3D “surface”, 50X
70	3	7	3	EXP 3D “surface”, 50X
71	3	8	3	EXP 3D “surface”, 20X
72	3	9	3	EXP 4C 141.61 µm, 5X
73	3	10	3	EXP 4C 141.61 µm, 50X
74	3	11	2	EXP 4C 141.61 µm, 50X
75	3	12	1	EXP 4C 141.61 µm, 50X
76	3	13	3	EXP 3D 8.33 µm, 5X
77	3	14	3	EXP 3D 8.33 µm, 50X
78	3	15	2	EXP 3D 8.33 µm, 50X
79	3	16	1	EXP 3D 8.33 µm, 50X

Picture #	Roll #	Exp. #	Position	Description
80	3	17	1	EXP 4C 149.94 µm, 50X
81	3	18	2	EXP 4C 149.94 µm, 50X
82	3	19	3	EXP 4C 149.94 µm, 50X
83	3	20	3	EXP 4C 149.94 µm, 20X
85	3	21	1	EXP 3D 16.66 µm, 50X
86	3	22	2	EXP 3D 16.66 µm, 50X
87	3	23	3	EXP 3D 16.66 µm, 50X
88	3	24	3	EXP 3D 16.66 µm, 20X
89	3	25	3	EXP 4C 158.27 µm, 5X
90	3	26	3	EXP 4C 158.27 µm, 50X
91	3	27	2	EXP 4C 158.27 µm, 50X
92	3	28	1	EXP 4C 158.27 µm, 50X
93	3	29	3	EXP 3D 24.99 µm, 5X
94	3	30	3	EXP 3D 24.99 µm, 50X
95	3	31	2	EXP 3D 24.99 µm, 50X
96	3	32	1	EXP 3D 24.99 µm, 50X
97	3	33	1	EXP 4C 166.6 µm, 50X
98	3	34	2	EXP 4C 166.6 µm, 50X
99	3	35	3	EXP 4C 166.6 µm, 50X
100	4	1	3	EXP 4C 166.6 µm, 20X
101	4	2	3	EXP 4C 166.6 µm, 5X
102	4	3	1	EXP 3D 33.32 µm, 50X
103	4	4	2	EXP 3D 33.32 µm, 50X
104	4	5	3	EXP 3D 33.32 µm, 50X
105	4	6	3	EXP 3D 33.32 µm, 20X
106	4	7	3	EXP 3D 41.65 µm, 5X
107	4	8	3	EXP 3D 41.65 µm, 50X
108	4	9	2	EXP 3D 41.65 µm, 50X
109	4	10	1	EXP 3D 41.65 µm, 50X
110	4	11	1	EXP 3D 49.98 µm, 50X
111	4	12	2	EXP 3D 49.98 µm, 50X
112	4	13	3	EXP 3D 49.98 µm, 50X*
113	4	14	3	EXP 3D 49.98 µm, 20X*
114	4	17	3	EXP 3D 58.31 µm, 5X
115	4	18	3	EXP 3D 58.31 µm, 50X
116	4	19	2	EXP 3D 58.31 µm, 50X
117	4	20	1	EXP 3D 58.31 µm, 50X
118	4	21	1	EXP 3D 66.64 µm, 50X
119	4	22	2	EXP 3D 66.64 µm, 50X
120	4	23	3	EXP 3D 66.64 µm, 50X
121	4	24	3	EXP 3D 66.64 µm, 20X

Picture #	Roll #	Exp. #	Position	Description
122	4	25	3	EXP 3D 74.97 µm, 5X
123	4	26	3	EXP 3D 74.97 µm, 50X
124	4	27	2	EXP 3D 74.97 µm, 50X
125	4	28	1	EXP 3D 74.97 µm, 50X
126	4	29	1	EXP 3D 83.30 µm, 50X
127	4	30	2	EXP 3D 83.30 µm, 50X
128	4	31	3	EXP 3D 83.30 µm, 50X
129	4	32	3	EXP 3D 83.30 µm, 20X
130	4	33	3	EXP 3D 91.63 µm, 5X
131	4	34	3	EXP 3D 91.63 µm, 50X
132	4	35	2	EXP 3D 91.63 µm, 50X
133	5	1	1	EXP 3D 91.63 µm, 50X
134	5	2	1	EXP 3D 99.96 µm, 50X
135	5	3	2	EXP 3D 99.96 µm, 50X
136	5	4	3	EXP 3D 99.96 µm, 50X
137	5	5	3	EXP 3D 99.96 µm, 20X
138	5	6	3	EXP 3D 108.29 µm, 5X
139	5	7	3	EXP 3D 108.29 µm, 50X
140	5	8	2	EXP 3D 108.29 µm, 50X
141	5	9	1	EXP 3D 108.29 µm, 50X
142	5	10	1	EXP 3D 116.62 µm, 50X
143	5	11	2	EXP 3D 116.62 µm, 50X
144	5	12	3	EXP 3D 116.62 µm, 50X
145	5	13	3	EXP 3D 116.62 µm, 20X
146	5	14	3	EXP 3D 124.95 µm, 5X
147	5	15	3	EXP 3D 124.95 µm, 50X
148	5	16	2	EXP 3D 124.95 µm, 50X
149	5	17	1	EXP 3D 124.95 µm, 50X
150	5	18	1	EXP 3D 133.28 µm, 50X
151	5	19	2	EXP 3D 133.28 µm, 50X
152	5	20	3	EXP 3D 133.28 µm, 50X
153	5	21	3	EXP 3D 133.28 µm, 20X
154	5	22	3	EXP 3D 141.61 µm, 5X
155	5	23	3	EXP 3D 141.61 µm, 50X
156	5	24	2	EXP 3D 141.61 µm, 50X
157	5	25	1	EXP 3D 141.61 µm, 50X
158	5	26	1	EXP 3D 149.94 µm, 50X
159	5	27	2	EXP 3D 149.94 µm, 50X
160	5	28	3	EXP 3D 149.94 µm, 50X
161	5	29	3	EXP 3D 149.94 µm, 20X
162	5	30	3	EXP 3D 158.27 µm, 5X

Picture #	Roll #	Exp. #	Position	Description
163	5	31	3	EXP 3D 158.27 µm, 50X
164	5	32	2	EXP 3D 158.27 µm, 50X
165	5	33	1	EXP 3D 158.27 µm, 50X
166	5	34	1	EXP 3D 166.6 µm, 50X
167	5	35	2	EXP 3D 166.6 µm, 50X
168	6	1	3	EXP 3D 166.6 µm, 50X
169	6	2	3	EXP 3D 166.6 µm, 20X
170	6	3	3	EXP 3D 166.6 µm, 5X
171	6	4	1	PVS "surface", 50X
172	6	6	1	PVS "surface", 20X
173	6	8	1	PVS "surface", 5X
174	6	10	2	PVS "surface", 50X
175	6	12	2	PVS "surface", 20X
176	6	14	2	PVS "surface", 5X
177	6	16	3	PVS "surface", 50X
178	6	18	3	PVS "surface", 20X
179	6	20	3	PVS "surface", 5X
180	6	30	n/a	scale at 5X
181	6	31	n/a	scale at 20X
182	6	32	n/a	scale at 50X

* indicates that an error in the position may have occurred here. May be off by 0.60.

Appendix C: Kinetic Release Data

This Appendix contains all the release data accumulated for this research, EXP 1 through 4.

-All data corrected for concentrations withdrawn from previous samples (see text).

EXP 1

Amount Benzoic Acid Released in grams versus Time in hours for EXP 1

Time (hr)	grams Benzoic Acid Released % Benzoic Acid 30.0	35.0	40.0	45.0	50.0	55.0
1	—	0.00669	0.00798	0.0111	0.00612	0.0105
2	0.0085	0.00955	0.01154	0.01396	0.01473	0.01665
3	0.01039	0.01148	0.01349	0.01752	0.01870	0.01983
4	0.01154	0.01293	0.01565	0.01961	0.02129	0.02283
5	0.01319	0.01419	0.01772	0.02210	0.02359	0.02584
6	0.01425	0.01536	0.01940	0.02411	0.02660	0.02826
7	0.01462	0.01632	0.02029	0.02582	0.02813	0.03049
8	0.01608	0.01800	0.02177	0.02785	0.03056	0.03303
10	0.01786	0.01938	0.02597	0.03058	0.03410	0.03749
12	0.01984	0.02146	0.02649	0.03373	0.03756	0.04146
14	0.02032	0.02305	0.02831	0.03629	0.04074	0.04785
16	0.02171	0.02445	0.03074	0.03876	0.04363	0.04867
20	0.02373	0.02715	0.03358	0.04382	0.04972	0.05480
24	0.02543	0.02878	0.03562	0.04701	0.05283	0.05915
28	0.02735	0.03111	0.03886	0.05092	0.05765	0.06422
32	0.02888	0.03305	0.04143	0.05384	0.06219	0.06922
40	0.03241	0.03691	0.04619	0.05987	0.06985	0.07763
48	0.03497	0.03980	0.05043	0.06548	0.07631	0.08616
56	0.03774	0.04340	0.05439	0.06952	0.08251	0.09391
64	0.03973	0.04592	0.05777	0.07498	0.08724	0.10059
96	0.04743	0.05625	0.07016	0.09096	0.10609	0.12571
112	0.05094	0.06031	0.07549	0.09851	0.11456	0.13734
128	0.05427	0.06498	0.08043	0.10324	0.12302	0.14801

Amount Benzoic Acid Released in grams versus Time in hours for EXP 1

(continued)

Time	grams Benzoic Acid Released % Benzoic Acid					
(hr)	30.0	35.0	40.0	45.0	50.0	55.0
152	0.05880	0.06777	0.08839	0.11442	0.13559	0.16471
176	0.06270	0.07722	0.09446	0.12307	0.14631	0.17760
200	0.06621	0.08241	0.10104	0.13172	0.15716	0.19452
224	0.07022	0.08819	0.10752	0.13997	0.16692	0.20654
248	0.07368	0.09302	0.11256	0.14770	0.17679	0.21916
272	0.07650	0.09704	0.11830	0.15639	0.22260	0.22865
296	0.07936	0.10079	0.12289	0.16114	0.24061	0.24080
320	0.08130	0.10333	0.12746	0.17789	0.24178	0.24998
368	0.08775	0.11437	0.13802	0.21166	0.24087	0.25815
416	0.09509	0.12015	0.14599	0.22533	0.24576	0.26727
464	0.09779	0.12674	0.15386	0.22573	0.23731	0.26935
512	0.10405	0.13333	0.16357	0.22788	0.24573	0.26773
560	0.10773	0.13971	0.16839	0.22507	0.24000	0.26910
608	0.11132	0.14634	0.17723	0.22427	0.23822	0.27053
656	0.11731	0.15300	0.18515	0.22740	0.24243	0.27190
704	0.11984	0.15665	0.18905	0.22439	0.24256	0.27219
752	0.12534	0.16128	0.19587	0.22336	0.24157	0.27035
800	0.12792	0.16298	0.20074	0.22439	0.23864	0.26859
848	0.13246	0.16767	0.20460	0.22338	0.24167	0.27175
896	0.13402	0.16735	0.20851	0.22233	0.24166	0.27089
944	0.13671	0.16915	0.21056	0.22736	0.24287	0.27317
992	0.13846	0.16903	0.20874	0.22461	0.24016	0.27270
1040	0.14116	0.16879	0.21274	0.22473	0.24235	0.27506
1088	0.14189	0.17058	0.20992	0.22489	0.24159	0.27442
1136	0.14453	0.17131	0.20984	0.22582	0.24164	0.27257
1184	0.14526	0.17007	0.20892	0.22287	0.23877	0.27087
1220	0.14784	0.17273	0.21079	0.22473	0.24168	0.27293
1268	0.14772	0.17050	0.20887	0.22385	0.24279	0.27345

Amount Benzoic Acid Released in grams versus Time in hours for EXP 1

(continued)

Time (hr)	grams Benzoic Acid Released % Benzoic Acid 30.0	35.0	40.0	45.0	50.0	55.0
1316	0.14935	0.17124	0.21090	0.22378	0.24284	0.27559
1364	0.15096	0.17291	0.21179	0.22365	0.24078	0.27371
1412	0.15056	0.17257	0.21262	0.22448	0.23967	0.27374
1460	0.15127	0.17135	0.21065	0.22534	0.24076	0.27195
1508	0.15190	0.17504	0.21153	0.22121	0.24169	0.27299
1556	0.15052	0.16972	0.20838	0.22106	0.23961	0.27103
1604	0.15123	0.16951	0.20844	0.22016	0.23875	0.27230
1652	0.15288	0.17221	0.21137	0.22108	0.23671	0.27042
1700	0.14994	0.16686	0.20920	0.21892	0.23557	0.26841
1748	0.15308	0.17147	0.21099	0.22068	0.23840	0.26835
1796	0.15074	0.16916	0.21091	0.22059	0.23642	0.26643
1844	0.15434	0.16978	0.21076	0.21838	0.23331	0.26640

EXP 2.

Amount Benzoic Acid Released in grams versus Time in hours for EXP 2

Time (hr)	grams Benzoic Acid Released % Benzoic Acid 30.0	35.1	40.4	43.1	50.1	55.1
24	0.02500	0.03350	0.03730	0.03820	0.05660	0.06220
36	0.03035	0.03727	0.04693	0.05311	0.06954	0.07729
48	0.03533	0.04546	0.05480	0.06091	0.08106	0.09006
60	0.03824	0.04780	0.06193	0.06875	0.09104	0.10363
72	0.04277	0.05514	0.06790	0.07723	0.10043	0.11486
96	0.04542	0.06143	0.07832	0.08047	0.11730	0.13314
120	0.05098	0.06514	0.08868	0.09220	0.13184	0.15399
144	0.05489	0.07228	0.09752	0.10381	0.14400	0.17165
168	0.06232	0.07892	0.10533	0.11889	0.15623	0.18909
192	0.06658	0.08763	0.11343	0.12843	0.16992	0.20332
216	0.07106	0.09206	0.12134	0.13648	0.18113	0.21847

EXP 3

Amount Release in mg versus Three-dimensional in seconds for EXP 3

Time$^{1/2}$ ($sec^{1/2}$)	mg Benzoic Acid Released % Benzoic Acid 5.9	8.2	10.6	15.4	20.5	25.2
207.85	—	4.79	7.61	10.30	—	—
293.94	4.86	6.54	9.72	13.46	17.20	21.60
360.00	5.69	7.46	11.60	15.84	19.39	25.22
415.69	6.46	8.65	12.87	16.93	22.10	28.46
464.76	7.20	9.39	14.13	18.82	23.82	30.81
509.12	8.10	10.41	14.92	20.43	25.96	33.50
587.88	8.81	13.67	16.60	24.74	28.80	36.28
657.27	9.70	12.03	17.78	23.96	31.56	40.99
720.00	10.69	14.90	19.18	26.70	33.95	44.23
777.69	11.45	15.89	20.61	28.38	35.96	46.71
831.38	11.62	15.98	21.64	29.76	37.69	49.12
881.82	12.79	16.97	22.86	31.22	40.00	51.89
929.52	13.22	17.86	24.11	32.47	41.34	54.18
974.89	14.00	18.76	25.25	33.16	43.57	56.48
1018.33	14.37	19.76	25.79	35.64	44.81	58.39
1059.72	14.95	20.67	27.03	35.82	46.35	59.52
1100.00	15.64	22.48	27.48	36.51	47.22	61.66
1138.42	16.22	23.91	28.63	38.22	49.77	64.01
1175.56	17.01	24.75	30.69	39.54	50.75	66.18
1212.02	17.40	26.39	30.93	40.57	52.43	71.25
1247.00	17.73	27.48	31.86	41.17	53.70	72.72
1281.41	18.25	28.57	—	42.87	55.06	75.21
1314.53	18.89	29.79	33.30	43.75	56.81	77.64
1346.85	18.93	30.71	33.84	44.27	57.49	78.46
1378.77	19.45	30.94	34.80	45.21	58.78	81.15
1409.61	19.86	32.23	35.42	45.98	59.32	82.13
1440.14	19.88	32.55	36.18	46.83	60.76	84.41
1469.69	20.20	33.25	36.73	47.46	62.04	85.30

Amount Release in mg versus Three-dimensional in seconds for EXP 3

(continued)

Time$^{1/2}$ ($sec^{1/2}$)	mg Benzoic Acid Released % Benzoic Acid					
	5.9	8.2	10.6	15.4	20.5	25.2
1498.67	20.72	34.06	37.56	48.57	63.43	87.47
1527.42	21.23	34.65	38.46	49.15	63.78	88.27
1555.31	21.25	34.86	38.99	50.05	65.26	90.83
1583.03	21.37	35.66	39.62	50.13	65.83	92.56
1636.46	22.39	38.06	41.24	54.42	68.69	94.78
1688.49	24.22	37.36	42.09	53.72	71.98	97.17
1738.97	23.13	39.08	43.01	56.73	71.90	100.31
1788.02	25.65	39.05	44.84	56.08	78.18	103.27
1835.76	24.30	41.19	45.92	59.73	76.95	105.73
1882.02	25.15	39.70	46.99	58.62	78.60	108.32
1927.43	25.59	42.02	48.35	61.95	80.22	110.02
1971.80	26.62	40.30	49.12	60.60	82.94	113.04

EXP 4

Amount Released in mg versus Three-dimensional in seconds for EXP 4

Time$^{1/2}$ (sec$^{1/2}$)	mg Benzoic Acid Released % Benzoic Acid 1.5	3.3	5.3	7.4	9.4	11.1
293.94	—	—	4.21	—	7.1	8.02
415.69	1.7	3.28	5.91	8.42	9.61	10.87
509.12	1.82	3.89	6.84	10.15	11.47	12.42
587.88	2.29	4.44	8.02	11.56	13.15	14.32
657.27	2.34	4.91	8.74	12.80	14.38	15.75
720.00	2.51	5.44	9.67	13.88	15.62	16.75
777.69	2.70	5.86	10.31	15.04	16.85	18.01
831.38	2.89	6.26	11.14	16.04	17.99	19.25
881.82	3.14	6.83	11.85	17.11	19.09	20.76
929.52	3.31	7.09	12.39	17.94	19.67	21.08
1018.23	3.62	7.82	13.54	19.62	21.51	23.89
1099.82	3.83	8.40	14.41	20.97	22.90	25.85
1175.76	4.17	8.80	15.00	22.19	24.62	28.51
1247.08	4.37	9.44	15.75	23.52	26.07	29.78
1314.53	4.71	10.08	16.82	24.71	27.39	32.62
1378.70	4.77	10.55	17.63	26.32	29.06	34.71
1440.00	4.94	10.93	17.86	27.47	30.49	36.29
1498.80	5.34	11.54	18.59	28.31	31.84	36.84
1555.38	5.44	11.96	19.24	29.30	33.05	39.14
1609.97	5.55	12.04	19.48	30.16	34.12	40.09
1662.77	5.77	12.52	20.11	31.08	35.54	41.64
1713.94	5.82	12.70	20.36	31.94	36.65	42.89
1763.63	5.97	12.97	20.70	32.70	37.63	43.60
1811.96	6.01	13.12	20.84	33.44	38.62	44.82
1859.03	6.12	13.46	21.11	33.48	38.97	44.81
1904.94	6.20	13.30	21.27	33.88	39.54	45.66
1949.77	6.14	13.13	20.77	34.22	40.00	45.78

Amount Released in mg versus Three-dimensional in seconds for EXP 4

(Continued)

Time$^{1/2}$ ($sec^{1/2}$)	mg Benzoic Acid Released % Benzoic Acid 1.5	3.3	5.3	7.4	9.4	11.1
1993.59	6.59	13.87	22.02	35.50	41.14	47.21
2036.47	6.47	13.54	21.76	35.36	41.22	47.31
2078.46	6.52	13.87	22.13	35.79	42.07	47.74
2119.62	6.66	14.07	22.44	36.00	42.04	47.83
2160.00	6.70	14.13	22.65	36.65	42.86	48.66
2199.64	6.79	14.21	22.81	36.60	42.93	48.59
2238.57	7.46	14.76	23.55	37.45	43.94	49.75
2276.84	6.92	14.57	23.52	37.51	43.92	49.97
2314.48	7.27	15.37	24.45	38.22	45.02	50.83
2351.51	7.21	15.24	24.27	38.26	45.04	51.07
2387.97	7.43	15.58	24.56	38.44	45.20	50.74
2423.88	7.49	15.46	24.65	38.38	45.12	50.91
2459.27	7.52	15.53	24.90	38.42	45.54	51.12
2494.15	7.43	15.59	24.77	38.55	45.56	50.94
2528.56	7.43	15.64	25.10	38.78	45.68	50.86
2562.50	8.32	16.47	26.08	40.87	47.61	53.74
2612.58	8.46	16.76	26.46	40.63	47.95	54.42
2661.73	8.22	16.82	26.74	40.54	47.94	54.06
2709.98	8.11	16.93	26.51	40.47	48.39	54.23
2757.39	8.05	17.34	27.04	41.18	49.05	55.33
2804.00	8.19	16.94	26.92	41.21	49.19	55.02
2849.84	8.21	17.11	26.90	40.93	48.98	54.90
2894.96	8.02	16.89	27.03	40.81	49.29	55.48
2939.39	8.10	17.05	26.51	40.71	48.39	55.43
2983.15	8.14	17.31	26.55	40.25	48.25	54.69
3026.28	8.14	17.12	26.48	39.78	47.78	54.39
3068.81	8.38	17.35	27.10	40.85	48.65	54.78
3110.76	8.09	17.16	26.70	40.36	48.09	55.36

Amount Released in mg versus Three-dimensional in seconds for EXP 4

(Continued)

Time$^{1/2}$	mg Benzoic Acid Released % Benzoic Acid					
(sec$^{1/2}$)	1.5	3.3	5.3	7.4	9.4	11.1
3152.14	8.05	17.10	26.78	40.23	48.22	55.37
∞	8.36	17.66	27.17	40.74	48.62	55.81